Adhesion and Beyond: CD44 in Ovarian Cancer Spheroids

BY

Joelle Devon Sacks
M.S., Northeastern University, 2012
B.A., Boston University, 2009

DISSERTATION

Submitted as partial fulfillment of the requirements for the degree of
Doctor of Philosophy in Biopharmaceutical Sciences
in the Graduate College of the
University of Illinois at Chicago, 2018

Chicago, Illinois

Defense Committee:

Maria Barbolina Ph.D., Chair & Advisor
Debra Tonetti Ph.D.
Hyun-Young Jeong Ph.D.
Joanna Burdette Ph.D., Medicinal Chemistry and Pharmacognosy
Andre Kajdacsy-Balla, M.D., Ph.D., Pathology

ACKNOWLEDGEMENTS

It is with great honor that I recognize those who have significantly influenced my pursuit of a career in scientific research and without whom the completion of this work would not have been possible.

First and foremost, my gratitude to Dr. Maria Barbolina, my thesis advisor, cannot adequately be put into words. I can honestly say that without her constant encouragement and passionate commitment to training me to think critically and plan strategically, I would not be the researcher I am today. Throughout my tenure at UIC, it has been an absolute privilege to work under the guidance of outstanding thesis committee members: Drs. Joanna Burdette, Debra Tonetti, Hyun-Young Jeong, & Andre Kajdacsy-Balla. Their remarkable scientific acumen, adeptness, and vigor are unparalleled. I am grateful for sharing their knowledge with me and helping me build a solid scientific foundation. More so, are those who made the last 5 years in the lab an enjoyable place to work every day. Drs Goda Muralidhar and Jia Xie as well as Hilal Gurler had been an integral part of the Barbolina lab since I began and whose presence enriched not only our professional environment, but personally, as well.

Finally, in addition to those who have contributed to the work described here, it is imperative that I recognize the 3 individuals who have been a constant beacon of hope and provided unfailing support during the completion of this thesis and throughout my life. I will likely never been able to adequately express my gratitude to my parents, Bruce and Deborah Sacks. Always providing a platform for me to explore and pursue my dreams, they have made possible my pursuit of higher education and always supported whatever academic and professional opportunities I sought. Without them this accomplishment would not have been possible. Lastly, without my husband, Fernando Suarez Perez, I often wonder how I would have gotten through these 5 years. His continuous moral support and encouragement kept my spirits up when things got tough and strengthened my desire to persist forward.

TABLE OF CONTENTS

TABLE OF CONTENTS (continued)

TABLE OF CONTENTS (continued)

LIST OF TABLES

TABLE PAGE

LIST OF FIGURES

LIST OF FIGURES (continued)

LIST OF FIGURES (continued)

LIST OF ABBREVIATIONS

AML	Acute myeloid leukemia
APC	Adenomatous polyposis coli
ARID1A	AT-rich interaction domain 1A
BRAF	v-Raf murine sarcoma viral oncogene homolog B
BRCA1	Breast cancer type 1 susceptibility gene
BRCA2	Breast cancer type 2 susceptibility gene
CA125	Cancer Antigen 125
CAM	Cell adhesion molecule
CD44s	CD44 standard isoform
CD44v	CD44 variant isoforms
CSC	Cancer stem cell
DAPI	Diamidino-2-phenylindole
DLX4	Distal-Less Homeobox 4
DNA	Deoxyribose nucleic acid
ECM	Extracellular matrix

EMT	Epithelial to Mesenchymal transition
EOC	Epithelial Ovarian Cancer
ERK	Extracellular signal-related kinase
ERM	Ezrin–radixin– moesin
ESEM	Environmental scanning electron microscopy
FAK	focal adhesion kinase
FIGO	International Federation of Gynecological and Obstetrics
FOXM1	Forkhead box M1
gRNA	Guide RNA
GSH	Glutathione
HAS	Hyaluronan synthase
HGSOC	High-grade serous ovarian carcinoma
HMDS	Hexamethyldisilazane
HMWHA	High molecular weight hyaluronan
HNSCC	Head and neck squamous cell carcinoma
HR	Homologous Repair
IgG	Immunoglobulin G

IP	Intraperitoneal
KRAS	Kirsten rat sarcoma viral oncogene homolog
LMWHA	Low molecular weight hyaluronan
MAPK	Mitogen-activated protein kinase
MCA	Multicellular aggregate
MDR	Multidrug resistance
MEM	Minimal essential media
MMP	Matrix metalloprotease
ncRNA	Non-coding RNA
NF-κB	Nuclear factor kappa-light-chain-enhancer of activated B cells
p53	Tumor protein p53
PARP	Poly(ADP-ribose) polymerase
PBS	Phosphate buffered saline
PCM	Pericellular matrix
PIK3CA	Phosphatidylinositol-4,5-bisphosphate 3-kinase catalytic subunit α
POSTN	Periostin
PTEN	Phosphatase and tensin homolog

qRT-PCR	Quantitative real-time polymerase chain reaction
RARRES3	Retinoic Acid Receptor Responder 3
RhoGDI2	Rho GDP-dissociation inhibitor 2
RNA	Ribose nucleic acid
ROS	Reactive oxygen species
RPMI	Roswell Park Memorial Institute
SEM	Scanning electron microscopy
SET	Solid pseudoendometrioid transitional
shRNA	Short hairpin RNA
STIC	Serous tubal intraepithelial carcinoma
TBST	Tris-buffered saline, Tween 20
TIAM1	T-Cell Lymphoma Invasion And Metastasis 1
TGFβ	Transforming growth factor beta
TCGA	The Cancer Genome Atlas
VEGF	Vascular endothelial growth factor
VPSEM	Variable Pressure Scanning Electron Microscope
ZEB2	Zinc finger E-box-binding homeobox 2

SUMMARY

Epithelial ovarian cancer is a leading cause of death from gynecological malignancies. Challenges in effectively treating patients with metastatic disease and preventing chemo-resistance can be attributed to the insufficient understanding of the biology and the mechanisms involved in ovarian cancer metastasis. Epithelial ovarian carcinoma (EOC) metastasis is characterized by the shedding of malignant cells from the surface of the primary tumor and their implantation onto the peritoneal surface lining the abdominal cavity in addition to more distant sites. This shedding of malignant cells from the primary site results as either single cells or free-floating multicellular aggregates, known as spheroids, in the ascites. Although single cells and spheroids may potentially seed metastases, considerable evidence now suggests that the aggregation of cells is important for anchorage-independent cell survival and growth, and spheroid formation may represent an important intermediate survival mechanism to facilitate EOC dissemination. This project, thus, aimed to characterize CD44s in EOC spheroids and its functional significance in epithelial ovarian carcinoma metastasis.

Recent studies have uncovered human transmembrane cell adhesion molecule CD44 standard (CD44s) isoform expression correlating with high grade and advance-stage ovarian carcinoma. Moreover, it has also been suggested that CD44s may be an important mediator of ovarian cancer cell implantation in the peritoneal cavity

enhancing the metastatic potential of ovarian cancer cells. Therefore, we investigated the functional significance of CD44 standard by means of *in vitro* culture experiments with ovarian cancer spheroids.

After characterizing 8 EOC cell lines, a spectrum of CD44 expression was observed and we chose two cell lines with high CD44s (ES-2 and SKOV-3) and two cell lines low in CD44s (OVCAR-4 and OVSAHO) for further testing. Interestingly, the high CD44s-expressing cell lines formed larger spheroids that adhered significantly faster to a monolayer of primary mesothelial cells. Silencing of CD44 using CRISPR/Cas9 in these 2 cell lines reduced spheroid formation suggesting that differential expression of CD44s plays a role in cell-cell adhesion. When we i.p. injected ES-2 $CD44^{-/-}$ cells into athymic nude mice, decreased ascites production and mesentery tumor burden were observed as well as increased overall survival. However, CD44 knockout also significantly increased metastasis to the lung suggesting a suppressive role for CD44 in EOC distant metastasis, as well. This data implies that CD44 enhances the metastatic potential in ovarian cancer spheroids and regulates organ-specific dissemination of ovarian cancer cells, favoring peritoneal dissemination. However, high CD44 expression prevents metastatic dissemination to distant sites, including lungs, thereby limiting its use as a therapeutic target for disease management.

CHAPTER 1: REVIEW OF CURRENT LITERATURE & SCOPE OF THESIS

1.1 Epithelial Ovarian Cancer

1.1.1 Introduction

Epithelial ovarian carcinoma (EOC) is the leading cause of death from gynecologic malignancies and the fifth leading cause of death in women (1). In the United States, an estimated 22,440 new cases of ovarian cancer will be diagnosed in 2017 and an estimated 14,080 will succumb to the disease (1). Ovarian cancer is the 11th most common cancer in women with a frequency of 2.6% and overall lifetime risk of 1 in 76 (2). However, it has the fifth highest mortality rate accounting for 5% of all cancer related deaths in women (1). Based on data collected from 2007-2013, five year survival of patients diagnosed with ovarian cancer is 46.5% (2). The relative survival is influenced to a large extent by the stage of the disease at the time of diagnosis. If the disease is diagnosed at an early stage and localized to the primary site, the five-year survival is 92.5% (2). While, diagnosis at the metastatic stage, when more than 60% of patients are diagnosed, leads to a five year survival rate of only 28.9% (2).

Ovarian cancer is diagnosed at an advanced stage primarily due to non-specific symptoms, including abdominal discomfort, bloating, gas, nausea, and urinary urgency, ambiguous and often mistaken for gastrointestinal problems (3) along with a lack in sensitive and reliable screenings methods for early detection. Therefore, as patients are diagnosed at late metastatic stages, there is minimal chance for long-term survival due to a lack of effective treatments for metastatic disease. While current standard of care, a combination of surgery

and chemotherapy, is efficient as initial treatment, in most cases EOC recurs within a few years and develops resistance to current therapy (4, 5). Prolonging patient remission is a challenge in clinical management of EOC stemming in part from an insufficient understanding of the biology and mechanisms supporting EOC metastasis.

1.1.2. Clinical Appearance and Management

Malignant tumors of the ovaries and fallopian tubes occur at all ages varying in histological subtype by age. For example, in women younger than 20 years of age, germ cell tumors predominate, while borderline tumors occur typically in 30 and 40 year old woman—10 or more years younger than in women with invasive EOC occurring typically after age 50 (1, 6). Risk factors established for EOC include many reproductive factors. Women who have never had children are twice as likely to develop EOC. First pregnancy at an early age, early menopause, and the use of oral contraceptives have also been associated with lower risks of ovarian cancer (7, 8).

Moreover, hereditary factors are associated with approximately 10% of ovarian and fallopian tube cancer. Women with germline mutations in BRCA1 and BRCA2, key proteins involved in homologous repair (HR) of DNA, have a substantially increased risk of ovarian, tubal, and peritoneal cancer—about 20%–50% with BRCA1 and 10%–20% with BRCA2 (9-12). Patients with a strong family history of epithelial ovarian, fallopian tube, or peritoneal cancers, particularly if there is a documented germline BRCA1/2 mutation, are advised to have a bilateral salpingo-oophorectomy at the completion of childbearing in order to reduce their

risk of developing cancer in these tissues (6). Otherwise, there are no other effective screening methods that reduce the mortality of ovarian, fallopian tube, or peritoneal cancers. Studies using CA-125, ultrasonography of the pelvis, and pelvic examination do not have an acceptable level of sensitivity and specificity, but trials are still ongoing in women in the general population aside from those in high-risk populations (13).

Roughly two thirds of all epithelial "ovarian" cancers are Stage III or Stage IV at diagnosis. Woman often present with symptoms including vague abdominal pain or discomfort, menstrual irregularities, or indigestion among other mild digestive disturbances, which may have even been present for only a few weeks (14, 15). As the disease progresses, abdominal distention and discomfort from ascites generally increase and may be associated with respiratory symptoms from increased intra-abdominal pressure or from the leakage of fluid into pleural cavities (6).

Current treatment strategies for advanced ovarian carcinoma consist of aggressive tumor debulking or cytroreductive surgery to remove as much of the tumor as possible. Postoperatively, all women, except those with early- stage disease, receive chemotherapy with platinum (carboplatin, rarely cisplatin) and taxane (Taxol). Carboplatin, or *cis*-Diammine-1,1-cyclobutane dicarboxylate platinum (II), is a member of the platinum family of chemotherapeutic drugs along with the earlier analogue, cisplatin. These compounds function by binding to the purine bases in DNA creating DNA adducts that lead to irreparable DNA damage and activation of apoptosis (16-18). Carboplatin is preferred over cisplatin in the

chemotherapeutic treatment of ovarian cancer, however, due to equivalent efficacy with improved off-target toxicity (19). On the other hand, the taxane family of drugs, which includes paclitaxel and docetaxel, are cytotoxic agents used to treat several different cancers by causing stabilization of the cellular microtubules thereby preventing the de-polymerization of cell microtubule assembly and arresting the cells in the metaphase of mitotic cell division (20-22). Patients who have undergone optimal debulking would ideally receive intraperitoneal (i.p.) delivery of these therapies as EOC is generally restricted to the abdominal cavity and pharmacodynamic studies show i.p. chemotherapy can achieve very high peritoneal drug concentrations (23).

Moreover, therapies including Bevacizumab, a humanized monoclonal antibody targeting vascular endothelial growth factor, have recently been approved for first-line treatment of advanced EOC in combination with standard chemotherapy and for platinum-sensitive as well as platinum-resistant recurrent EOC (24), while olaparib, a poly(ADP-ribose) polymerase (PARP) inhibitor received its 2017 approval as maintenance therapy in patients with platinum-sensitive, relapsed EOC and a BRCA1/2 mutation following at least two lines of previous chemotherapy (25). If disease returns in less than 6 months following platinum chemotherapy, it is considered “platinum resistant,” and choice of chemotherapy is selected from a variety of medications that have all shown similar ability to shrink cancer (liposomal doxorubicin, gemcitabine, topoisomerase inhibitors) (26). The median interval to first recurrence in EOC is 18 to 24 months, and after recurrence, generally 70% of advanced stage

EOC relapses becoming increasingly more difficult to treat with poor overall survival prompting the need for new and better treatments for metastatic disease (27).

1.1.3 Histopathology

EOC is a highly heterogeneous disease classified by histological subtypes in 2 general groups, Type I and Type II, defined by distinct clinicopathological and molecular genetic features. Type I tumors include endometriosis-related tumors, clear cell, seromucinous and mucinous carcinomas, which are generally low grade and develop in a stepwise fashion from well-established benign precursors—in most cases, borderline tumors (28). They are generally confined to the ovary, progress slowly, and account for only 10% of deaths from ovarian cancer (28). Moreover, they are relatively genetically stable, however, present with frequent somatic mutations involved in the phosphatidylinositol-4,5-bisphosphate 3-kinase catalytic subunit α (PIK3CA)/phosphatase and tensin homolog (PTEN), catenin β1, Kirsten rat sarcoma viral oncogene homolog (KRAS)/B-Raf proto-oncogene, serine/threonine kinase (BRAF)/mitogen-activated protein (MAP) extracellular signal-related kinase (ERK), and AT-rich interaction domain 1A (ARID1A) chromatin remodeling pathways (28).

Type II tumors, on the other hand, are invariably high grade and composed, for the most part, of high-grade serous carcinomas (HGSOC) that can be further divided into morphologic (usual or solid pseudoendometrioid transitional (SET)) and molecular subtypes (immunoreactive, proliferative, differentiated, and mesenchymal) (28). These tumors are currently thought to develop rapidly from serous tubal intraepithelial carcinomas (STICs) of the fallopian tube

fimbriae (29) and are highly aggressive presenting in advanced stage in more than 75% of cases (28). They display marked chromosomal instability, ubiquitous TP53 mutations, and frequent abnormalities in homologous recombination repair, retinoblastoma protein, cyclin E1, forkhead box M1 (FOXM1), and Notch3 pathways (Figure 1) (28).

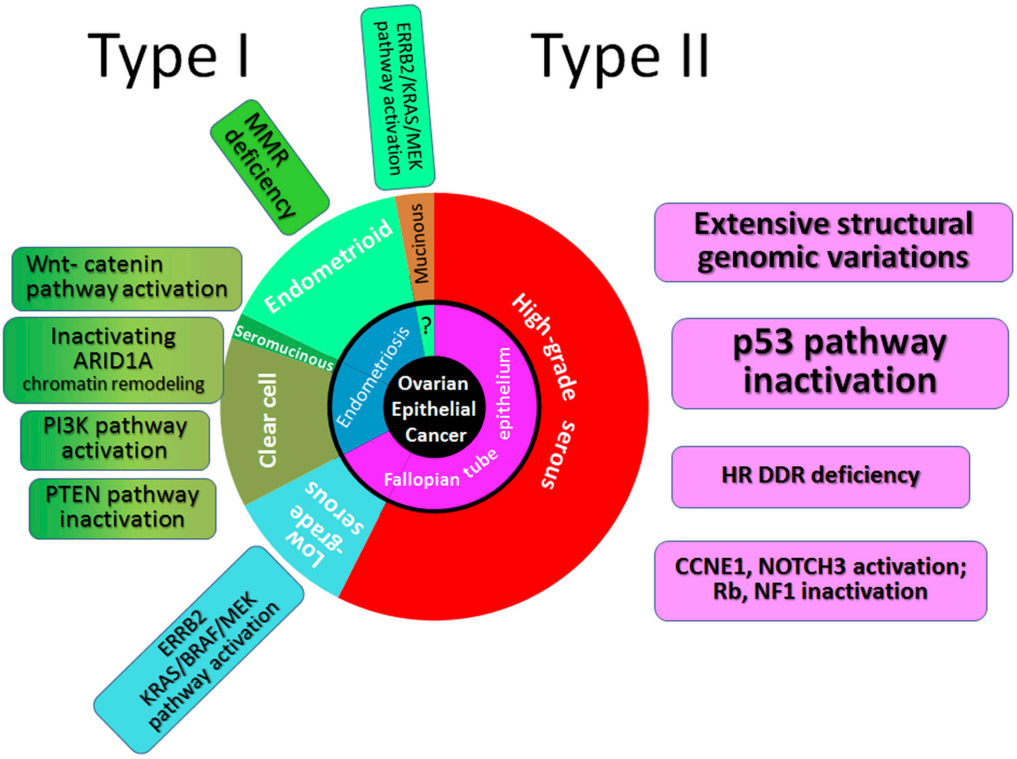

Figure 1. Sub classifications of ovarian cancer histologic subtypes (28).

The revised dualistic model in the pathogenesis of ovarian epithelial cancer. Type I carcinomas comprise low-grade serous, clear cell, endometrioid, and mucinous carcinomas. Seromucinous carcinomas and malignant Brenner tumors are rare and not shown. Type II carcinomas are largely composed of high-grade serous carcinomas. Carcinosarcoma and undifferentiated carcinoma are relatively uncommon and not illustrated. The areas in individual histotypes reflect their relative prevalence. The inner circle indicates the likely cell of origin of the different type I and type II neoplasms. The origin of mucinous carcinomas is not well established and is discussed in the text. The molecular pathway alterations that characterize each tumor subtype are summarized in the square boxes. Some of the pathway abnormalities are shared by some tumor types and they are shown in two-color fill in boxes. ARID1A, AT-rich interaction domain 1A; BRAF, B-Raf proto-oncogene, serine/threonine kinase; CCNE1, cyclin E1; ERRB2, estrogen-related receptor β2; HR DDR, homologous

recombination-mediated DNA damage repair; KRAS, Kirsten rat sarcoma viral oncogene homolog; MEK, mitogen-activated protein (MAP) extracellular signal-related kinase (ERK) kinase; MMR, DNA mismatch repair; NF1, nuclear factor 1; PI3K, phosphatidylinositol 3-kinase; PTEN, phosphatase and tensin homolog; Rb, retinoblastoma protein.

(Figure and caption originally published in Kurman, RJ, Shih, leM. The Dualistic Model of Ovarian Carcinogenesis: Revisited, Revised, and Expanded. American Journal of Pathology. 2016;4:734-6. doi: 10.1016/j.ajpath.2015.11.011.)

In addition to classification of subtypes by clinicopathological and molecular genetic features, EOC are classified based on degree of differentiation, or grade (30). The International Federation of Gynecological and Obstetrics (FIGO) have defined the most common grading system. The FIGO system is based on architectural criteria depending on the ratio of glandular or papillary structures relative to areas of solid tumor growth with Grades 1, 2, and 3 correspond to <5%, 5–50%, and >50% solid growth, respectively (31). Finally, classification of the disease by stage of tumor progression I-IV is used to determine therapeutic strategies. In 2014, the Gynecologic Oncology Committee of FIGO revised tumor staging to incorporate ovarian, fallopian tube, and peritoneal cancer in the same system due to the histologic, molecular, and genetic evidence showing that the majority of tumors classified as high-grade serous carcinomas of the ovary or peritoneum originate in the fimbrial end of the fallopian tube (29, 32, 33).

1.2 EOC Tumor Progression

1.2.1 Metastatic Dissemination

The high mortality of EOC is largely explained by the fact that the majority of patients present with advanced disease when the disease is widely metastatic within the peritoneal cavity.

Metastasis of EOC can occur via the transcoelomic, hematogenous, or lymphatic route. Of these, however, transcoelomic metastasis is the most common, and is responsible for the greatest morbidity and mortality in women with this disease because they occur so frequently and have the capacity to affect multiple vital organs within the abdomen, including the gastrointestinal and genitourinary systems (34). HGSOC is currently thought to spread form the fallopian tube fimbrae to involve the ovaries first, and then metastasize either by direct extension from the ovarian/fallopian tumor to neighboring organs (uterus, omentum, sigmoid colon) or detachment of the cancer cells from the primary tumor mass and taken up by the natural flow of peritoneal fluid within the abdominal cavity (34). The formation of this malignant ascites, can result in raised intra-abdominal pressure and subsequent abdominal distention and discomfort, early satiety leading to dietary deficiency, impaired circulation of blood and lymphatic vessels, and respiratory dyspnea (34). Other common secondary sites for regional metastasis are the peritoneum, which covers the entire abdominal cavity, the right diaphragm, and the small bowel mesentery are preferentially colonized (23). Unlike most other cancers, EOC rarely disseminates through the vasculature. However, pelvic and/or para-aortic lymph nodes can be involved (35), a risk factor for development of distant metastasis (pleura, lung, liver, bone) consistent with late stage disease in one third of ovarian cancer patients (36).

1.2.2 Spheroids

The primary mode of distant metastasis involves the shedding of cells from the primary tumor, which can then aggregate as spheroids within the abdominal cavity, then settle onto

the peritoneal surface followed by disaggregation and implantation in the mesothelial lining where metastatic outgrowth can occur (37-39). In ascites, shed EOC cells can be found as individual cells and/or multicellular spheroids (40, 41). Although both populations of cells may potentially seed metastases, the aggregation of cells has been reported to be important for anchorage-independent cell survival and growth (42), and, therefore, spheroid formation may represent an important intermediate survival mechanism to facilitate EOC dissemination. Therefore, understanding the role of cells, specifically in spheroids, in malignant ascites will be integral for understanding EOC metastasis. While the function of multicellular spheroids in metastatic disease remains to be fully elucidated, there is evidence to suggest that they play an important role in metastatic disease (39).

The most important function of a multicellular tumor spheroid is to create an anchorage-independent *in vivo* tumor microenvironment that can support mechanisms of cell survival through cell–cell adhesion, depending largely on the expression and activity of certain cell–cell adhesion molecules (CAMs) N- and E-cadherin (43, 44), as well as upregulation or expression of proteins associated with spheroid compaction, including vimentin (45). Cells must express at least one CAM, otherwise they would not be able to aggregate or subsequently compact (46, 47). Successful metastasis then requires the remodeling of these CAMs, as the spheroids disaggregate on the mesothelium of the peritoneum, while extracellular matrix (ECM) adhesion molecules (integrins) anchor the spheroid to the sub-mesothelial ECM (48, 49). Invasion of tissues requires additional protease activation (matrix metalloproteases (MMP)) for the degradation of the basement membrane and complete

establishment of a metastatic lesion (39). The microenvironment *in situ* appears capable of supporting these functions through exposure to secreted growth factors and chemokines that are found in the ascitic fluid (50). These mechanisms are potentially very complex and further delineating them will be crucial for the development of new therapies that specifically target spheroid-mediated metastasis (39).

Recently, it has become apparent that spheroids within malignant ascites represent a significant impediment to efficacious treatment of late stage EOC. *In vivo*, spheroids are present in the malignant ascites of EOC patients, while *in vitro* cultured spheroids are capable of tumorigenesis *in vivo* and display a reduced response to chemotherapeutic drugs when compared to monolayers (51, 52). A major problem associated with the current generation of chemotherapy agents is that they do not address the anchorage- and vascular-independent growth conditions associated with a 3-dimensional structure that has formed and/or grown in suspension. Penetration of small molecule inhibitors that rely on diffusion through the plasma membrane must pass through multiple layers of cells to reach the inner cells of these compact multicellular structures. Thus, spheroid formation may represent a key component of platinum/taxane- sensitive recurrence if cells in the core of the spheroids are less exposed overall to drug. However, a better understanding of spheroid biology is necessary for the identification of new treatment opportunities for the sustained treatment of metastatic EOC (39). New methodologies that specifically target spheroid-mediated disease progression still need to be developed, as well. New experimental therapies that utilize antibody-directed therapy to focus treatment at the tumor site while minimizing systemic exposure to cytotoxic

agents is ongoing (53), and will hopefully provide promising directions for the treatment of spheroid-mediated EOC metastases.

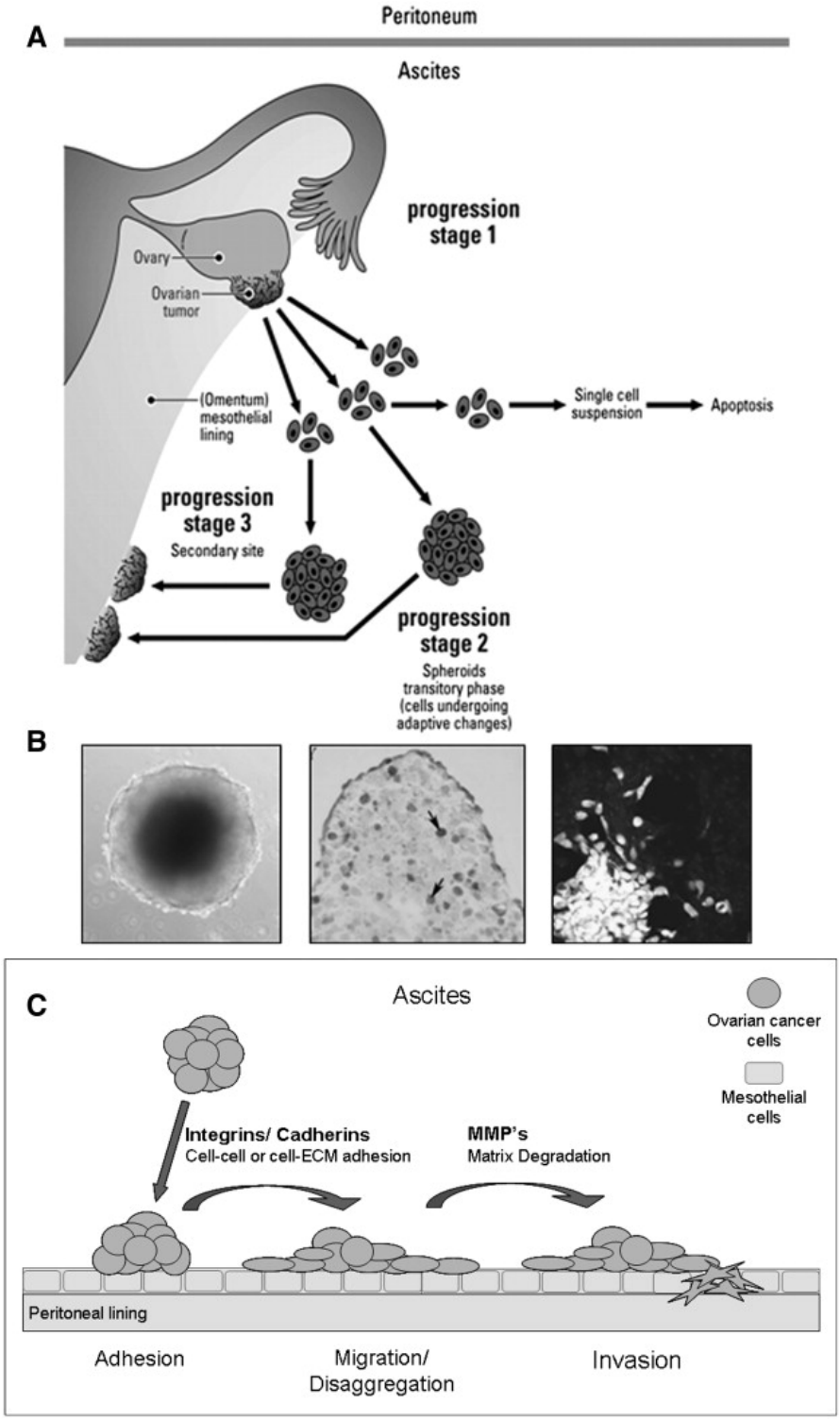

Figure 2. Model of ovarian cancer progression (39).

(A) Diagrammatic representation of our hypothesis of Ovarian Cancer progression (reproduced with permission from [19]). (B) In vitro assays using HEY ovarian cancer spheroids after 4 days of culture. Phase contrast image of a HEY spheroid (left panel, magnification 200×), cryostat section of a HEY spheroid probed for Ki67 expression (middle panel, arrows, magnification 400×) and Cell-Tracker labeled HEY spheroid (light cells) disaggregating on a mesothelial monolayer (LY9, dark cells just visible in the background) (right panel, magnification 400×). (C) Outline of how spheroids in ascites would be able to establish metastatic lesions. Multicellular ascites spheroids attach to and disaggregate on the mesothelial lining of the peritoneal cavity, facilitated by the action and/or remodeling of the cadherins and integrins. Then through the activity of MMPs cells are able to infiltrate the mesothelial lining and ECM. MMP — matrix-metalloprotease; ECM — extracellular matrix.

(Figure and caption originally published in Shield, K., et al. Multicellular spheroids in ovarian cancer metastases: Biology and pathology. Gynecologic Oncology. 2009;113:143-8. doi: 10.1016/j.ygyno.2008.11.032.)

1.2.3 Extracellular Matrix in the Microenvironment

The extracellular matrix (ECM) is a highly organized three-dimensional structure with many physiological and pathological roles. In addition to maintaining tissue integrity, ECM also regulates cell migration, cellular differentiation, and proliferation and provides a reservoir of cytokines and growth factors (54). ECM is an essential component of the tumor microenvironment, and cancer development and progression are associated with increased ECM deposition and crosslinking. The chemical and physical signals elicited from ECM are necessary for cancer cell growth and invasion, and it has been shown that cancer cells are an active and important component in ECM remodeling. These ECM functions are summarized in Figure 3. ECM molecules, such as Periostin (POSTN), fibronectin, and hyaluronan, are important components of the metastatic niche (55). The potential of ovarian cancer cells to disseminate and metastasize into the peritoneal cavity is ruled by, among others, the ECM composition (56). The ECM of epithelial ovarian tumors comprises a variety of molecules

including the collagen superfamily and noncollagenous proteins such as glycoproteins, proteoglycans, and hyaluronan. Elevated levels of laminin-γ2, collagen types I and III, periostin, fibronectin, versican, hyaluronan (HA), and its receptor CD44 have all been associated with a poor prognosis of ovarian cancers (57, 58). Periostin, for example, is detected in the ascites of ovarian cancer patients (59) and associated with late-stage disease and ovarian cancer relapse (60). Periostin has also been reported to increase the motility of the ovarian cancer cells and their adhesion to the peritoneum via integrins αvβ3 and αvβ5 (59). Fibronectin, on the other hand, activates the α5β1-integrin/c-Met/FAK/Src dependent signaling pathway, contributing to ovarian cancer invasion and metastasis (61). Moreover, we have shown that versican regulates the development of peritoneal metastasis (62). While, it has also been shown that HA to CD44 triggers direct cross-signaling between different signaling pathways (63-68), and it is this function which is thought to be involved in increased motility, adhesion, and invasion of cancer cells as well as tumor growth in ovarian cancer (69, 70).

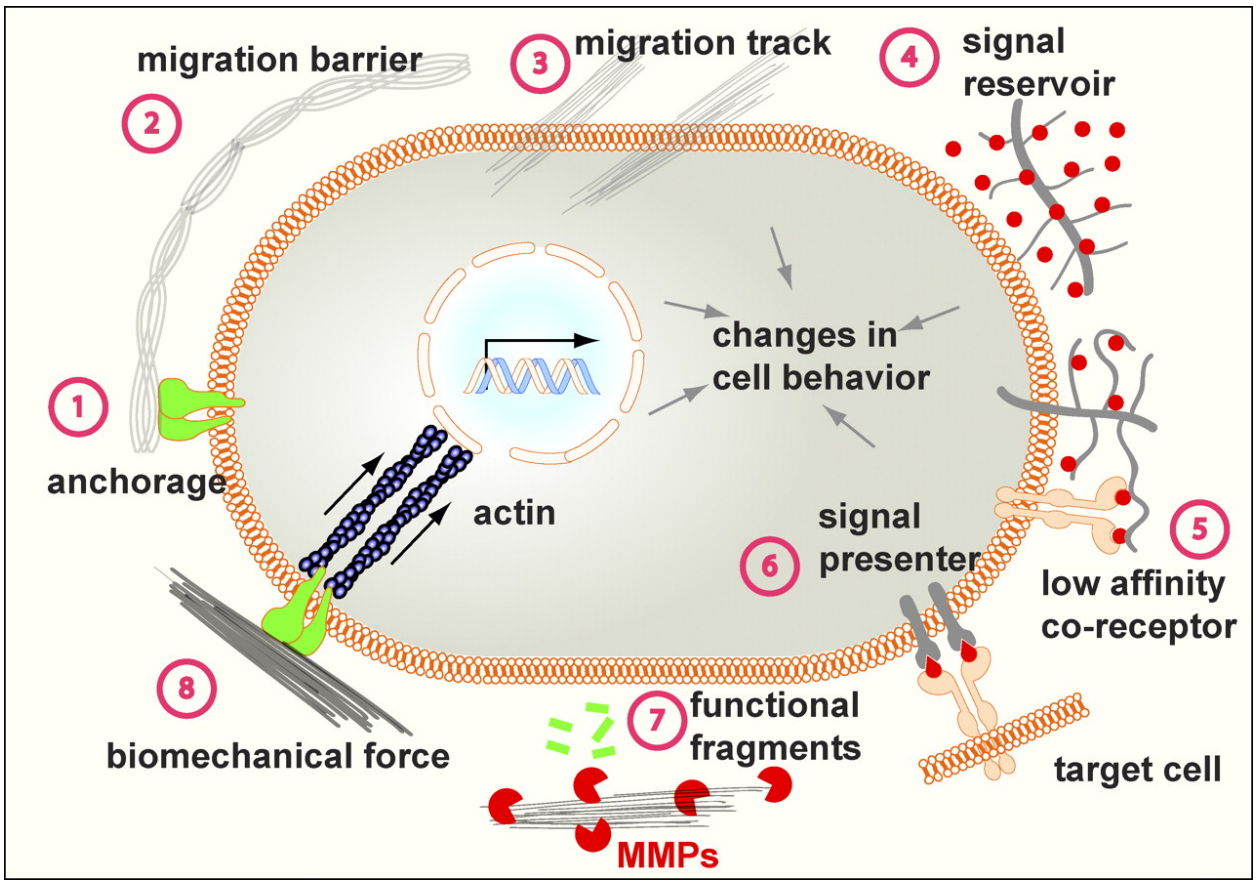

Figure 3. Mechanisms of ECM function. The versatile functions of the ECM depend on its diverse physical, biochemical, and biomechanical properties. Anchorage to the basement membrane is essential for various biological processes, including asymmetric cell division in stem cell biology and maintenance of tissue polarity (stage 1). Depending on contexts, the ECM may serve to block or facilitate cell migration (stages 2 and 3). In addition, by binding to growth factor signaling molecules and preventing their otherwise free diffusion, the ECM acts as a sink for these signals and helps shape a concentration gradient (stage 4). Certain ECM components, including heparan sulfate proteoglycans and the hyaluronic acid receptor CD44, can selectively bind to different growth factors and function as a signal coreceptor (stage 5) or a presenter (stage 6) and help determine the direction of cell–cell communication (Lu et al., 2011). The ECM also direct signals to the cell by using its endogenous growth factor domains (not depicted) or functional fragment derivatives.

(Figure and caption originally published in Lu, P., et al. The extracellular matrix: A dynamic niche in cancer progression. Journal of Cell Biology. 2012;196:395. Doi: 10.1083/jcb.201102147)

1.3 CD44 in Cancer

1.3.1 Protein Structure

Members of the CD44 family of transmembrane glycoproteins (also referred to as HCAM, Pgp-1, Hermes antigen, and lymphocyte homing receptor) belong to a class of cell adhesion receptors involved in a variety of cellular processes including the regulation of growth, survival, differentiation, and motility (71). The amino-terminal globular protein domain of CD44 is encoded by the first five non-variable exons of the CD44 gene and contains motifs that function as docking sites for several components of the extracellular matrix including hyaluronan (HA), which CD44 binds with a particularly high affinity, as well as collagen, laminin, and fibronectin. Exons 6–15 encode variant exons v1–v10, which are either completely excluded in the smallest CD44 isoform, CD44s, or included in various combinations in the extracellular domain leading to CD44 variant isoforms (Figure 3). Up to ten different CD44 isoforms have been reported due to differential splicing of the 10 variant exons (72, 73). The transmembrane region contains 23 hydrophobic amino acids and 1 cysteine residue, and is thought to be involved in CD44 oligomerization and association with lipid rafts (74, 75). Finally, the c-terminus cytoplasmic-tail region contains motifs that direct CD44 basolateral localization or subdomain localization during cell migration, and it mediates CD44 interactions with intracellular binding partners. Although CD44 has no intrinsic kinase activity, the cytoplasmic tail interacts with a variety of signaling mediators and contains binding sites for the actin-cytoskeleton adaptor proteins, which facilitate association of CD44 with the cytoskeleton responsible for the associated phenotypes (76-79). Moreover, the cytoplasmic tail contains 6 potential serine phosphorylation sites that are phosphorylated by

protein kinase C and Rho kinase as a means of regulating association of intracellular proteins to CD44 during signaling transduction (80). The CD44 family is further compounded by several post-translation modifications including *N*- and *O*-glycosylation (81). There are many reports about the physiological roles of CD44 and its activity in various diseases, but a detailed understanding of molecular mechanisms is mostly lacking (82).

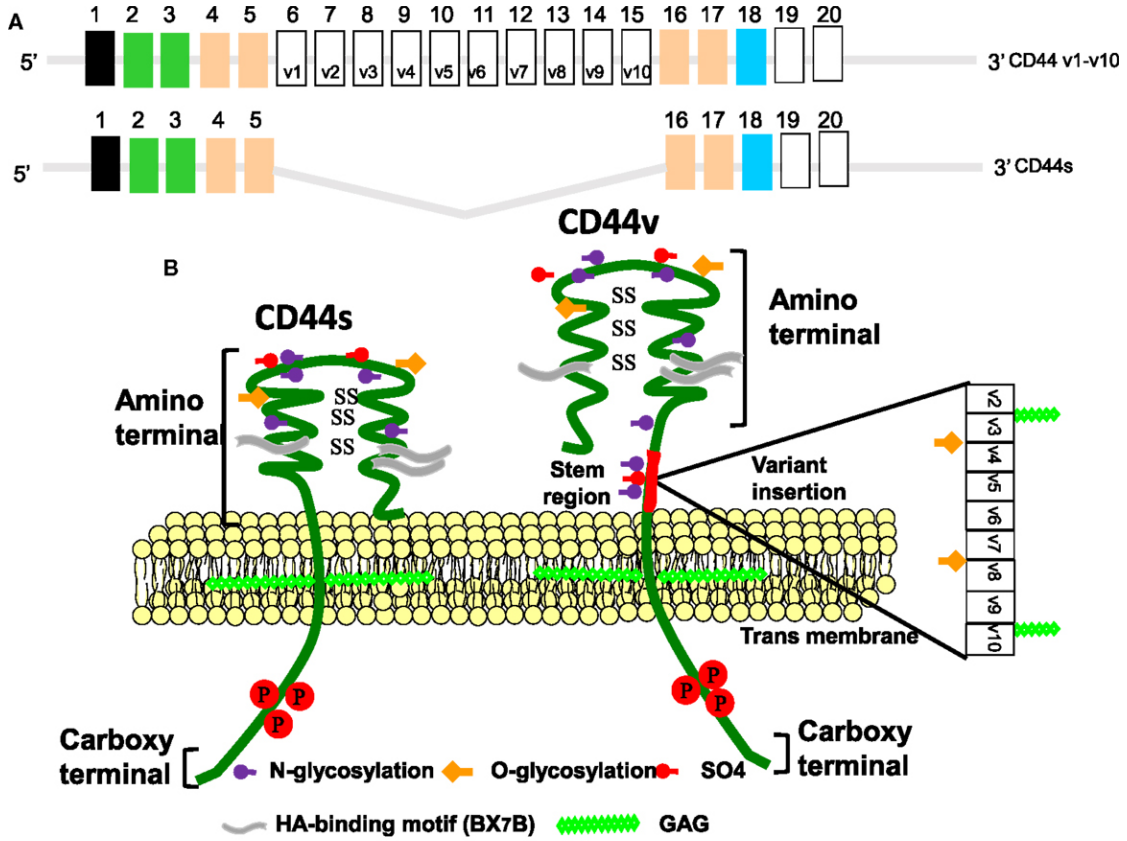

Figure 4. Mouse CD44 gene and protein structure (83).

(A) Model structure of alternative splicing in CD44. CD44 pre-mRNA is encoded by 20 exons in mice and 19 exons in humans. The common standard CD44s (hematopoietic) form contains no extra exons, and the protein has a serine motif encoded in exon 5 that can initiate synthesis of a chondroitin sulfate or dermatan sulfate chain. Alternative splicing of CD44 predominantly involves variable insertion of 10 extra exons with combinations of exons 6–15 and spliced in v1–v10 into the stem region, of which v3 encodes a substitution site for a heparan sulfate chain. Variable numbers of the variant exons can be spliced in epithelial cells, endothelial cells, and inflammatory monocytes and also are upregulated commonly on neoplastic transformation depending on the tissue. (B) Model structure of alternatively

spliced CD44 proteins. The CD44 protein is composed of an extracellular N-terminal domain, a stem region in the extracellular domain close to the transmembrane region, where the variant exon products (red/violet circles) are inserted, the transmembrane region, and the carboxyl terminal cytoplasmic tail. There are multiple sites for N-glycosylation (purple circles) and O-glycosylation (orange circles), and a sulfation domain. The N-terminal portion contains highly conserved disulfide bonds as well as 2 BX7B motifs, both of which are essential for HA binding. CD44 is subjected to extensive glycosylation, sulfation, and attachment of glycosaminoglycans (GAG) that contribute to regulation of the HA-binding activity. The C-terminal cytoplasmic tail contains several phosphorylation sites that regulate the interaction of CD44 with the cytoskeletal linker proteins, as well as with SRC kinases.

(Figure and caption originally published in Misra, S., et al. Interactions between Hyaluronan and Its Receptors (CD44, RHAMM) Regulate the Activities of Inflammation and Cancer. Frontiers in immunology. 2015;6:16. doi: 10.1016/j.ajpath.2015.11.011.)

The non-sulfated glycosaminoglycan hyaluronic acid (HA) is the principle ligand of CD44. HA is a polymer of repeating disaccharide units D-glucuronic acid and N-acetyl-D-glucosamine and can range in size from small oligosaccharides to millions of Daltons. The size of the HA is important for its physiological functions. HA of a high molecular weight (HMWHA) is typically >500 kDa and can naturally bind multivalently to more surface receptors across a larger area of the cell than low molecular weight (LMWHA) typically between 10 and 500 kDa. This difference in the number of bound HA receptors allow different sizes of HA to have different signaling effects (84). HA is synthesized in humans by HA-synthases HAS1, HAS2, and HAS3 on the cytoplasmic side of the plasma membrane and then expelled into the extracellular space. HA is synthesized by many cells, but mesenchymal cells are the major source of HA. It is degraded by the hyaluronidase family of enzymes, HYAL1, HYAL2, HYAL3, and HYAL4 (85).

1.3.2 Diagnostic and Prognostic Indictor

There is now substantial evidence that CD44 variant isoforms are aberrantly expressed in many human tumors. In some instances, such as with colorectal carcinomas, the expression of CD44 variants predict poor prognosis (86). Interestingly, the upregulation of CD44 expression seems to be an early event in colon carcinogenesis (87) and requires adenomatous polyposis coli (APC) gene inactivation (88). There are some tumor types, however, including neuroblastomas and prostate carcinomas, in which the absence of CD44 expression (including CD44 variants) correlates with transformation and poor prognosis (89, 90). Interestingly, overexpression of CD44 in prostate carcinoma cells even suppressed metastatic behavior (91). In most cancers, the misregulated expression of CD44 is not the result of CD44 mutations. Instead, genes that are implicated in promoting carcinogenesis control the patterns of CD44 expression in cancer cells. Alternative splicing, for example, is under the control of mitogenic signals including the Ras–MAP kinase cascade (92, 93). In addition, the loss of different subunits of the SWI/SNF chromatin remodeling complex, which are mutated in numerous cancers, results in the loss of CD44 transcription (94, 95). Aberrant CD44 expression is therefore inextricably linked to genetic alterations that lead to tumor growth and metastasis (71).

1.3.3 Cellular Functions

The diversity in cellular activity is a result of variable expression of CD44 variant isoforms, post-translational modifications, and binding by a variety of ligands. CD44 signaling has been shown to be important in cancer metastasis and tumor growth, but can be broken down into

two primary areas: HA-dependent and HA-independent signaling. HA-independent signaling relies on interactions between CD44's intracellular domain and cytoskeletal proteins or membrane-associated kinases. CD44 signaling that is HA independent is largely reliant on CD44's position in lipid rafts. Association between CD44 and other signaling proteins is often regulated through CD44's interaction with members of the ezrin–radixin–moesin (ERM) protein family and merlin that initiate association with cytoskeletal elements and assemble intracellular complexes that are important in signal transduction (84). The complexes that are bound to CD44 differ depending on the extracellular conditions and can act as a molecular switch that specifies cell growth arrest or proliferation (96). In other words, CD44 proteins function as interpreters of the extracellular environment and direct the switch between growth- and invasiveness-permissive and non-permissive states (71). Moreover, CD44 can also act as a co-receptor for signal transduction, including with the ERBB receptor tyrosine kinase family, in a complex involving interchain disulfide bonds (64). CD44 can be co-immunoprecipitated with ERBB1 (also known as EGFR/HER1), ERBB2 (also known as HER2/neu), ERBB3 (also known as HER3) and ERBB4 in several cell lines and primary cells (64, 97, 98). However, co-receptor, functions are exerted by CD44s or CD44 splice variants so one might speculate that different CD44 splice variants function as co-receptors for different receptor tyrosine kinases (71).

HA-dependent signaling relies on two CD44 molecules being cross-linked allowing other CD44-associated signaling proteins to interact with each other (84). The affinity of CD44 for hyaluronan seems to be modulated from inside the cells, as its binding affinity is upregulated

by mitogenic stimuli, influenced by glycosylation of the extracellular domains (99) and possibly also by the phosphorylation of specific serine residues in the cytoplasmic tail of CD44 (71). However, the signaling pathways seen in HA-dependent CD44 signaling are almost identical to those seen in HA-independent signaling. Thus, HA binding to CD44 may bring CD44 in close proximity to other signaling receptors allowing for direct association and interaction between receptors and their signaling complexes in a tightly localized lipid raft (100-102). Interestingly, the binding of hyaluronan to CD44 also triggers hyaluronan metabolism (103). Hyaluronan can be taken up by cells in a CD44-dependent manner (104). So, at least under some circumstances, CD44 might itself be involved in the regulation of the pericellular hyaluronan matrix, thereby providing another mechanism by which CD44 could influence adhesion and de-adhesion to the ECM (71).

1.3.4 Marker of Stemness

Cancer stem cells (CSCs) represent a unique subpopulation of self-renewing oncogenic cells thought to be responsible for cancer initiation, progression, and metastasis (105, 106). The stemness and subsequent expansion of CSCs are believed to be highly influenced by changes in microenvironmental signals. Hyaluronan (HA), a major component of the extracellular matrix, has been demonstrated to provide a favorable microenvironment for the self-renewal and maintenance of stem cells (107), while interactions between HA and its receptor, CD44, propagate the stemness of CSCs . HA–CD44 interactions evoke a wide range of signals required for CSC self-renewal and maintenance and have become a prominent marker of CSCs in several types of cancer (108-111). Increasing evidence suggests that HA plays a central role

in epithelial-to-mesenchymal transition (EMT) during embryonic development and malignant progression (112). Transcriptional networks that drive EMT (e.g., Snail, Twist, and Zeb1) have also been found to dynamically change during HA-induced EMT. Importantly, HA binding with CD44 was suggested to induce Twist expression following CD44 nuclear translocation (113) thereby implicating CD44 as a key player in CSC signaling. Moreover, several studies have highlighted the essentiality of CD44 in CSC self-renewal and maintenance. In head and neck squamous cell carcinoma (HNSCC), $ALDH^{high}/CD44^{high}$ cells exhibited similar self-renewal and tumor-initiating properties as CSCs through the suppression of BMP signaling (114). Although its precise mechanism remains undefined, CD44 may act as an intracellular scaffold protein for Smad1, and their interactions may potentiate the long-term survival of CSCs by regulating BMP/Smad signaling (115).

CD44 also plays a critical role in the preservation and multidrug resistance (MDR) of CSCs by transmitting survival and anti-apoptotic signals in both HA-dependent and HA-independent manners (116). HA–CD44 interactions have not only been shown to induce MDR1 expression in breast and ovarian cancer cells (117), but also upregulate multidrug resistance protein 2 in non-small cell lung cancer cells, specifically through the CD44s isoform (118). Furthermore, CSCs effectively gain a survival/growth advantage by adapting their metabolism and maintaining cellular redox homeostasis. CD44 has been demonstrated to contribute to antioxidant status in cancer cells (119) and also control reactive oxygen species (ROS) defense by altering cellular glutathione (GSH) synthesis (120) suggesting CD44 can maintain low levels of ROS and orchestrate protective mechanisms against oxidative stress-mediated damage.

Therefore, growing evidence indicates CD44 is not only a common marker of CSCs, but plays a leading role in maintaining their stemness by enhancing cell survival and conferring resistance to chemotherapy and oxidative stress (116).

1.3.5 Therapeutic Development Efforts

In several types of tumors, CD44 together with other cell surface markers characterizes cancer stem cell populations. Mechanistically, CD44 proteins act as receptors for hyaluronan, co-receptors for receptor tyrosine kinases or G-protein-coupled receptors, or provide a target for metalloproteinases (121). For all these reasons, targeting CD44 may be a successful approach in cancer therapy. As CD44 is the main receptor for hyaluronan, and the hyaluronan binding domain exists in all CD44 isoforms, much effort has focused in blocking the CD44-HA interaction based on abundant evidence that the CD44-HA interaction is involved in tumor progression (122, 123). It has been shown that the interference with the binding of CD44 expressed on tumor cells to HA using either the soluble CD44 ectodomain as a competitor or antibodies that specifically block the binding of HA to CD44, impaired tumor growth and metastasis in breast cancer cells (124, 125), while HA oligosaccharides had similar effects in inhibiting tumor growth *in vivo* (125). Pan-CD44 monoclonal antibodies have been shown to reduce tumor growth, metastasis and post-radiation recurrence of pancreatic xenograft tumors (126), while have also been reported to drastically decrease the leukemic population in mice transplanted with human acute myeloid leukemic stem cells, as well (127). Furthermore, isoform-specific antibodies have been reported, including those against CD44v6, where a radiolabeled CD44v6 monoclonal antibody showed selective tumor

targeting and high tumor uptake in a nude mouse squamous cell carcinoma xenograft (128). In addition to antibody-based targeting of CD44, other strategies have been employed using DNA aptamers targeting CD44v10 in breast cancer (129) and peptides mimicking CD44v6 for blocking the coreceptor function of CD44v6 for c-Met and VEGFR-2 in endothelial cells thereby impeding angiogenesis (130). In an effort to develop new and effective treatment strategies for advanced-stage ovarian cancer patients, CD44 is also being explored as a therapeutic target. Instead of interfering with the function of CD44 proteins, these studies have aimed at inhibiting CD44 expression in tumor cells. One recent report tested a dendrimer-based drug delivery system for carrying paclitaxel and siRNA targeted to CD44 mRNA while another constructed PLGA nanoparticles with short hairpin RNA (shRNA) against focal adhesion kinase (FAK) and CD44 for enhancing antitumor effects in an ovarian cancer mouse xenograph (131, 132). Both showed a high therapeutic potential for combinatorial treatment of ovarian carcinoma using novel nanoscale drug delivery systems. These CD44 targeting approaches are summarized in Figure 5. Although only few approaches have made it as far as clinical trials, the scientific progress in the last few years suggests strong prospects for anti-CD44 therapies.

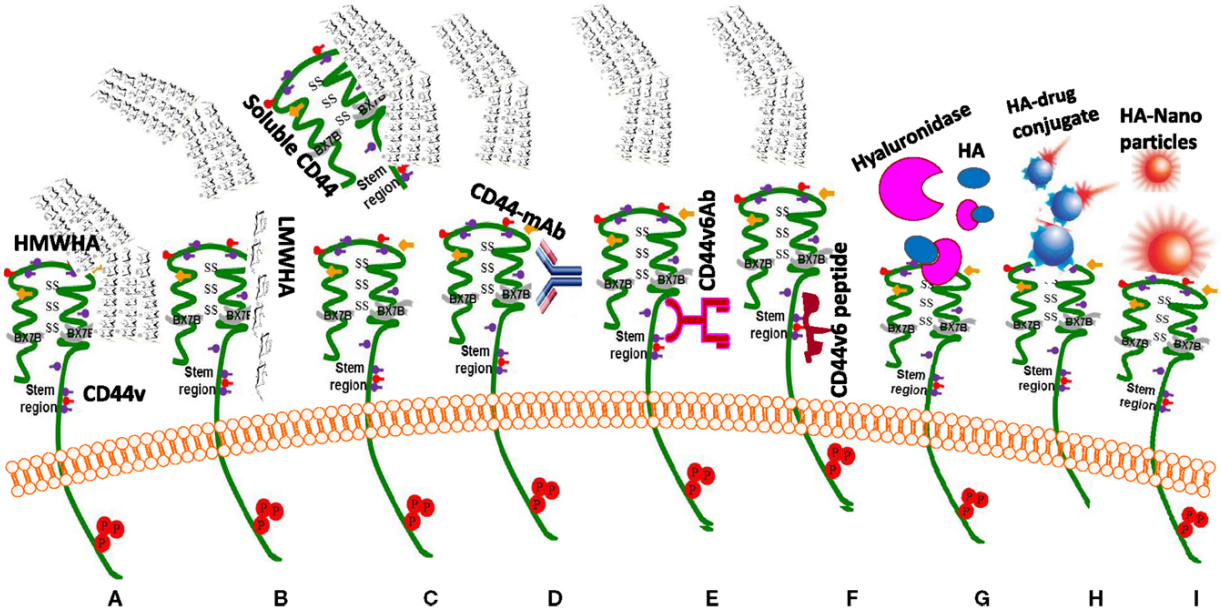

Figure 5. Drug targeting approaches to exploit HA-CD44 interaction in cancer treatment. (A) HMWHA-CD44v interaction induces inflammation and tumor growth; most common blocking reagents against CD44 isoforms: (B) LMW HA inhibits the binding of HMWHA; (C) sol-CD44 competes with HMWHA to bind with CD44v; (D). CD44-blocking monoclonal antibody (CD44-mAb); (E) antibodies against CD44v6; (F) peptides blocking binding of HA with CD44v6; (G) enzymatic hydrolysis by hyaluronidase cleaves the HMWHA to small fragments and blocks the HA-CD44v6 interaction; (H) targeting HA receptor with HA-drug conjugate; (I) targeting "HA receptor" with "HA nanoparticles (83).

(Figure and caption originally published in Misra, S., et al. Interactions between Hyaluronan and Its Receptors (CD44, RHAMM) Regulate the Activities of Inflammation and Cancer. Frontiers in immunology. 2015;6:16. doi: 10.1016/j.ajpath.2015.11.011.)

NOTE:

Section 1.4.1 and 1.4.2 have been previously published by Sacks et al. in Sacks, JD and Barbolina, MV. Expression and Function of CD44 in Epithelial Ovarian Carcinoma. Biomolecules, 2015. 5(4): p. 3051-3066.

1.4 CD44 in EOC

1.4.1 Expression Profile in EOC

CD44 is expressed in the majority of epithelial ovarian carcinomas (133-135). Expression of CD44 and specific isoforms in epithelial ovarian carcinoma has remained a controversial topic, as highlighted in a 2011 report, which reviewed some of the conflicting data on CD44 expression and its correlation with metastasis and survival outcome (54). The authors pointed out that several studies have suggested that patients with CD44s positive tumors have a significantly shorter disease-free survival than patients with CD44 negative tumors (135-137), while in contrast, other studies have demonstrated that high CD44s expression is associated with improved ovarian cancer outcome (138-140). Additionally, other studies have found no association between CD44s or CD44 variant expression with ovarian cancer metastasis or survival outcome (141-143). They concluded that differences between the studies could be attributed to technical factors, including the use of different antibodies and detection methods. Moreover, the cohorts of ovarian cancer patients examined in the various studies were highly heterogeneous and composed of patients with variable tumor types, stages, and courses of therapy. Recently published studies are in support of CD44 association with unfavorable prognosis in epithelial ovarian carcinoma (133, 134, 144-146). Specifically, a recent study conducted using patient-matched primary tumor samples showed higher expression levels of CD44 in metastatic and recurrent tumor tissues when compared with its primary counterparts and a significant correlation between CD44 expression and decreased disease-free, as well as overall survival (146). This group also reported overexpression of CD44 in the recurrent tumors generated using a xenograft mouse model

exposed to paclitaxel treatment, providing evidence that CD44 may directly participate in chemoresistance; although, the underlying mechanisms were not MDR1-dependent. Similar results were reported by Zhang, et al. showing that CD44 expression associated with high-grade and advanced-stage ovarian carcinoma (147). In further support, another group demonstrated that CD44 expression was also significantly increased in patients with metastasis (144). However, no significant differences in CD44 expression was observed between paired primary and peritoneal metastases (144). This contradiction to Gao et al. could be attributed similarly to the highly heterogeneous collection of ovarian cancer patients analyzed in these studies.

1.4.2 Stemness Marker and Sphere-Forming Cells

While CD44 is low to absent in normal ovarian epithelial cells (138, 141), CD44 has been identified as a potential marker for normal stem-like epithelial cells in the distal end of the fallopian tube (148). However, CD44 is used as a marker for cancer stem cell (CSC) detection in a variety of cancers,(84). The search for ovarian CSCs has largely been based on the exploitation of properties that are associated with "stemness" in other systems, particularly the expression of specific "stemness" markers on the cell surface. Studies on the properties of these "stem" cells in ovarian cancer using an Aldefluor assay to isolate ALDH1-bright (ALDH1br) cells from epithelial ovarian cancer cell lines, revealed greater stem-like properties, enrichment in CD44, and association with chemoresistance and poor clinical outcome (149). Other reports have showed that $CD44^+$ status along with $CD117^+$ is a marker of ovarian cancer-initiating cells (150), while when $CD44^+CD117^+$ cells were compared using two-

dimensional (2D) culture versus a three-dimensional (3D) culture system, $CD44^{+}CD117^{+}$ cells possessed not only CSC properties, but also exhibited increased chemoresistance in 3D compared to 2D culture, suggesting a more relevant model for studying CSC response to anticancer drugs (151, 152).

Since sphere-forming ability is known to be one of the properties of CSCs, it was intriguing that fresh primary high-grade serous ovarian carcinoma biopsies cultured under serum-free conditions produced floating spheres, which overexpressed stem cell genes and CSC markers, including CD44 (153). Moreover, spheroid cells from human ovarian cancer cell lines were found to be enriched for cells with cancer stem cell-like characteristics such as upregulation of stem cell genes, self-renewal, high proliferative and differentiation potential, and high aldehyde dehydrogenase (ALDH) activity, and these cells were more aggressive in growth, migration, invasion, scratch recovery, clonogenic survival, anchorage-independent growth, and more resistant to chemotherapy *in vitro* (154). Furthermore, an anti-CD44 monoclonal antibody A3D8 was employed to investigate its effects and mechanisms on the proliferation and apoptosis of sphere-forming cells in the human ovarian cancer cell line SKOV-3. Results showed that A3D8 inhibited proliferation of sphere-forming cells and induced apoptosis in these cells causing S-phase arrest and deregulation of the cell cycle (155). Therefore, this provides evidence that CD44 contributes to the aggressive properties of spheroid cells and ovarian cancer pathogenesis, thus, requiring further investigation.

1.4.3 Metastasis

Both CD44s and CD44 variants play complex roles in tumor progression and metastasis (65, 156, 157). Previous research has shown that human ovarian tumor cells can bind HA via membrane CD44 (158). CD44 has also been shown to mediate ovarian carcinoma cell adhesion to peritoneal mesothelial cells (69), while other *in vivo* studies have suggested that CD44s is required for human ovarian cancer cell adhesion to mesothelial cell surface HA (156). Therefore, it has been established that ovarian cancer cell adhesion to mesothelial cell monolayers is mediated, at least in part, by the interaction between HA and CD44 (159). Moreover, dependence of CD44 on versican, a large HA-binding proteoglycan, has been shown in ovarian cancer where HA and versican form a pericellular matrix around CD44-expressing ovarian cancer cells that further promotes their motility and invasion *in vitro* (160). Studies in our lab demonstrated that versican is involved in facilitating both ovarian cancer cell and spheroid adhesion to mesothelial cell monolayers. Likewise, both spheroids and cells with reduced expression of versican demonstrated significantly impaired ability to generate peritoneal tumors suggesting that versican functions in regulating the development of peritoneal metastasis originating from single cells and spheroids (62). This further supports a role for CD44 together with HA and versican in a number of key steps needed for ovarian cancer metastasis. However, mechanisms that induce expression of CD44 in ovarian cancer are poorly understood. A recent study found that expression of CD44 was induced by the transcription factor DLX4 via enhanced activity of NF-κB stimulated by inflammatory cytokine IL-1β, a transcriptional target of DLX4. High expression of DLX4 is associated with reduced survival of ovarian cancer patients and found to stimulate attachment of ovarian tumor cells

to peritoneal mesothelial cells in vitro and increase the numbers of peritoneal implants in xenograft models (161). DLX4, therefore, might contribute to poor outcomes in ovarian cancer, in part, by promoting peritoneal implantation of tumor cells via enhanced CD44 expression and tumor-mesothelial cell interactions in an NF-κB-dependent manner. Further investigation into the cross-talk between CD44 and inflammatory signaling in ovarian cancer will hopefully lead to a better understanding of more effective focal points for therapeutic intervention. Moreover, post-transcriptional regulation of CD44 by multiple non-coding RNAs (ncRNA) including miRNAs and lncRNAs has been described in a variety of cancers (162-164). Although miR-199a was reported to target CD44 in ovarian cancer (165), additional studies are needed to further characterize these CD44 regulatory mechanisms in EOC.

1.5 Motivation

For quite some time, the role of CD44 in ovarian cancer progression and metastasis has remained unclear. However, many lines of evidence indicate that CD44 organizes a signaling platform by which cancer cells survive and grow in addition to seeding metastases. The published reports highlighted in this review provide further evidence that CD44 is an important player in ovarian tumor growth and metastasis. Greater understanding of the functions of CD44 isoforms at the molecular level and identification of specific CD44 isoforms on EOC cells will allow new strategies to be directed more discerningly against tumor cells. Finally, there is a hypothesis that CD44 function varies during different stages of tumor growth, from initiation to formation of metastases in breast cancer (166), which has yet to be explored in the context of EOC. Based on current understanding, CD44 remains promising as a therapeutic target in

ovarian cancer and, thus, warrants further evaluation. Since spheroids have a suggested important function in metastasis of EOC, we hypothesized that CD44s enhances cell-cell adhesion and metastatic potential in ovarian cancer spheroids.

1.6 Scope and Organization of Thesis

The objective of this work was to characterize the functional role of CD44s in EOC spheroids in the context of epithelial ovarian cancer metastasis. Several approaches were taken to thoroughly explore the variety of functions of CD44s in EOC cells and spheroids. Experiments performed are organized as follows:

- Chapter 2 describes the observed patterns of CD44 expression in EOC tumor tissue and cell lines.
- Chapter 3 examines the functional significance of CD44s in spheroid formation.
- Chapter 4 assesses the functional importance of CD44s in EOC cell adhesion.
- Chapter 5 evaluates the functional role of CD44s in EOC cell growth and proliferation.
- Chapter 6 assesses the functional significance of CD44s in EOC cell migration, invasion, and EMT
- Chapter 7 examines the functional importance of CD44s in EOC metastasis.
- Chapter 8 summarizes the key findings of this thesis and outlines future directions of research warranting further investigation based on the findings described here.

CHAPTER 2: EXPRESSION PATTERNS OF CD44 IN EOC TUMORS AND CELL LINES

2.1 Introduction

In order to establish whether there was any correlation between CD44 expression in tumor tissue and overall survival in patients we needed to analyze a large number of patients. Therefore, accessing CD44 expression data along with a large set of matching patient characteristics collected by TCGA from over 500 women was a suitable tool for identifying in what population of individuals CD44 expression was most significant and how the expression of CD44 might vary at different ages and stages of tumor development—both from an overall total CD44 perspective, as well as through CD44s and variant isoform pattern analysis.

Hence, raw CD44 expression data was obtained and re-analyzed yielding an intriguing correlation between CD44 and overall survival in EOC patients. Importantly, however, that data showed CD44 expression had greater significance in overall survival of late stage disease. This was followed up by assessment of isoform expression differences in late stage patients using a tissue cDNA array and pPCR with primers specific for variants 2, 6, and 8, the standard isoform bridging the splice junction of standard exons 5 and 15, as well as within standard exon 5, which is contained in all isoforms, for total CD44 expression quantification. Identification of CD44s as seemingly playing a more important role in late stage EOC led to profiling CD44 isoform expression in EOC cell lines and their spheroids with RT-qPCR as well as western blot for use in further functional studies on CD44s.

Taken together, the data in this chapter demonstrates an important role for CD44 in the progression of EOC with CD44s isoform as the more significant contributor in late stage disease.

2.2 Materials & Methods

2.2.1 Cell Lines. Human ovarian carcinoma cell lines of serous histotype originating from malignant cells in ascites, OVCAR4, and SKOV-3 were obtained from the NCI Tumor Cell Repository (Detrick, MD). The human ovarian carcinoma cell line of serous histotype originating from a surgical tumor specimen, ES-2, and another human ovarian carcinoma cell line, CAOV3, originating from malignant cells in the ascites, were obtained from Dr. M.S. Stack (University of Notre Dame, ID). The human ovarian carcinoma cell lines of serous histotype originating from abdominal metastasis, OVSAHO, and malignant cells in ascites, Kuramochi, were obtained from the Japanese Collection of Research Bioresources Cell Bank (Osaka, Japan). SKOV-3, ES-2, and CAOV-3 were propagated in minimal essential media (MEM) (Corning) supplemented with 10% fetal bovine serum (FBS) (Sigma-Aldrich), 0.5% penicillin/streptomycin (Corning), 0.4% amphotericin B (Corning), and 0.22% g/ml sodium bicarbonate (Santa Cruz Biotechnology) for no longer than fifteen consecutive passages. OVCAR-4, OVSAHO, and Kuramochi were propagated in Roswell Park Memorial Institute (RPMI) 1640 media supplemented with 10% FBS, 0.5% penicillin/streptomycin, 0.4% amphotericin B, and 0.2% g/ml sodium bicarbonate for no longer than fifteen consecutive passages. All cells were kept at 37°C and 5% CO_2

in a humidified incubator, and were routinely tested for Mycoplasma, cellular morphology and average doubling time. All cell lines were propagated from stocks originally obtained from cell banks, authenticated using STR analysis, and stored in aliquots for future use. SKOV-3 cell line revealed a 100% match to the DNA profile of SKOV-3 from ATCC. Each aliquot was further propagated for no longer than 20 consecutive passages or 4 months, whichever came first.

2.2.2 CD44 Expression Analyses of TCGA Datset. Data from The Cancer Genome Atlas (TCGA) database for serous ovarian adenocarcinoma were downloaded from cbioportal and plotted as CD44 expression $Log_{2(\text{median centered ratio})}$ vs percent survival. Patients with incomplete survival information as well as patients who died due to causes other than ovarian carcinoma were excluded; total of 557 specimens were included in the analyses. Based on the value of median CD44 expression, defined as CD44 expression $Log_{2(\text{median centered ratio})}$ at 50% survival, the data set was divided in two, including specimens with CD44 expression ≥2.6, termed "high CD44 expression" (n=157; red line), and specimens with CD44 expression < 2.6, termed "low CD44 expression" (n=400; blue line). Overall survival of patients expressing high and low levels of CD44 was plotted and analyzed with Kaplan-Meier plot using Prism 7 software. Relationship between patients' survival and CD44 expression at different FIGO stages was analyzed by breaking down the specimens into three groups: 1) Stage I and II (n=32; green line), 2) Stage III (n=430; blue line), and 3) Stage IV (n=83; red line). Survival was plotted and analyzed with Kaplan-Meier plot using Prism 7.0 software. Overall survival of patients with Stage III or IV

disease expressing high (n=139) and low (n=374) levels of CD44 was plotted and analyzed with Kaplan-Meier plot using Prism 7 software. The relationship between patients' survival and CD44 expression at different menopausal status was analyzed by dividing the specimens into pre- (<51 years old, n=130; blue line) and post-menopausal (>51 years old, n=427; red line) groups. Median CD44 expression was found for each group, and it equaled to 3.3 for pre- and 2.6 for post-menopausal patients. Survival was plotted and analyzed with Kaplan-Meier plot using Prism software.

2.2.3 Quantitative Real-Time PCR (qRT-PCR). qRT-PCR was performed using MyiQ (Bio-Rad) according to the manufacturer's instructions. Primers were designed to be specific for CD44 variants using IDT PrimerQuest Tool (https://www.idtdna.com/primerquest). CD44s: forward primer 5'-AAAGGAGCAGCACTTCAGGA-3' (spanning splice junction of exons 5 and 15) and reverse primer 5'-TGTGTCTTGGTCTCTGGTAGC-3' binds across exons 5 and 15 (spanning the exon-exon junction); CD44v2: forward primer 5'- ACAGCAACCAAGAGGCAAGA-3' and reverse primer 5'- AGCCATTTGTGTTGTTGTGTGA-3'; CD44v3: forward primer 5'-TGCAACTCACCACAACAGGT-3' and reverse primer 5'-GCCTGATCCAGAAAAACTGAGG-3'; CD44v4: forward primer 5'- CAGTTTCAACCACACCACGG-3' and reverse primer 5'-CCGGATTTGAATGGCTTGGG-3'; CD44v5: forward primer 5'- CACACCCTCCCCTCATTCAC-3' and reverse primer 5'- CGACCGCCATCTTGCTTACT-3'; CD44v6: forward primer 5'-CTCACAGTCCAGGCAACTCC-3' and reverse primer 5'- TTGGCGATATCCCTCATGCC-3'; CD44v7: forward primer 5'- CAGCTCATACCAGCCATCCA-3' and reverse primer 5'-

TGGGGTGTGAGATTGGGTTG-3’; CD44v8: forward primer 5’- ACGCTTCAGCCTACTGCAAA-3’ and reverse primer 5’- CGCGTTGTCATTGAAAGAGGT-3’; CD44v9: forward primer 5’-CCTCATTGAAACAGAGCAGAGT-3’ and reverse primer 5’-ACTGCTTGATGTCAGAGTAGAAGT-3’; CD44v10: forward primer 5’-CAGGTGGAAGAAGAGACCCA-3’ and reverse primer 5’- GGTCCTGCTTTCCTTCGTGT-3’; All CD44: forward primer 5’- CCGCTATGTCCAGAAAGGA-3’ and reverse primer 5’-CTGTCTGTGCTGTCGGTGAT-3’ (both bind exon 5 expressed in all isoforms); and a housekeeping gene control Ribosomal Protein L19 (RPL19): forward primer 5’-CAATGAAATCGCCAATGCCAACTC-3’ and reverse primer 5’- TGGACCGTCACAGGCTTGC-3’. Primer specificity was determined using serial dilutions of the template and by examination of the product melting curves. Total RNA was isolated from cells using SV Total RNA Isolation System (Promega) and first-stranded cDNAs were synthesized from 700 ng total RNA using iScript™ cDNA synthesis kit (Bio-Rad) in a 20 µL-reaction. 0.8 µL of reverse transcription product was used for qPCR. SYBR Green was used for qPCR as a double-stranded DNA-specific fluorophore. PCR was conducted by initial denaturation for 10 min at 95°C followed by 40 cycles of 95°C for 15 sec and 60°C for 1 min using the PerfeCTa SYBR Green FastMix for iQ (Quanta Biosciences). To determine the specificity of the PCR primers, the melting curves were collected by denaturing the products at 95°C, then cooling to 65°C, and then slowly melting at 0.5°/sec up to 95°C.

2.2.4 Tissue Microarray

The expression profile of CD44 variant isoforms in patients tissues was determined by performing qPCR as described above on a TissueScan™ Cancer Tissue array of cDNA from 48 ovarian cancer patient tumor samples of all 4 stages obtained from Origene (HORT101)—7 normal, 16 stage I, 3 stage II, 19- stage III, 3 stage IV. Briefly, PCR was conducted by initial denaturation for 10 min at 95°C followed by 40 cycles of 95°C for 15 sec and 60°C for 1 min using Fast SYBR® Green (Thermo) and all CD44 primers as above on a ViiA7 (Applied Biosystems, Inc.).

2.2.5 Western Blot. Cells were collected and lysed in RIPA lysis buffer (50mM Tris-HCl (pH 7.4), 150mM NaCl, 1% Triton X-100, 1% sodium deoxycholate, 0.1% SDS (Thermo Scientific, Rockford, IL) supplemented with Halt Protease Inhibitor Cocktail (Thermo) and PhosStop phosphatase inhibitor cocktail tablets (Roche) according to manufacturer's guidelines. Cell lysates (20 µg) were electrophoresed on 10% SDS-polyacrylamide gels under reducing conditions (167), electroblotted to a polyvinylidene difluoride membrane (168), blocked with 10% goat serum in Tris buffered saline with 0.1% tween (TBST) for 1 h at room temperature (25°C). Membranes were incubated overnight at 4 °C with 1:1000 anti-human CD44 monoclonal antibody (DF1485) from Santa Cruz Biotechnologies (Dallas, TX) in 5% goat serum in TBST. Secondary antibody was goat anti-mouse horseradish peroxidase (Santa Cruz Biotechnology) (1:2000). Proteins were visualized using Amersham ECL Prime Detection Reagent (GE Healthcare)

on a Bio-Rad gel documentation system. Blots were performed in triplicate and densitometry analyses were determined using Quantity One software (Bio-Rad) according to the manufacturer's instructions.

2.3 Analysis of CD44 Expression in Patient Tumor Samples

High vs low CD44 expression does not predict a difference in survival in patients with epithelial ovarian carcinoma (Figure 6). Data from The Cancer Genome Atlas (TCGA) database for serous ovarian adenocarcinoma were analyzed in Oncomine and plotted as CD44 expression $Log_{2(\text{median centered ratio})}$ vs percent survival (Figure 6A, left panel). Based on the value of median CD44 expression, defined as CD44 expression $Log_{2(\text{median centered ratio})}$ at 50% survival, the data set was divided in two, including specimens with CD44 expression ≥2.6, termed “high CD44 expression” (red line), and specimens with CD44 expression < 2.6, termed “low CD44 expression” (blue line). Overall survival of patients expressing high and low levels of CD44 was plotted and analyzed with Kaplan-Meier plot using Prism 7 software (Figure 6A, center panel). Average overall survival of patients with high and low CD44 expression is indicated in the table (Figure 6A, right panel). CD44 expression has a more profound affect on survival in advanced stage III and IV EOC patients than in early Stage I/II EOC patients (Figure 6B). Data from The Cancer Genome Atlas (TCGA) database for serous ovarian adenocarcinoma were analyzed in Oncomine plotted as CD44 expression $Log_{2(\text{median centered ratio})}$ vs percent survival (Figure 6B, left panel) subdivided by stages I/II, III, and IV. High vs low CD44 expression does not predict a difference in survival in patients with serous

ovarian carcinoma at FIGO Stages III and IV. The specimens in groups containing Stage III and Stage IV samples (n=513) were combined into one group with “high” and “low” CD44 expression (red and blue lines, respectively) corresponding to cases with higher than median CD44 expression and lower than median CD44 expression (2.05 for Stage III and IV only). Overall survival of patients with Stage III or IV disease expressing high and low (Figure 6B, center panel) was not significantly different. Average overall survival of patients at Stage III and IV disease with high and low CD44 expression is indicated in the table (Figure 6B, right panel).

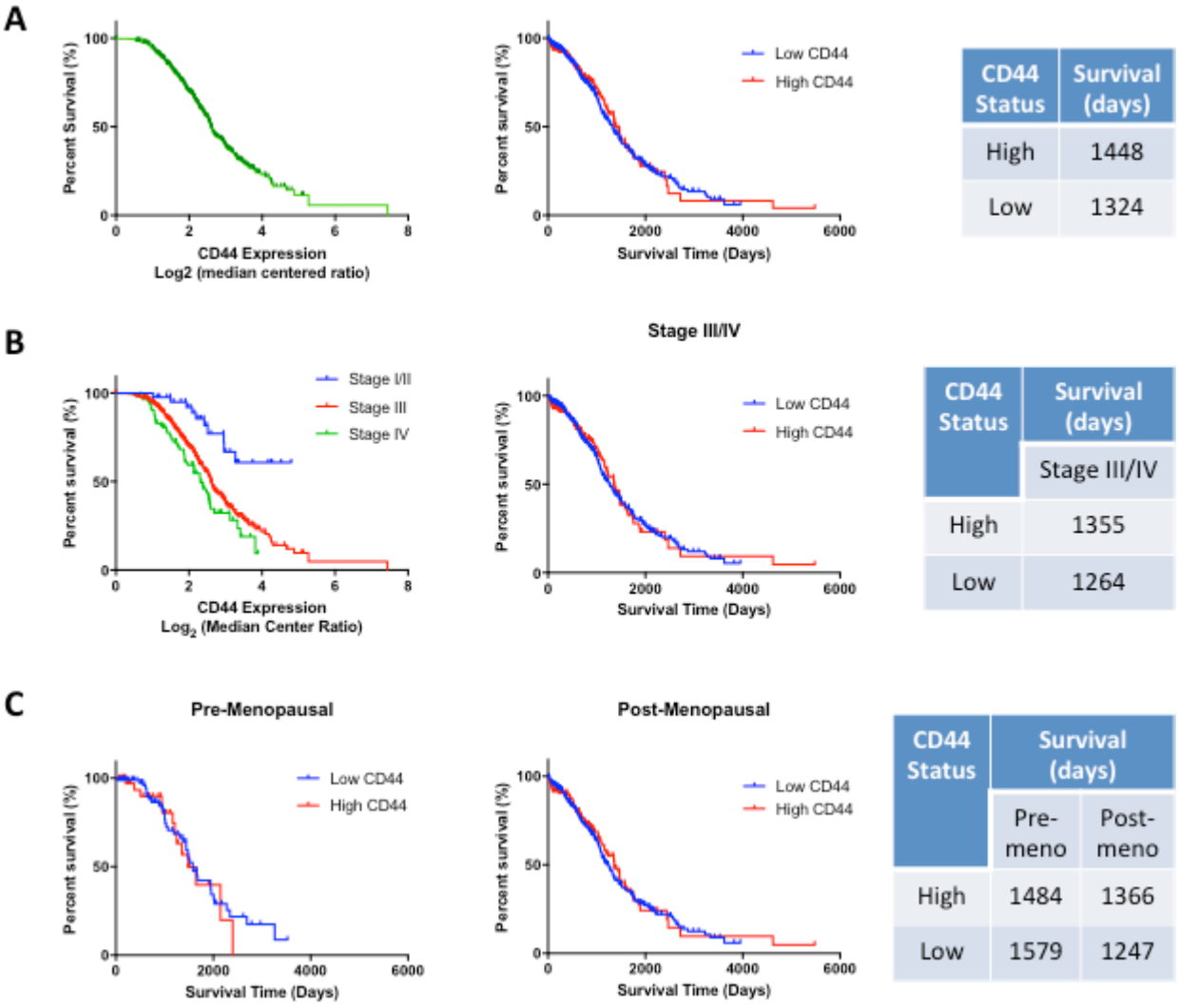

CD44 Status	Survival (days)
High	1448
Low	1324

CD44 Status	Survival (days)
	Stage III/IV
High	1355
Low	1264

CD44 Status	Survival (days)	
	Pre-meno	Post-meno
High	1484	1366
Low	1579	1247

Figure 6. High vs low CD44 expression is not predictive of survival in EOC patients. B (left panel), p<0.0001, Log-rank (Mantel-Cox) test, p<0.0002, Gehan-Breslow-Wilcoxon test. A (center panel), B (center panel) and C (left and center panel), p=n.s., Log-rank (Mantel-Cox) test, p=n.s., Gehan-Breslow-Wilcoxon test

High vs low CD44 expression does not predict a difference in survival in pre- or post-menopausal patients with serous ovarian carcinoma (Figure 6C). Overall survival of patients of pre-menopausal age with high (n=130) and low (n=90) CD44 expression was plotted and analyzed (Figure 6C, left panel) revealing no significant difference, while analysis of overall

survival of patients of post-menopausal age with high (n=117) and low (n=310) CD44 expression (Figure 6C, center panel) also revealed no significant difference. Average overall survival of patients of both pre- and post-menopausal age with high and low CD44 expression is indicated in the table (Figure 6C, right panel). It is important to remember that TCGA expression data on CD44 includes all variants of transcribed CD44 mRNA and does not delineate between them. Due to the complex nature of CD44 signaling, it is reasonable to assume that overall expression in EOC may not be as important as pre-mRNA splicing and the resulting functional protein isoforms.

Since there are few reliable antibodies commercially available for looking at CD44 variant isoforms specifically, we used PCR to profile the expression of CD44 in patient samples using an array of cDNA from 35 serous EOC tissues of normal (n=7), stage I (n=7), stage II (n=1), stage III (n=17), and stage IV (n=3) (Figure 7). Among these samples, total overall CD44 expression remained unchanged between early EOC (stage I/II) and late EOC (stage III/IV). However, the ratios of CD44v2, v4, and v6 to the CD44s isoform are significantly decreased in late stage EOC compared to early stage indicating that in the entire tumor cell population, expression of the standard isoform gains greater importance in late stage ovarian cancer and suggest the relevance of variant expression to be substantially reduced.

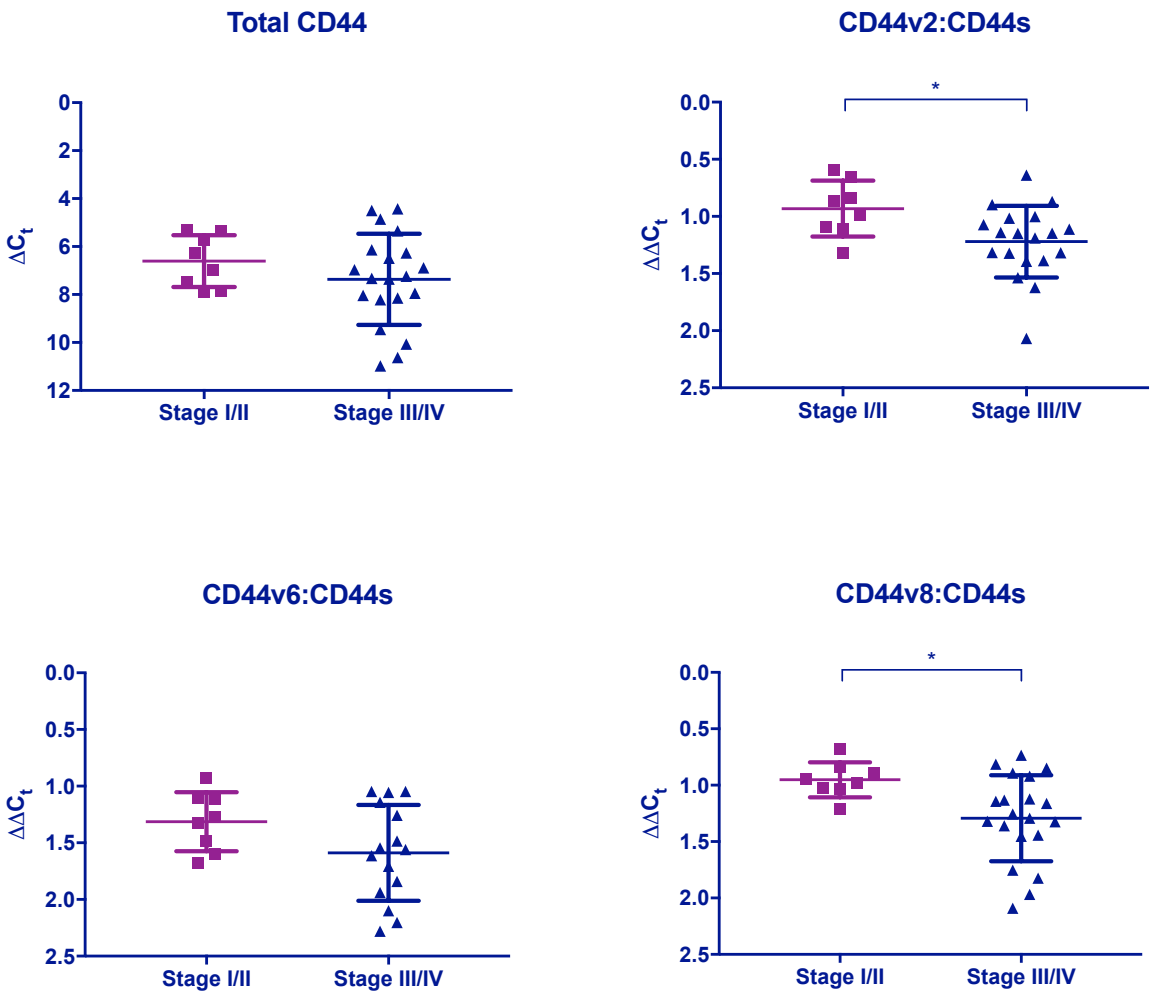

Figure 7. Reduction in CD44v isoforms compared to CD44s in advanced stage serous EOC tissue. CD44v2 to CD44s expression ratio (upper right panel) (*p=0.02, Mann-Whitney U); CD44v6 to CD44s expression ratio (lower left panel) (p=n.s.); CD44v8 to CD44s expression ratio (lower right panel) (**p*=0.02, Mann-Whitney U).

2.4 Quantifying CD44 Isoform Expression in EOC Cell Lines

Moving forward, the goal of the following experiments was to establish the patterns of expression of CD44 standard and variants in serous ovarian carcinoma cell lines and their spheroids. These experiments were performed using ES-2, SKOV-3, OVCAR-4, and OVSAHO

with an initial assessment in OAW28, Kuramochi, OVKATE, and CAOV-3. We found 2 general groupings of CD44 isoform expression in our cell lines. Standard CD44 (CD44s)-high compared to overall variant and standard CD44 (CD44s)-low compared to overall variant expression. The highest total CD44 expressing cell lines were ES-2, SKOV-3, and CAOV-3. However, ES-2 (Figure 8, row 1, left) and SKOV-3 (Figure 8, row 1, right) have very high CD44s expression compared to all the variants, while CAOV-3 expressed similar CD44s compared to many of the different variants—V3, V5, V9. As CAOV-3 does not form true spheroids, this cell line was excluded from further study. OVCAR-4 and OAW28 expressed moderate levels of total CD44, however OAW28 expressed predominately variant isoforms (Figure 8, row 3, left), while OVCAR-4 expressed similar levels of CD44s as CD44 variants (Figure 8, row 2, left). Lower expressers of total CD44 include OVSAHO (Figure 8, row 2, right) and Kuramochi (Figure 8, row 3, right), however, CD44s expression appears lower than variants in OVSAHO, while Kuramochi has higher CD44s expression compared to variants. This was further observed at the protein level using Western blot where ES-2 and SKOV-3 expressed high standard CD44, which appears at 80-95kDa, variant CD44 isoforms at higher molecular weights (Figure 9). On the other hand, OVCAR-4 and OVSAHO expressed low CD44s compared to variant expression. Therefore, ES-2 and SKOV-3 were selected for further study as predominately CD44s expressing cell lines (CD44s-hi) and OVCAR-4 and OVSAHO for CD44s moderate to low-expressing cell lines (CD44s-lo), which exhibit similar levels of CD44s compared to the variants.

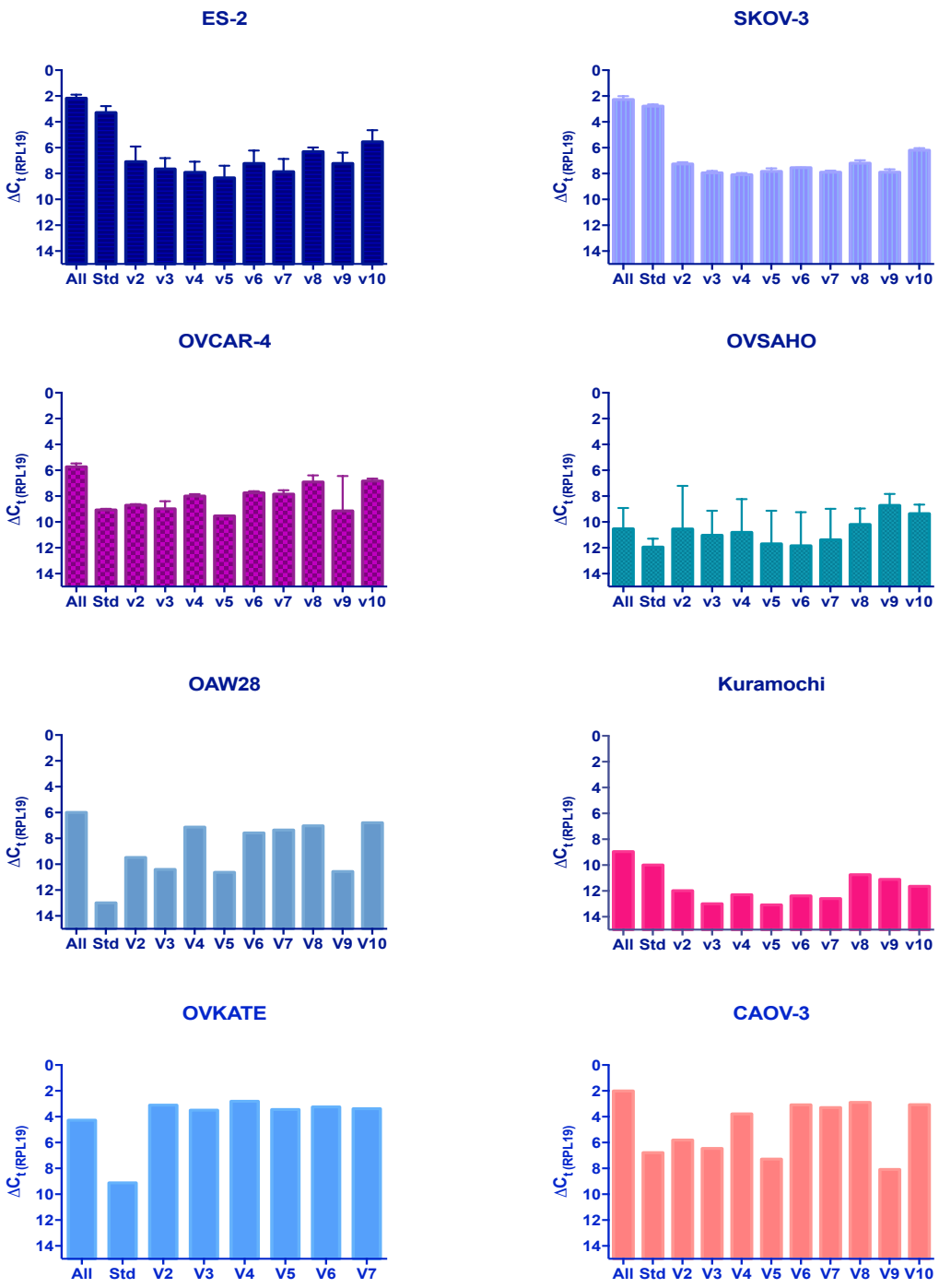

Figure 8. CD44 messenger RNA expression in human EOC cell lines. CD44 mRNA was determined by reverse transcription-polymerase chain reaction using 11 sets of primers. Primer set 1 detected all isoforms of CD44, while primer set 2 specifically detected CD44s and sets 3-11 specifically detected CD44v2, v3, v4, v5, v6, v7, v8, v9, and v10, respectively. Top 4 cell lines, N=4; Bottom 4 cell lines, N=1.

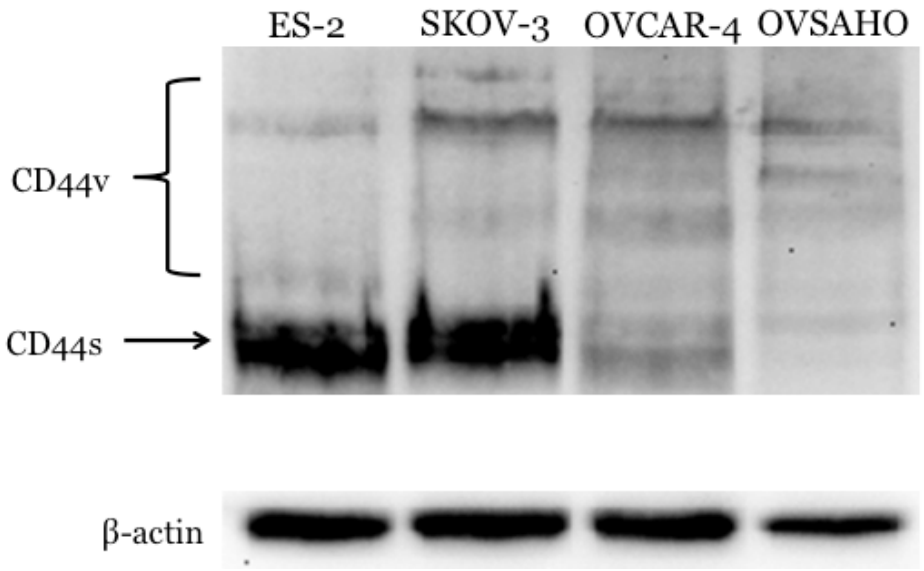

Figure 9. CD44 protein expression in human EOC cell lines. Pan-CD44 was determined by western blot analysis. CD44s, CD44 standard isoform; CD44v, variant CD44 isoforms. β-actin was used as a loading control for protein. Figure representative of 4 individual replicates.

CHAPTER 3: CD44S IN SPHEROID FORMATION

3.1 Introduction

While the previous experiments identified the advanced stage of patient at which CD44 seems most influential in survival and CD44s isoform is more highly expressed in these patients, it provides no real insight into the functional role CD44s may play in EOC. Since the development of peritoneal metastases in EOC is regulated, to a large extent, by the ability of shed ovarian tumor cells to survive and subsequently attach to and infiltrate the mesothelial lining of the abdominal cavity, and spheroid formation may represent an important intermediate survival mechanism that facilitates this dissemination, it was important, to next, assess the role of CD44s in formation of spheroids.

As described in chapter 1, section 1.4.2, CD44 is an important player in sphere-forming cells. Spheroid-forming cells of a gastric cancer cell line had upregulated CD44 expression (169). $CD44^{+}CD117^{+}$cells isolated from SKOV-3 ovarian cancer cell line formed non-adherent spherical clusters (151), and treatment with a CD44 antibody reduced sphere-forming cell proliferation and significantly increased apoptosis in sphere-forming cells isolated from ascites, bulk tumor, and the SKOV-3 cell line (155). Thus, given the relevance of CD44 in sphere-forming cells, spheroids were chosen as the model to study the functional significance of CD44s in EOC.

We needed to first determine the CD44 expression and localization using immunofluorescence within our cell lines throughout spheroid formation—from single cells

in suspension at time of seeding all the way through complete spheroid formation. But since spheroids are a three-dimensional entity, we had to develop a methodology for immunohistochemical staining where their structure could be preserved. This was achieved by suspending fixed spheroids in an agarose pellet that could be paraffin-embedded in blocks similar to fixed tissue samples.

Finally, in order to study its affect on spheroid formation, we needed to knockdown CD44 expression. We chose to use CRISPR/Cas9 for gene knockout as this method results in permanent changes at the genomic level and loss-of-function. Moreover, it has a higher efficiency at performing bi-allelic gene modifications, as well. Thus, we could establish stable CD44 knockdown clones in high CD44s-expressing cell lines as a useful tool for functional studies in EOC cells.

3.2 Materials & Methods

3.2.1 Spheroid Formation Assay.

Spheroids were generated using an agarose overlay method described previously (170). Briefly, non-adhesive agarose plates were prepared by solidifying agarose solution (0.5% in complete culture media) in cell culture plates. EOC cells were released from the monolayers with 0.05% trypsin/EDTA solution, suspended in media containing 2% fetal bovine serum at a concentration of $1x10^6$ cells/mL. 1 mL of this solution was added atop of the solidified agarose, supplemented with the addition of 2 mL of 2% serum containing media, and incubated for 24-72 h at 37°C and 5% CO_2. Spheroids were defined as having a diameter greater than 30 μm and

were visualized using bright field microscopy with their diameters measured using AxioVision software (Zeiss). Spheroids were collected from the media with gentle centrifugation for 1 min at 100 × g to separate any single cells and cell debris from the spheroids. Cells were released from the spheroids with 0.05% trypsin/EDTA for manual counting.

3.2.2 Immunohistochemistry of Spheroids. Single cells and spheroids were fixed in suspension in 4% paraformaldehyde for 15 minutes, centrifuged for 2 mins at 100 x g, resuspended in 100% ethanol wash for 30 minutes, centrifuged as before, and then stored in suspension in 70% ethanol overnight. The next day, spheroids were pelleted and resuspended in liquefied 0.5% agarose in PBS and allowed to solidify briefly at 4°C in an eppendorf tube. The solidified pellet was then carefully removed from the tube and placed in a cassette for paraffin-embedding as described previously (171). Slides containing 0.3 µm sections of paraffin-preserved single cells or spheroids were rehydrated by incubation in xylenes and graded ethanol solutions followed by blocking of peroxidase activity with 3% H_2O_2 for 10 min. Antigen retrieval was achieved through incubation at 95°C for 15-min in sodium citrate buffer, pH 6.0. After cooling to room temperature, sections were blocked with 10% goat serum in PBS. Primary mouse anti-human CD44 antibody clone MEM-263 was obtained from Novus (Littleton, CO) and mouse anti-human CD44 antibody clone DF1485 were obtained from Santa Cruz Biotechnology (Dallas, TX), diluted 1:1000 in 1% goat serum in PBS, and incubated overnight at 4°C. Secondary anti-mouse IgG-Alexafluor 488 (Invitrogen) was diluted

1:2000 in 1% goat serum in PBS, and incubated 20 min at RT. Cell were counterstain with diamidino-2-phenylindole (DAPI) for 15 minutes at a concentration of 10 μg/ml. Slides were washed and mounted using ProlongGold (Invitrogen, Carlsbad, CA). Fluorescent imaging was performed using a Zeiss AxioObserverD.1 fluorescent microscope

3.2.3 Generation of CD44 Knockout Cell Lines. CRISPR/CAS9 plasmids were designed and created by the UIC Genome Editing Core using the pX330 vector backbone (Addgene) inserted with a guide RNA (gRNA) sequence directed towards exon 1 of CD44 immediately downstream of the start codon. One vector, Guide 1, coded for gRNA against CD44 DNA sequence 5'- AGTTTTGGTGGCACGCAGCC -3' while a second vector, Guide 2, coded for gRNA against CD44 DNA sequence 5'- TGGACAAGTTTTGGTGGCAC -3'. 100ng of CRISPR plasmid DNA (Guide 1) and 100ng of CRISPR plasmid DNA (Guide 2) were co-transfected with 400ng pPGKpuro plasmid DNA (Addgene) using Lipofectamine™ 3000 (ThermoFisher) according to manufacturer's instructions. Cells were selected with 2μg/mL puromycin for 4 days and then seeded for single cell clones. Confirmation of protein knockdown was confirmed using western blot for CD44 as described above followed by detection of genomic mutation in CD44 gene using both Surveyor® Mutation Detection from IDT (Coralville, IA) according to manufacturer's instructions as well as Sanger sequencing through the UIC DNA Services Core. Briefly, the kit uses Surveyor Nuclease to recognize and cleave mismatches in DNA due to the presence of small insertions or deletions in one or more copies of the gene.

3.2.4 Scanning Electron Microscopy (SEM). Spheroids were transferred to fine porous holders (Falcon) that were soaked in a container containing 4% glutaraldehyde/PBS and fixed for 2 hr. The holders were immersed in 0.1 M PBS for 30 min. The spheroids were then dehydrated by placing the holder in serial concentrations of ethanol (25%, 50%, 75%, 95%/water for 30 min each, and then absolute ethanol for 1 hour). The spheroids were dried using hexamethyldisilazane (HMDS) (Sigma), mounted on aluminum stubs with carbon tape as an adhesive, and sputter-coated with 8.0nm of Platinum/Palladium using a Cressington 208 HR Resolution Coater. Exterior surfaces were imaged using a Secondary Electron detector (SE) with a Hitachi S-3000N Variable Pressure Scanning Electron Microscope (VPSEM) at the University of Illinois Chicago, Electron Microscopy Service Facility.

3.2.5 Particle Exclusion Assay. In culture, cells with large amounts of surface-associated HA often exhibit prominent pericellular coats which can be visualized on living cells by their ability to exclude particles (172-174). The outline of the coat is revealed as a halo around individual cells (175). The particles used in this study were horse red bloods cells (Lampire) after fixation in 1.5% paraformaldehyde overnight. ES-2 cells were plated at 1 $x10^5$ cells/ 2mL in complete media in uncoated glass bottom P35 plates and allowed to adhere overnight. The medium was removed and replaced with 750 µL of a suspension of fixed red blood cells ($5x10^7$ cells/ml) in PBS. The particles were allowed to settle for approximately 15 min, and then observed and photographed

using a Zeiss Laser Scanning Microscope (LSM) 710 outfitted with a 63x/1.46 Oil alpha Plan-Apochromat objective.

3.3 CD44 Expression During Spheroid Formation in EOC Cell Lines

As spheroid formation may represent an important intermediate survival mechanism that facilitates EOC dissemination, we assessed the role of CD44s in formation of spheroids. We observed quite significant CD44 staining in the cell membrane of cells throughout the whole spheroid in ES-2 and SKOV-3, very minimal CD44 in OVCAR-4, and almost none in OVSAHO (Figure 14). In 24 hours, ES-2 cells was able to form spheroids of around 100 microns in diameter that continued to grow over time reaching >300 μM in 7 days of continued culture (Figure 10). While SKOV-3 took 2 days longer to form spheroids of 100 microns in diameter, they successfully did so, like ES-2, also continued to grow over time, as well, though not quite to the same extent as ES-2 (Figure 11). However, at 3 days in suspension culture, OVCAR-4 (Figure 12) and OVSAHO (Figure 13) formed spheroids of only 60-75 microns, which never grew much larger and maintained a size less than 100 microns throughout continued culture.

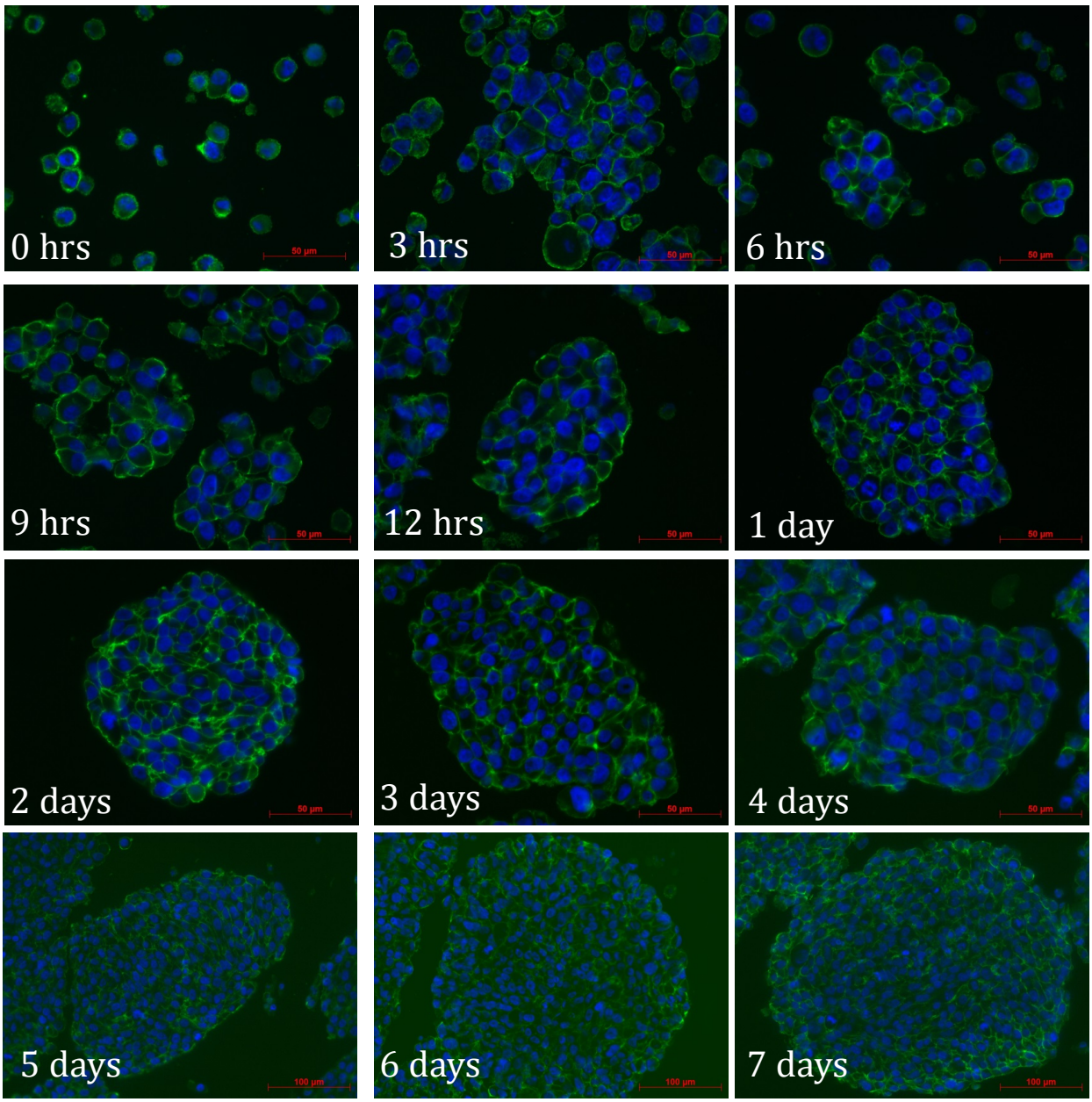

Figure 10. CD44 expression in ES-2 spheroids over 7 days. ES-2 spheroids collected at each time point were paraffin-embedded and cut into 3 µm sections. Expression of CD44 was examined with immunofluorescence staining. Nuclear DNA was stained using 4',6-diamidino-2-phenylindole (DAPI). Images superimposed on blue and green channels are shown. Bar, 50 micron (0 – 4 days) or 100 micron (5 – 7 days).

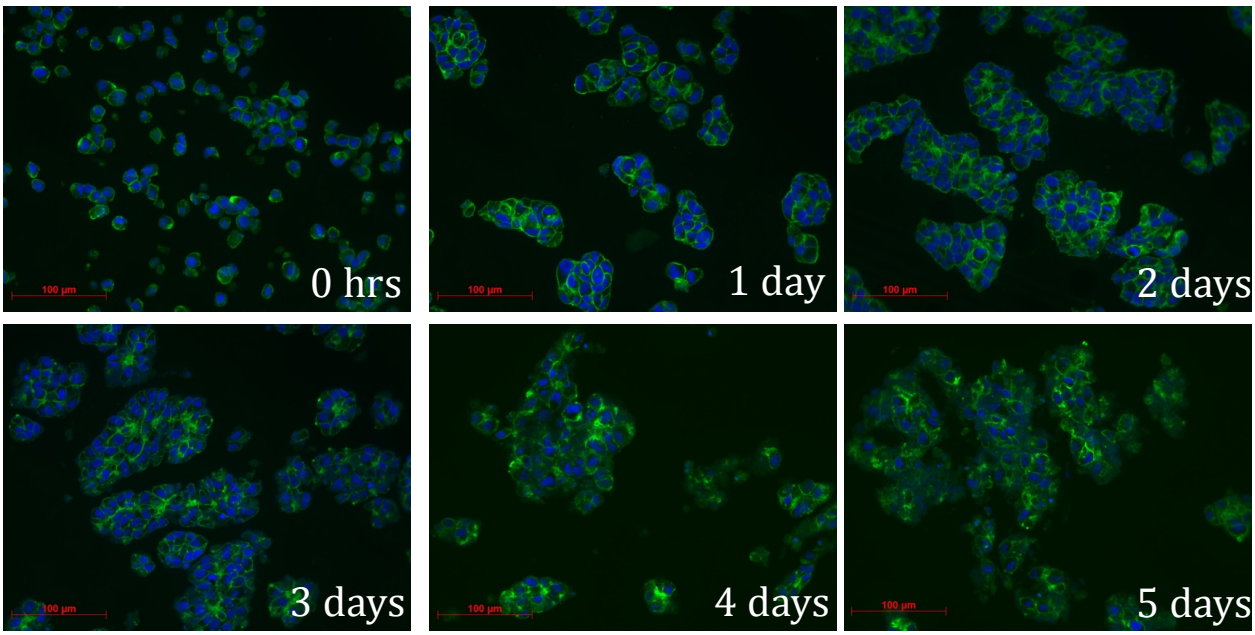

Figure 11. CD44 expression in SKOV-3 spheroids over 5 days. SKOV-3 spheroids collected at each time point were paraffin-embedded and cut into 3 µm sections. Expression of CD44 was examined with immunofluorescence staining. Nuclear DNA was stained using 4',6-diamidino-2-phenylindole (DAPI). Images superimposed on blue and green channels are shown. Bar, 100 micron.

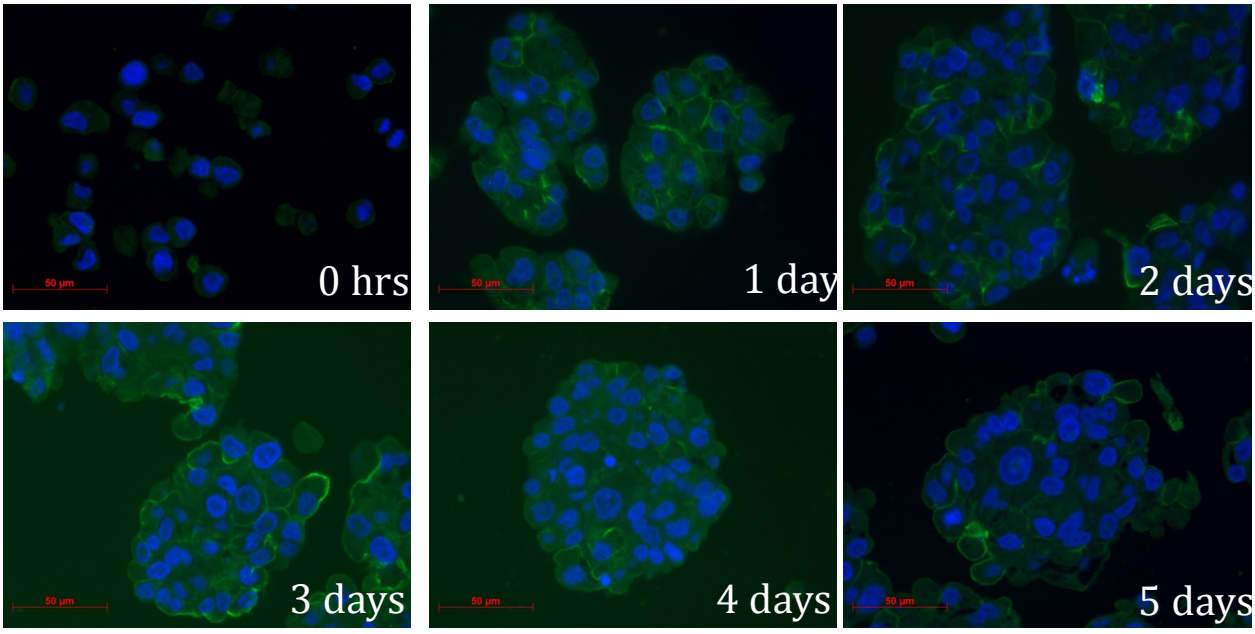

Figure 12. CD44 expression in OVACR-4 spheroids over 5 days. OVCAR-4 spheroids collected at each time point were paraffin-embedded and cut into 3 µm sections. Expression of CD44

was examined with immunofluorescence staining. Nuclear DNA was stained using 4',6-diamidino-2-phenylindole (DAPI). Images superimposed on blue and green channels are shown. Bar, 50 micron.

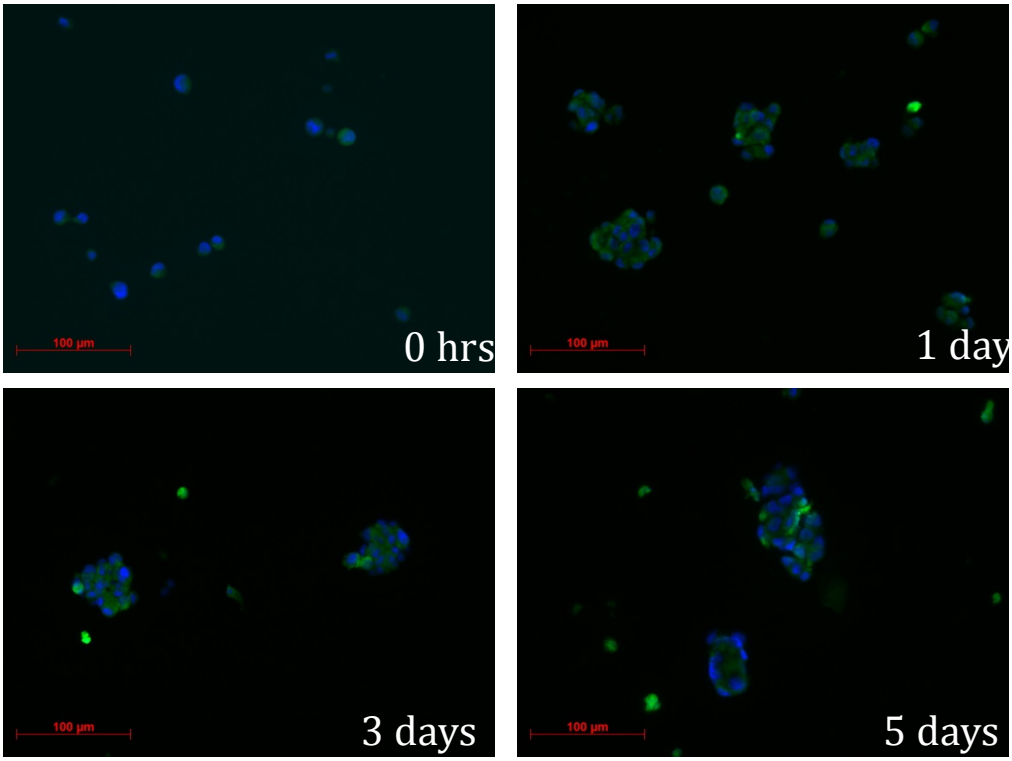

Figure 13. CD44 expression in OVSAHO spheroids over 5 days. OVSAHO spheroids collected at each time point were paraffin-embedded and cut into 3 µm sections. Expression of CD44 was examined with immunofluorescence staining. Nuclear DNA was stained using 4',6-diamidino-2-phenylindole (DAPI). Images superimposed on blue and green channels are shown. Bar, 100 micron.

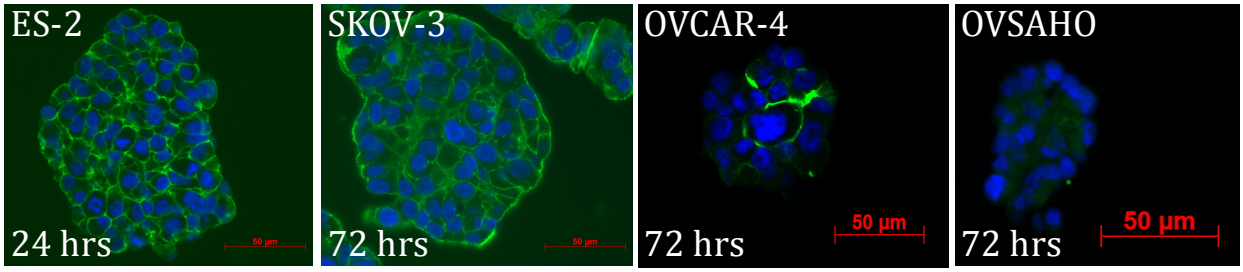

Figure 14. CD44 expression in CD44s-high spheroids vs CD44-low spheroids. ES-2, SKOV-3, OVCAR-4, and OVSAHO spheroids were paraffin-embedded and cut into 3 µm sections.

Expression of CD44 was examined with immunofluorescence staining. Nuclear DNA was stained using 4',6-diamidino-2-phenylindole (DAPI). Images superimposed on blue and green channels are shown. Bar, 50 micron.

Furthermore, 100% of ES-2 and SKOV-3 cells seeded form spheroids whereas only 60-75% of OVCAR-4 and only about 50% of OVSAHO cells seeded go into spheroids (Figure 15, right panel). Therefore, in large spheroids we observed a very high intensity of CD44 expression, which we know is predominately the CD44s isoform. Since many more of the cells highly expressing CD44s can actually form spheroids, this suggests a strong correlation between increased CD44s expression and the capability of forming spheroids in EOC.

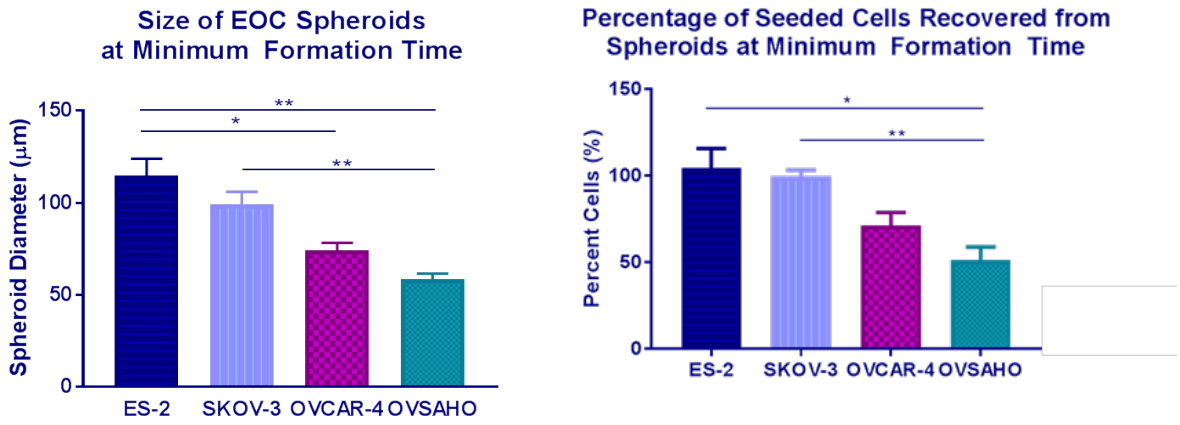

Figure 15. CD44s expression correlates with size and number of EOC spheroids formed. EOC spheroid size (left panel) and percent of seeded cells forming spheroids (right panel) after 24-72 hours for CD44s-high (ES-2, SKOV3) and CD44s-low (OVCAR-4, OVSAHO) expressing cell lines. Left panel N=12, *p<0.005, **p<0.0001, One-Way ANOVA, Tukey's Post-Hoc test. Right panel N=4, *p=0.0121, **p=0.025, One-Way ANOVA, Tukey's Post-Hoc test.

3.4 Spheroid Formation of SKOV-3 $CD44^{-/-}$ Cells

SKOV-3 CRISPR-generated $CD44^{-/-}$ clones were characterized for protein knockdown using western blot (Figure 16, left panel). 3 clones (C2, C5, and C6) were chosen for CD44 gene mutation confirmation using Surveyor endonuclease. A bp region of exon 1 in the CD44 gene surrounding the CRISPR gRNA target site was amplified using PCR. The resulting product was mixed with parental wildtype CD44 PCR product, denatured, re-hybridized, and treated with Surveyor nuclease creating 2 cleavage products for every bp insertion or deletion present in the sample. Clone 2 and clone 6 displayed 2 cleavage bands below the full-length amplicon indicative of a single mutation at the same, or roughly the same, location in each gene allele (Figure 16, right panel). On the other hand, clone 5 exhibited 3 cleavage bands indicative of 2 mutations. Clone 6 was submitted for sequencing and confirmed to have 1 adenosine deletion 2bp after the start codon on one copy of the CD44 gene and the other copy of the gene with a guanine insetion 2 bp after the start codon. ES-2 clone 7 was also confirmed for CD44 gene mutation using Surveyor. Similar to SKOV-3 clones 2 and 6, the only ES-2 clone initially isolated with CD44 protein reduction (Figure 19, left panel), clone 7, displayed 2 cleavage bands below the full-length amplicon indicative of a single mutation at the same, or roughly the same, location in each gene allele (Figure 19, right panel). Sequencing confirmed one copy with an adenosine and guanine inserted in place of cytosine immediately following the start codon, while the other copy of the gene has a cytosine deleted 2 bp downstream of the start codon. These are indicative of frameshift mutations resulting in loss-of-functional protein. All clones were seeded in non-adherent culture conditions for 3 days and measured for the number of cells in spheroids

out of 1 million cells seeded. All clones were tested against the parental cell line as well as a scrambled vector clone and vector only clone averaged together as controls. CD44 stable knockdown cells exhibited significantly reduced spheroid formation as determined through the reduced number of cells forming spheroids after 72 hours (Figure 17). Furthermore, using brightfield microscopy we observed a reduction in the size of the spheroids that do form (Figure 18).

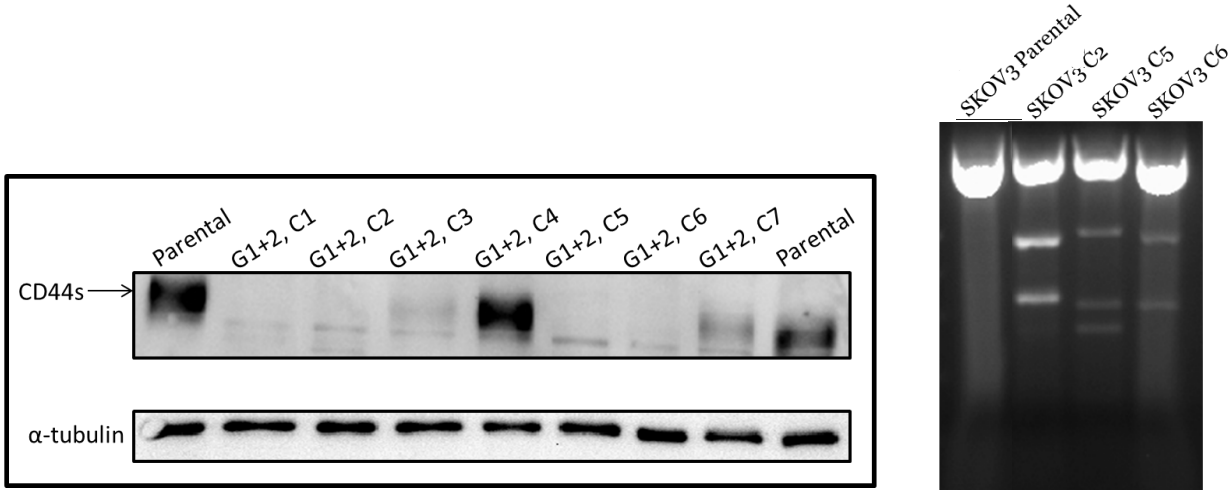

Figure 16. CD44 protein and genomic DNA characterization of SKOV-3 CD44$^{-/-}$ isogenic clones. Pan-CD44 was determined by western blot analysis for clones 1-7 (left panel). CD44s, CD44 standard isoform. Parental SKOV-3 cell lysate was used as a positive control for CD44s protein expression. α-tubulin was used as a loading control for protein. Mutation in exon 1 of CD44 gene was determined by Surveyor® Mutation Detection Kit and DNA visualized using agarose gel electrophoresis (right panel). Top MW band=full length amplified CD44 DNA flanking CRISPR target site. Lower MW bands=DNA cleavage products from base pair mismatching after hybridization of clone mutant DNA with parental wildtype DNA and exposure to Surveyor nuclease.

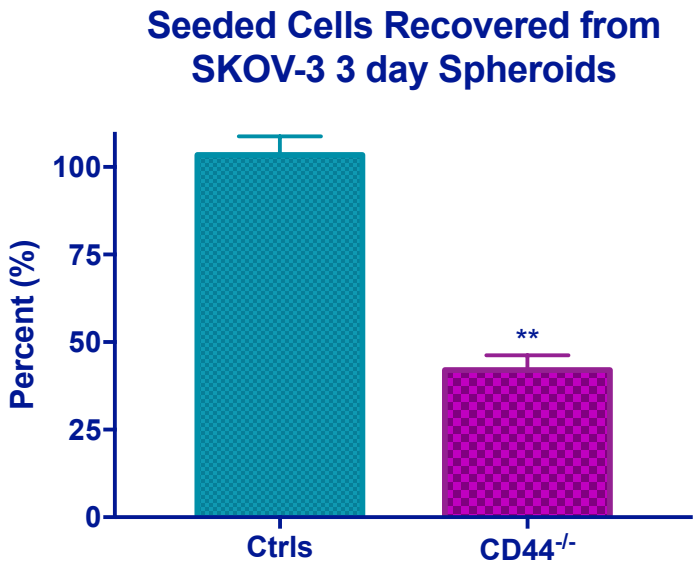

Figure 17. CD44s expression reduces SKOV-3 spheroid formation. % of seeded SKOV-3 cells recovered from spheroids after 72 hours. N=7, **p<0.0001, Mann-Whitney U

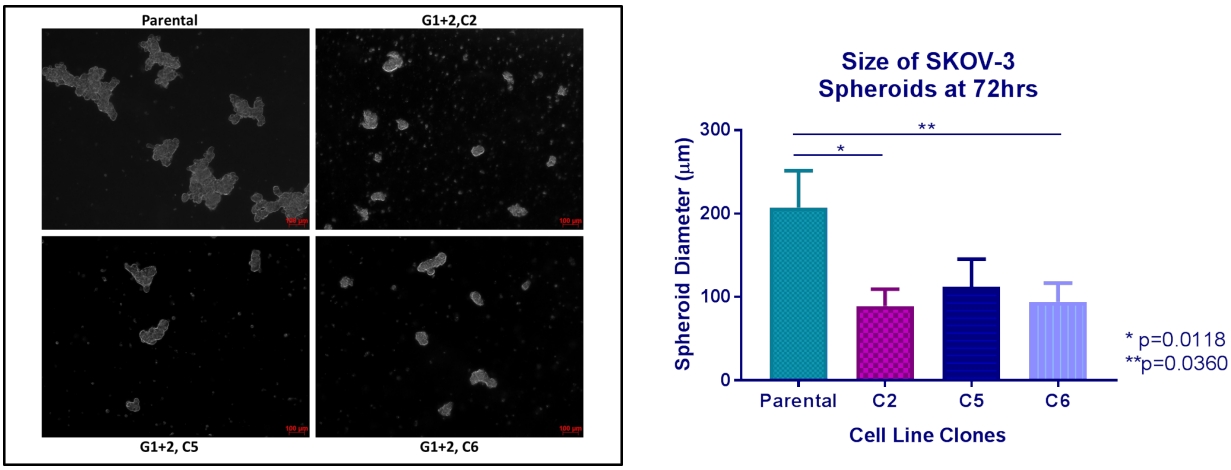

Figure 18. SKOV-3 spheroid size reduction in CD44$^{-/-}$ isogenic cell lines. SKOV-3 CD44$^{-/-}$ clones in spheroids after 72 hours visualized using brightfield microscopy (left panel). SKOV-3 parental spheroids were used as a control. Average spheroid diameter is shown (right panel). N=20, *p=0.0118, **p=0.0360, student's t-test.

3.5 Spheroid Formation of ES-2 CD44$^{-/-}$

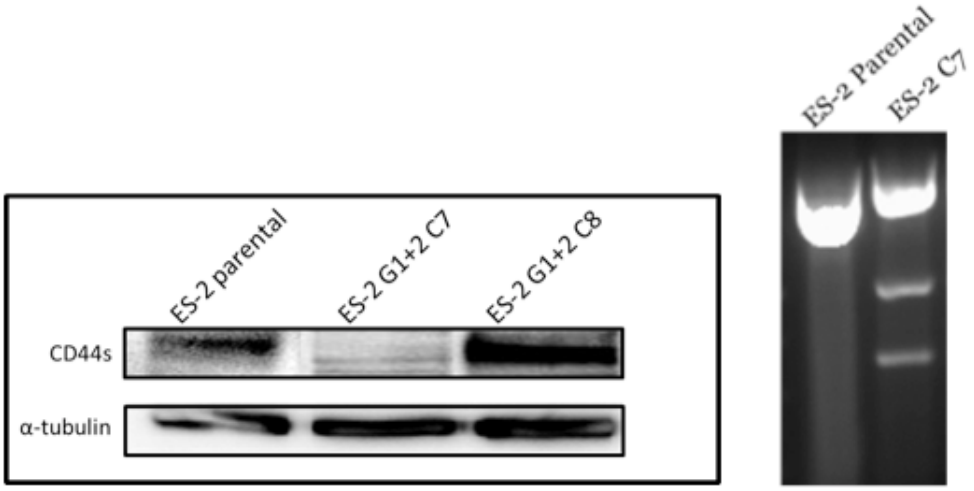

Figure 19. CD44 protein and genomic DNA characterization of ES-2 CD44$^{-/-}$ isogenic cell lines. Pan-CD44 was determined by western blot analysis for clones 7 and 8 (left panel). CD44s, CD44 standard isoform. Parental ES-2 cell lysate was used as a positive control for CD44s protein expression. α-tubulin was used as a loading control for protein. Mutation in exon 1 of CD44 gene was determined by Surveyor® Mutation Detection Kit and DNA visualized using agarose gel electrophoresis (right panel). Top MW band=full length amplified CD44 DNA flanking CRISPR target site. Lower MW bands=DNA cleavage products from base pair mismatching after hybridization of clone mutant DNA with parental wildtype DNA and exposure to Surveyor nuclease.

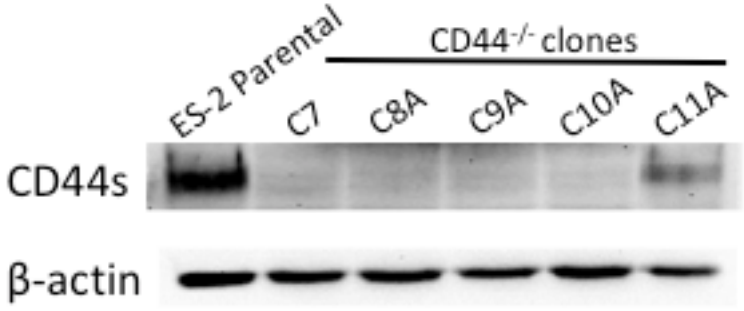

Figure 20. CD44 protein in newly generated ES-2 CD44$^{-/-}$ isogenic cell lines. Pan-CD44 was determined by western blot analysis for a second round of CRISPR-generated CD44$^{-/-}$ clones 7A – 11A. CD44s, CD44 standard isoform. Parental ES-2 cell lysate was used as a positive control for CD44s protein expression. ES-2 clone 7 generated and validated previously was

used as a negative control for CD44s expression. β-actin was used as a loading control for protein.

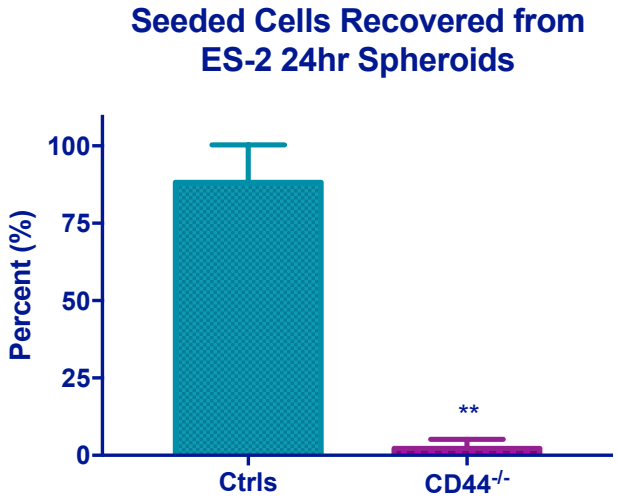

Figure 21. Silencing CD44s expression eliminates ES-2 spheroid formation. % of seeded ES-2 CD44$^{-/-}$ clone 7 cells recovered from spheroids after 24 hours. N=5, $^{**}p<0.0001$, Mann-Whitney U.

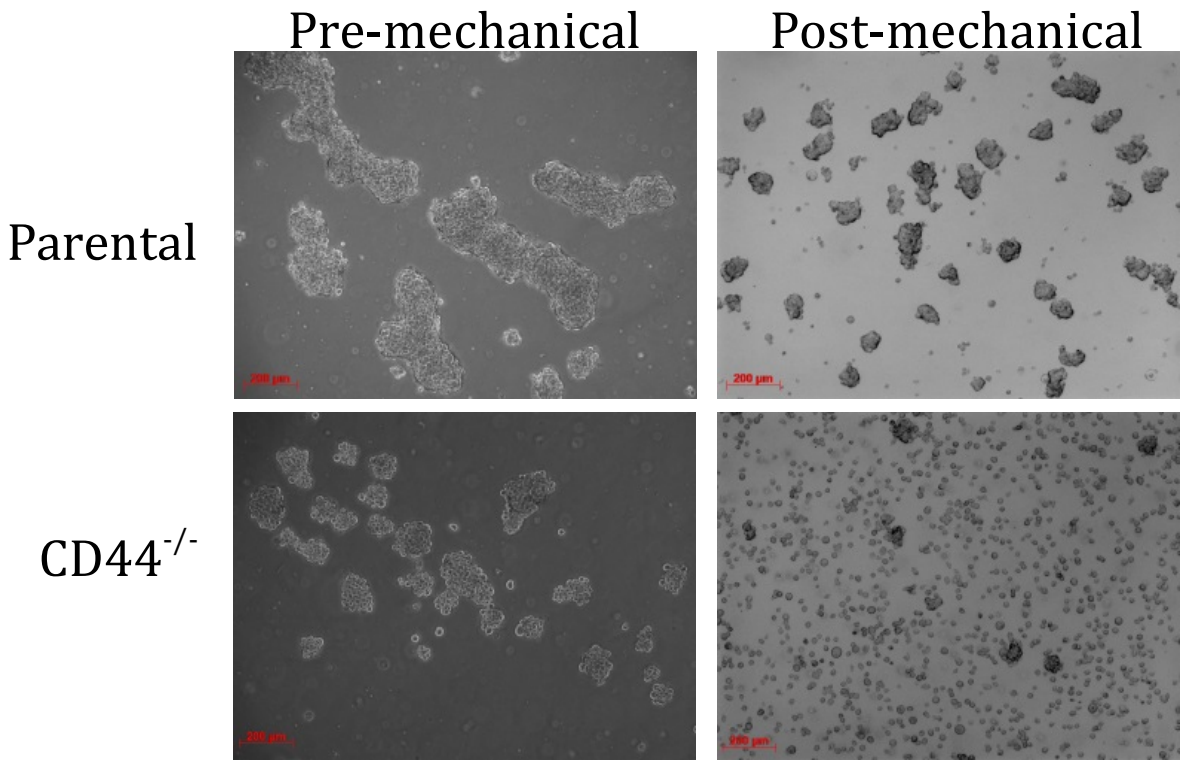

Figure 22. CD44$^{-/-}$ cells form multicellular aggregates that easily disaggregate upon mechanical disruption. Bright-field images of 24hr ES-2 parental spheroids before and after gentle pipetting compared to multicellular aggregates of ES-2 CD44$^{-/-}$ cells, which disperse into single cells with gentle pipetting.

In order to better understand the structural changes that occur in these cells after CD44 knockdown, we viewed these cells using scanning electron microcopy. Parental ES-2 spheroids have an extensive network of tight intercellular connections (Figure 23, upper left panel), while the CD44-silenced cell aggregates exhibit only loose intercellular connections (Figure 23, upper right panel). Furthermore, not only is the tightness of these connections reduced, but there is also a significant reduction in the number of intercellular connections these cells make with each other when CD44 expression is silenced seen at higher magnification, 3500X (Figure 23, lower panels). This shows visually that when CD44 is knockdown in ES-2 cells, they are unable to form the same number of intercellular connections, and those connections that they are able to form are very loose, appearing flimsy and unstable.

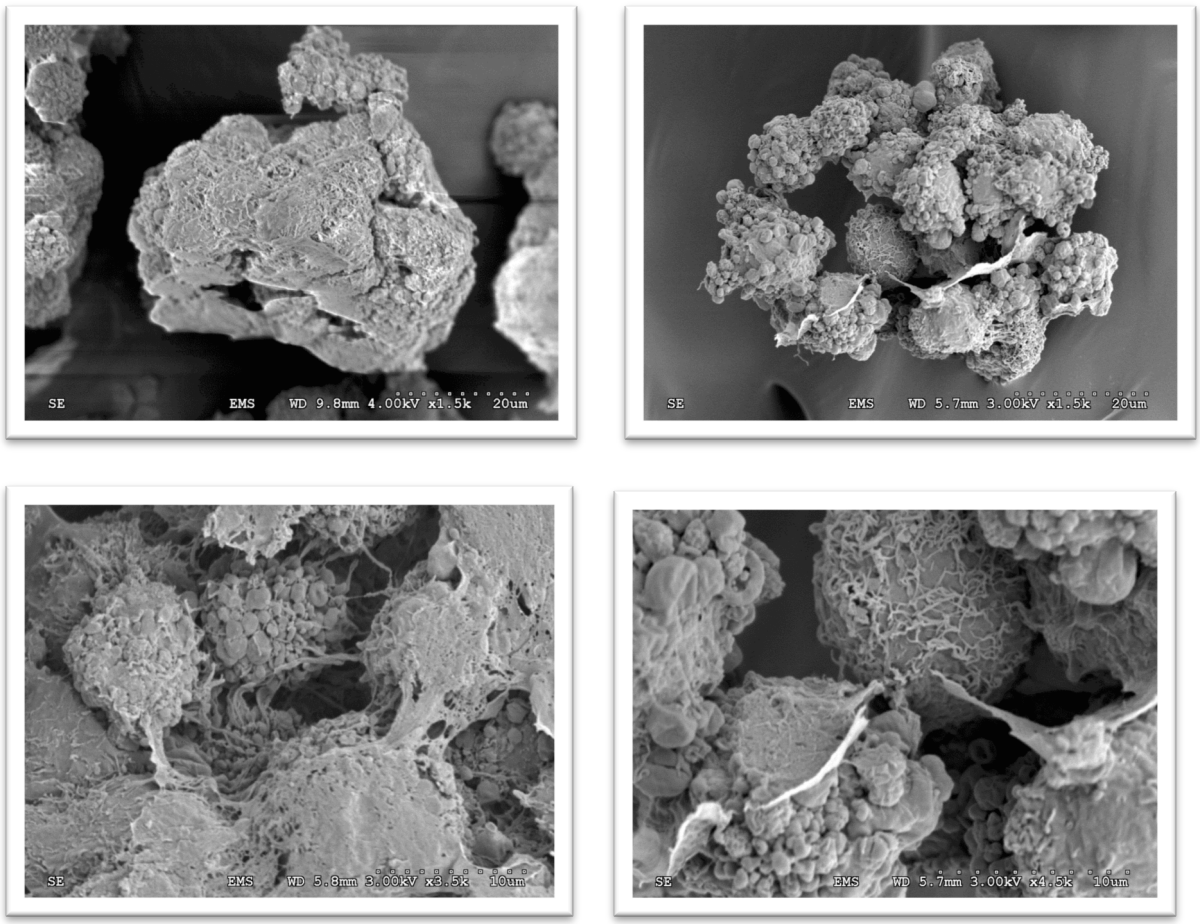

Figure 23. SEM images of ES-2 parental spheroids and CD44$^{-/-}$ multicellular aggregates. Bar, 20 micron (top panel), 10 micron (bottom panel); 1500X magnification (top) 3500X magnification (bottom).

Finally, CD44 plays and important role in the formation of pericellular matrix (PCM), also termed pericellular sheath or glycocalyx—an area that is both biochemically and biomechanically distinct from the extracellular matrix (ECM) (176). This sheath is dependent on hyaluronan retention at the cell surface through binding to its receptor CD44. Now, this coat has multiple important roles, from serving structural and mechanochemical functions,

to the regulation of cell division and motility, as well as cancer progression and metastasis, and has previously been reported as necessary for sphere formation in rabdhomyosarcoma (176). Since this coat is highly hydrated, it appears in ES-2 parental spheroids as a collapsed sheath surrounding the cells due to the dehydration process necessary for electron microscopy (Figure 24). Importantly, however, the CD44 knockout clone has no evidence of pericellular sheath formation in cell aggregates as we saw in the parental spheroids.

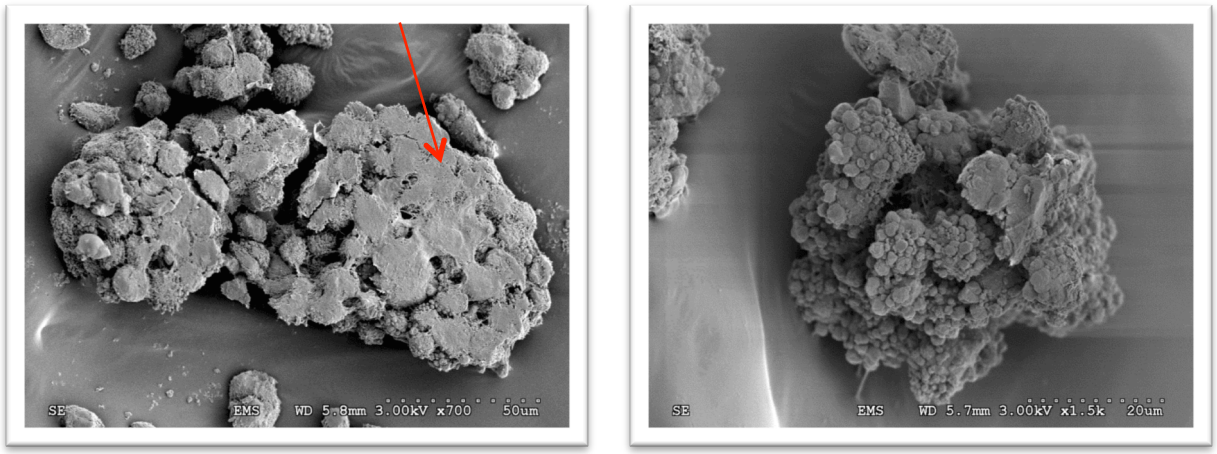

Figure 24. CD44 gene silencing may reduce pericellular sheath formation on ES-2 spheroids. SEM images of an ES-2 parental spheroid and a CD44$^{-/-}$ multicellular aggregate. Arrow, pericellular matrix. Bar, 50 micron (left panel), 20 micron (right panel); 700X magnification (left) 1500X magnification (right).

However, to more definitively assess the presence of a PCM, a particle exclusion assay was employed, but no apparent pericellular matrix was observed in two-dimensional monolayer culture (Figure 25). This, does not rule out, however, the formation of PCM during spheroid formation in 3D. Though, we did not have the tools to visualize PCM in fixed *hydrated*

spheroids —known as wet-SEM (177) or environmental SEM (ESEM) (178)—with the technology available at the UIC electron microscopy core.

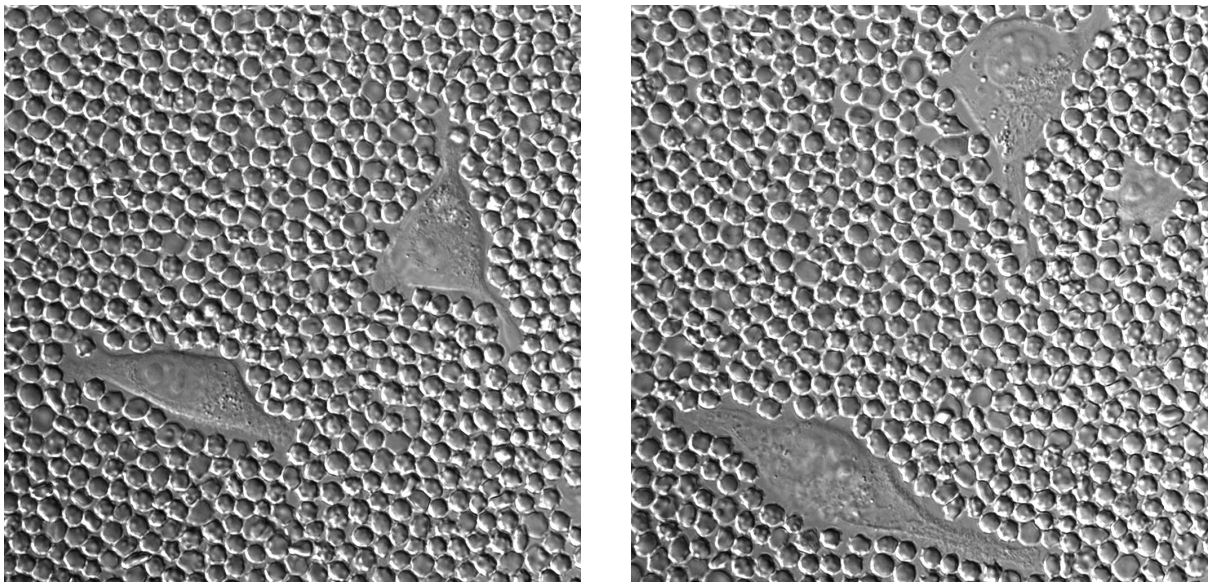

Figure 25. Lack of pericellular matrix in 2D cultured ES-2 cells observed by particle (red blood cell) exclusion assay. Red blood cells diameter = 7 μm

CHAPTER 4: CD44S IN CELL ADHESION

4.1 Introduction

Metastasis of ovarian cancer is distinguishable from that of many other types of cancers in that after detaching from the primary tumor site, cancer cells adhere and implant around the peritoneal cavity and organs, which are covered by a continuous monolayer of mesothelial cells (179) (180). Previous research in understanding this process has implicated a role for CD44 in adhesion of ovarian cancer cells to mesothelial cells, a crucial step in peritoneal metastasis.

One study linked CD44 with β1-integrin in mediating ovarian cancer cell adhesion to peritoneal mesothelial cells (181), and this binding was shown to be associated with expression of CD44s isoform in another study (156). Moreover, inhibition of CD44 using an antibody *in vivo* was reported to limit intra-abdominal implantation in a human ovarian cancer xenograft, and interestingly, the cell line they used in their studies was shown to predominately express the standard isoform of CD44. Therefore, all of these reports point to an important functional role for CD44 in the progression of peritoneal metastasis through enhanced mesothelial adhesion, with evidence for a specific CD44s isoform association as depicted in Figure 26.

Since the experiments in Chapters 2 and 3 identified CD44s gaining importance in late stage EOC and implicated CD44s as an important component for spheroid formation, the next set

of experiments sought to determine the role of CD44s in spheroid adhesion to mesothelial cells *in vitro*. By testing their adhesion capability in the presence and absence of functional CD44 to a monolayer of mesothelial cells, we could get an idea of the metastatic phenotype of these cells and the role of CD44s in contributing to that.

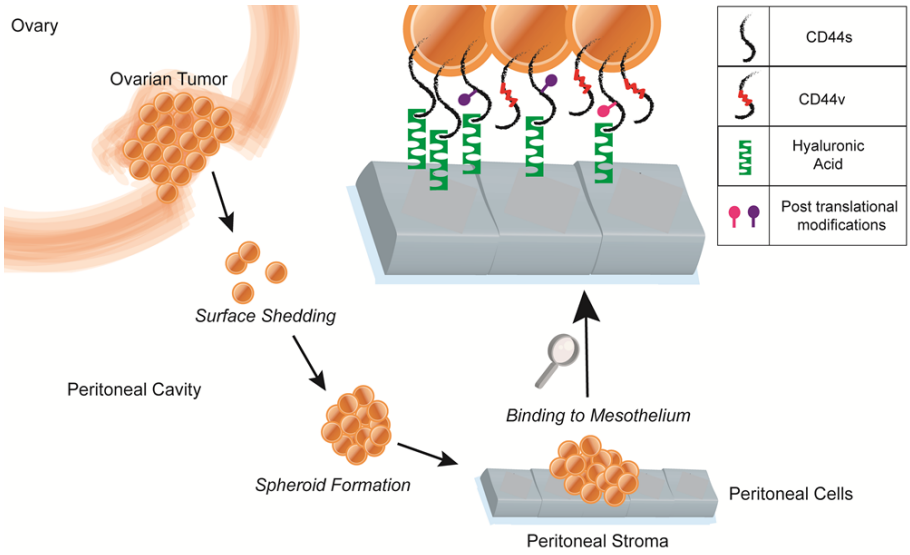

Figure 26. Schematic representation of proposed EOC spheroid adhesion to peritoneal mesothelial cells via CD44s binding to hyaluronan in the ECM.

4.2 Materials & Methods

4.2.1 Mesothelial Cell Adhesion.

The human immortalized peritoneal mesothelial cell line LP-3 was obtained from the Coriell Aging Cell Repository (Camden, NJ) and cultured in a 1:1 mixture of medium 199 (Sigma-Aldrich) and MCDB 105 (Sigma-Aldrich) supplemented with 15% fetal bovine serum, 10 ng/mL epidermal growth factor, 0.4 µg/mL hydrocortisone, 10 mL/L sodium pyruvate, 5 mL/L nonessential amino acids, and 2 mM glutamine in a humidified incubator with 5% CO_2 at 37°C for 5–7 passages. For the assay, LP-3 was cultured in 6-well plates to confluence. To study adhesion of spheroids,

ES-2 cells were released from monolayers with 0.05% trypsin/EDTA solution, resuspended in serum-free cell culture media, and fluorescently labeled with 8 μL Vybrant DiO (Invitrogen) per 1 x 10^6 cells for 30 mins at 37°C. Cells were then cultured for spheroid formation as described above followed by incubation with 10 ug/mL of function-neutralizing mouse anti-CD44 (BU75) from Ancell (Bayport, MN), which blocks binding of HA to CD44, or normal mouse IgG in serum-free media for 30 mins at 37°C. Then, the spheroids were plated over the confluent monolayer of LP-3 cells (in triplicate per condition) in serum-free media. The fluorescently labeled spheroids were allowed to adhere to the mesothelial monolayer for 30 mins, 1 hours, 2 hours, and 4 hours. Subsequently, at each time point the monolayers were washed twice with PBS and fixed with 4% paraformaldehyde. Adherent cells were visualized by green fluorescent signals using a Zeiss AxioObserverD.1 fluorescent microscope. The six well plates were divided into 20 individual grids to enable manual counting of adherent DiO-labeled spheroids by fluorescent microscope and averaged. The experiments were performed three times for statistical analysis using GraphPad Prism 7.0. Spheroids smaller than 30 μm or larger than 275 μm were not used in statistical analysis.

Additional experiments were performed to evaluate the degree of adhesion of ES-2 $CD44^{-/-}$ MCA and single cells compared to parental spheroids and single cells, respectively, on a monolayer of LP-3 mesothelial cells in six well plates. As before, ES-2 cells were fluorescently labeled with Vybrant DiO and immediately plated over the LP-3 monolayer (in triplicate per condition) as single cells or seeded for 24hr spheroid

formation as described previously followed by plating over the LP-3 monolayer. To the LP-3 cells were added 10,000 fluorescently labeled ES-2 cells or spheroids/MCAs of 1.5 x 10^5 cells. The degree of adhesion was represented by percent of adhering cells, which was determined by taking the number of adherent cells divided by the number of cells seeded initially. With spheroids/MCA, the number of adherent spheroids is relative to the number of anti-IgG pre-treated or ES-2 parental adherent spheroids at 4 hours. The percent of adhesion was examined at 30 min, 1 hour, 2 hours, and 4 hours by gently removing non-adhering cells with a PBS rinse. The six well plates were divided into 20 individual grids to enable manual counting of adherent DiO-labeled spheroids by fluorescent microscope and averaged. The experiments were performed three times for statistical analysis using GraphPad Prism 7.0.

4.3 CD44 Function-Neutralizing in CD44s-hi EOC Cell to Mesothelial Cell Adhesion

In order to model *in vitro* the initial process of ovarian cancers cell metastasis, we used a co-culture system of human LP-3 peritoneal mesothelial cells with ES-2 cells. Primary mesothelial cells were seeded until 100% confluence, and ES-2 cells stained with DiO were seeded as single cells, spheroids, or multicellular aggregates on the mesothelial cell monolayer. We assessed the adhesion of ES-2 spheroids to an LP-3 mesothelial monolayer following pre-treatment of the spheroids with either a CD44 function-neutralizing antibody or IgG control. The CD44 antibody recognizes the hyaluronan-binding domain effectively blocking binding of hyaluronan to the CD44 expressed on the cell surface of these spheroids.

We saw that ES-2 spheroids showed significantly faster adhesion to the LP-3 cells, overall, and this adhesion was reduced by 50% on average at each time point for spheroids treated with CD44 antibody (Figure 27).

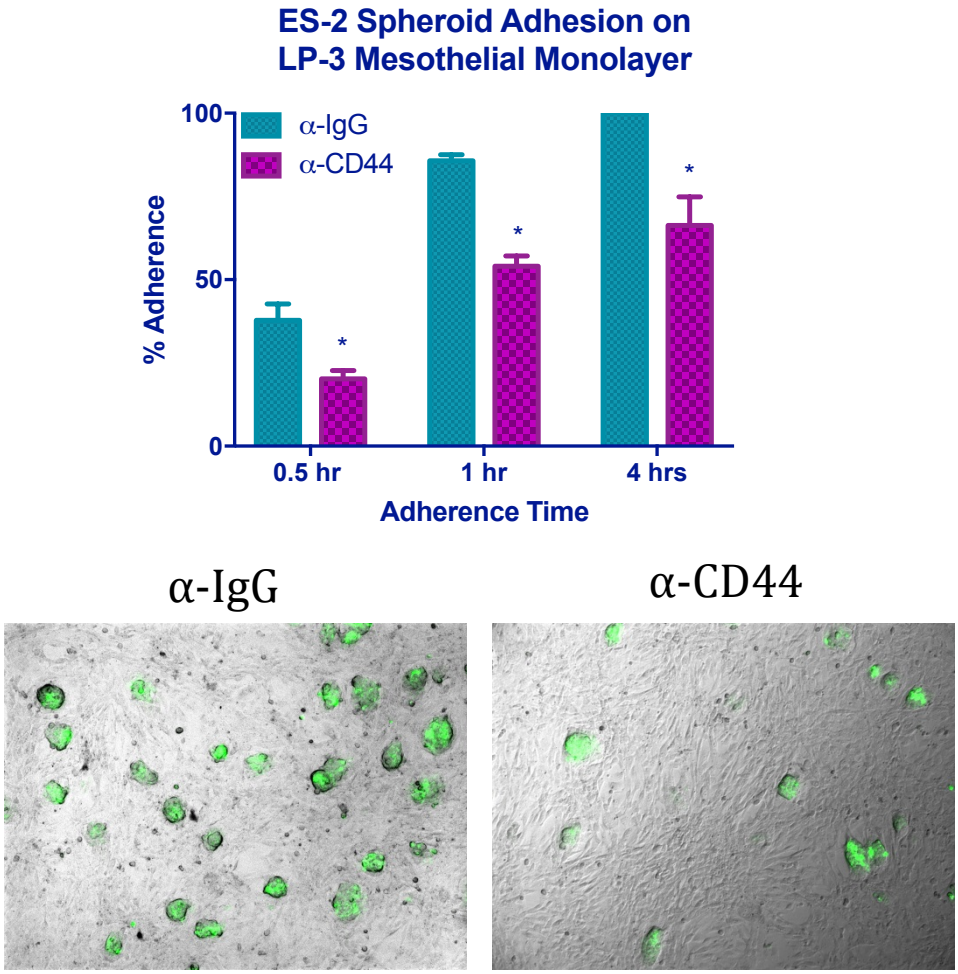

Figure 27. CD44 function-neutralizing antibody reduced ES-2 spheroid adhesion to mesothelial cells. Percent adhesion of anti-CD44 pre-treated compared to mouse IgG pre-treated ES-2 spheroids on LP-3 mesothelial cell monolayers. Spheroids shown in green. N=3, *p<0.005; student's t-test.

4.4 CD44 Expression-Silenced in CD44s-hi EOC Cell to Mesothelial Cell Adhesion

Moreover, when we silenced CD44 in ES-2 cells, we observed a similar 2-fold reduction in single cell adhesion (Figure 29) and multi-cell aggregate adhesion to mesothelial cells compared to the parental CD44s-expressing spheroids (Figure 28). This agrees with previously reported findings that binding of ovarian cancer cells to peritoneal mesothelium *in vitro* is mediated by standard CD44 (156). Therefore, we conclude that adhesion of ovarian cancer single cells and spheroids to mesothelial cells depends on the presence of standard CD44 expression.

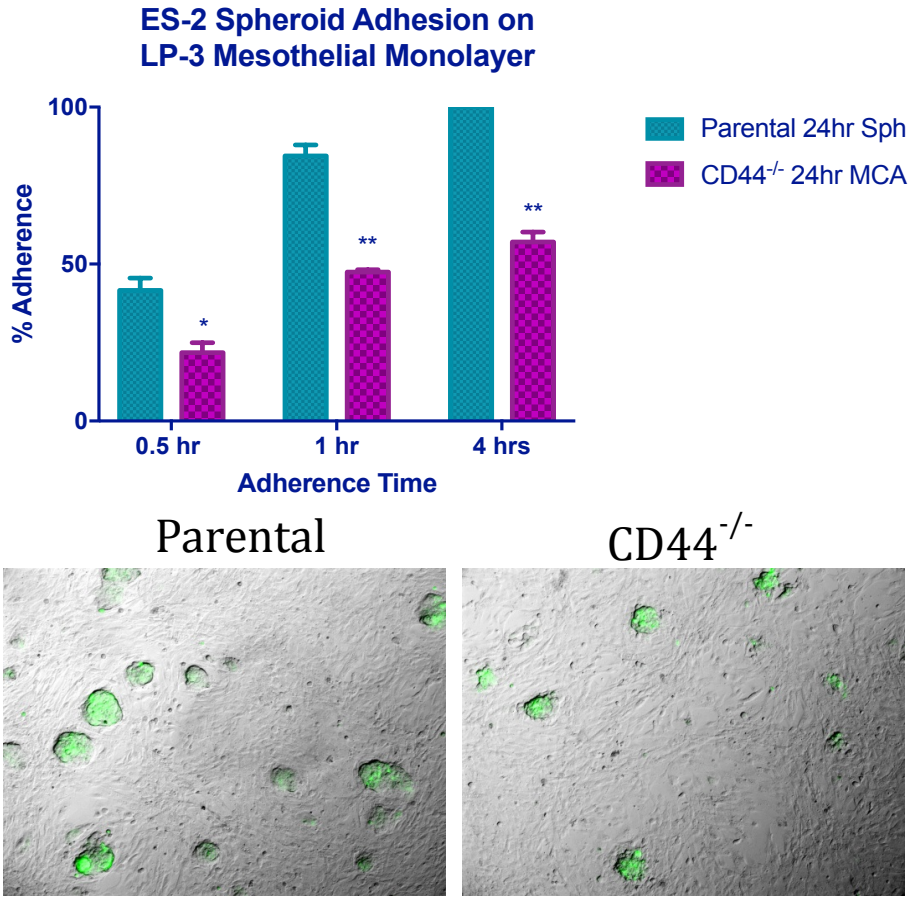

Figure 28. CD44 gene silencing reduced ES-2 MCA adhesion to mesothelial cells. Percent adhesion of ES-2 CD44$^{-/-}$ MCAs compared to parental spheroids on LP-3 mesothelial cell

monolayers (top panel). LP-3 cells with attached ES-2 spheroids (bottom left panel) and CD44$^{-/-}$ MCAs (bottom right panel), Green – spheroids. N=3,*p<0.005,**p<0.0001; student's t-test.

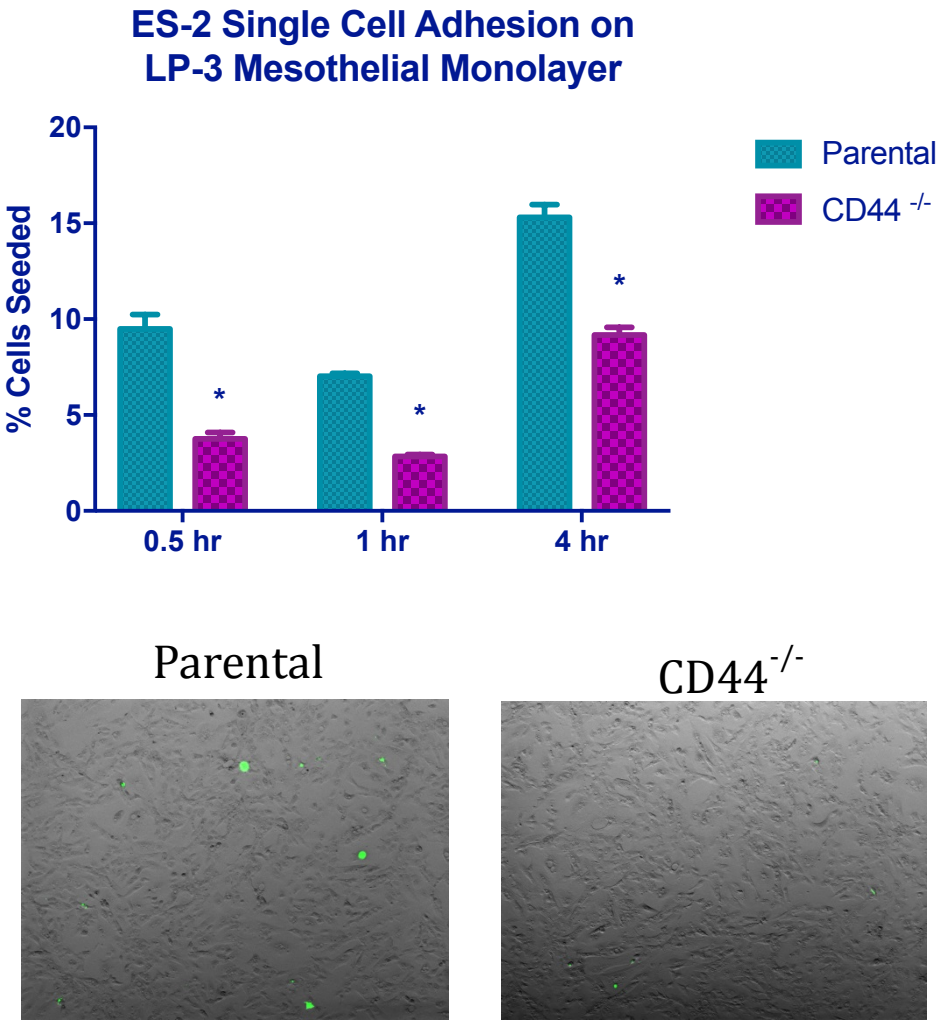

Figure 29. CD44 gene silencing reduced ES-2 single cell adhesion to mesothelial cells. Percent adhesion of ES-2 CD44$^{-/-}$ single cells compared to parental single cells on LP-3 mesothelial cell monolayers (top panel). LP-3 cells with attached ES-2 single cells (bottom left panel) and CD44$^{-/-}$ single cells (bottom right panel), Green – ES-2 cell. *p<0.0001; N=3, Sidak's post- hoc test.

CHAPTER 5: CD44S IN CELL GROWTH AND PROLIFERATION

5.1 Introduction

When the CD44 knockout clones were first isolated, it was observed that they grew slower compared to their parental counterparts as more days passed before the need to passage cells to larger culture dishes. Moreover, co-localization of CD44 with the nuclear proliferation marker Ki-67 *in vivo* and *in vitro* has been described in meningioma (182) and numerous other studies have reported a decrease in cell growth associated with reduction or neutralization of CD44. CD44 knockdown with shRNA decreased cell proliferation in colon cancer cells (183) and breast cancer cells (184) while antibody ligation of CD44 in acute myeloid leukemia (AML) cells (185, 186) as well as ovarian cancer cells also reduced their proliferation (155). These provide evidence for an important functional role for CD44 in cell proliferation.

Since the experiments in the previous chapters implicated CD44s as an important component for spheroid formation, we hypothesized that CD44s may enhance EOC cell growth and proliferation, and the next set of experiments sought to quantify the difference in cell growth rate that had been observed during clone establishment. This was achieved using two assays. WST-1 reagent produces a highly water soluble formazan upon uptake by metabolically active cells, allowing a direct and user-friendly colorimetric measurement of cell viability and proliferation (187). The clonogenic (or colony forming) assay enables an assessment of the differences in reproductive viability (capacity of cells to produce progeny;

i.e. a single cell to form a colony of 50 or more cells) between parental cells and genetically manipulated cells (188).

5.2 Material & Methods

5.2.1 Cell Proliferation Assay.

The effect of CD44 expression knockdown on proliferative activity was determined using a WST-1 assay kit (Takara Bio) by plating 5,000 ES-2 parental control cells and $CD44^{-/-}$ cells in a 96-well plate and incubating for 24 hours. Viability was then evaluated according to manufacturer's instructions by incubating WST-1 reagent with cells for 1 hour followed by measurement of OD_{440} as a readout. Values are shown relative to parental control cells.

5.2.2 Clonogenic Assay.

700 ES-2 parental and $CD44^{-/-}$ cells were plated into p60 culture dishes and incubated in complete media for 10 days. Cells were fixed in 4% paraformaldehyde for 5 mins and then incubated with 0.2% crystal violet for 30 mins at RT. Excess crystal violet was washed off using diH_2O and allowed to air dry. Quantitation of crystal violet staining was performed by extracting dye using 100% methanol for 1 hr with agitation and absorbance read at 600nm using a Promega Plate Reader.

5.3 Cell Proliferation

We also investigated the effect of suppressing the expression of standard CD44 on proliferation in ES-2 cells. With standard CD44 expression eliminated, cell growth was

inhibited by 58.47 ± 13.2% compared to parental control cells in WST-1 assay (P<0.01; Figure 30). Thus, knockout of CD44 expression resulted in approximately 2.5- to 3-fold reduction in cell growth.

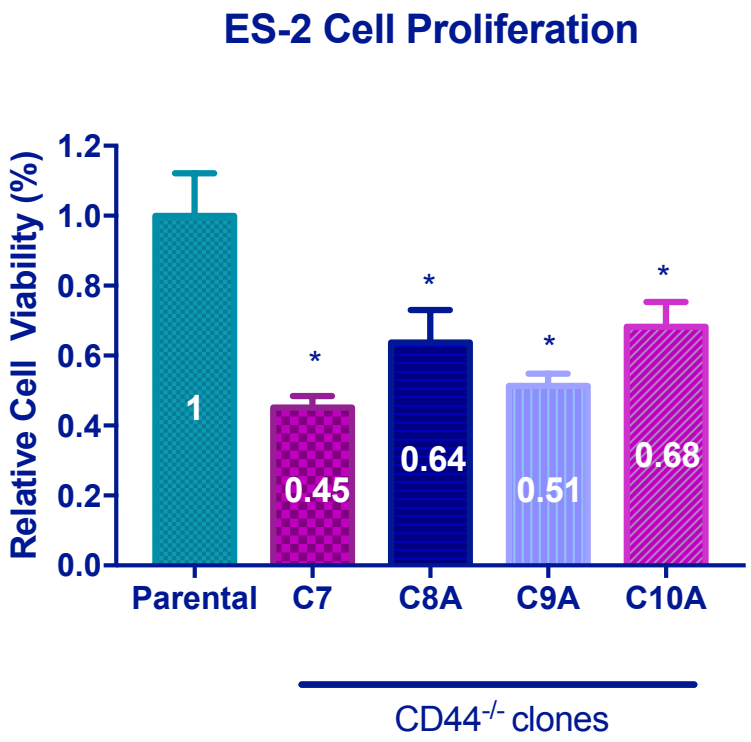

Figure 30. CD44s expression regulates proliferation in ES-2 cells. Relative proliferation rate of ES-2 $CD44^{-/-}$ cells compared to parental in 2D culture quantified by WST-1 assay. N=9,*p<0.0001; Mann-Whitney U.

5.4 Colony Formation

Similar to WST-1 assay results, clonogenic assay showed a decrease in colony density of ES-2 $CD44^{-/-}$ cells compared with parental control cells (Figure 31, left panel) and 69.5 ± 2% inhibition of cell growth (P<0.001; Figure 31, right panel). This is similar to other reported cancer models, which observed reduced proliferation with CD44 knockdown (183, 184), or

with anti-CD44 antibody treatment in SKOV-3 ovarian cancer cells (189) suggesting that ovarian tumor formation and growth, as well, may be affected by CD44s expression.

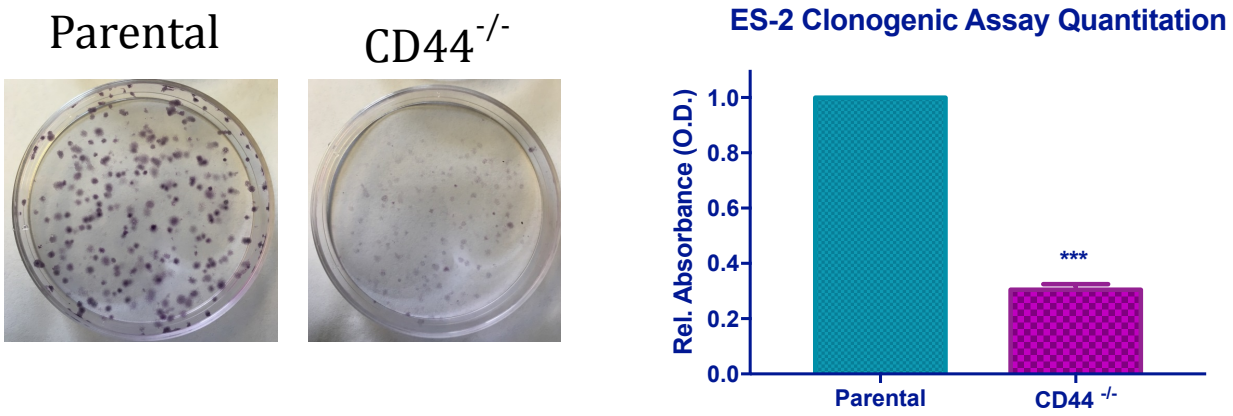

Figure 31. CD44s regulates colony cell growth. Images of ES-2 cells subjected to clonogenic assay (left panel) and quantitation of colony formation (right panel) by solubilizing crystal violet cell staining and measuring absorbance at 590nm. ***p<0.0001; student's t-test, N=3

CHAPTER 6: CD44S IN CELL MIGRATION, INVASION, AND EMT

6.1 Introduction

Metastasis requires tumor cell dissemination to different organs from the primary tumor. Dissemination is a complex cell motility phenomenon that requires the molecular coordination of the protrusion, chemotaxis, invasion and contractility activities of tumor cells to achieve directed cell migration (190). Invasiveness is one of the key attributes of aggressive cancers. Epithelial-Mesenchymal transition (EMT) is a complex biological process in which an epithelial cell undergoes multiple changes to acquire mesenchymal features associated with enhanced invasiveness. While invasion is dependent on migration, invasion requires different mechanics—enhanced migration is not a phenotypic requirement of EMT, and migration and invasion can be uncoupled during carcinoma-associated EMT (191).

One group reported that CD44s, but not CD44v, is localized in invadopodia, and shRNA-mediated depletion of CD44s abolished invadopodia activity, preventing matrix degradation and decreasing tumor cell invasiveness (192). CD44s-mediated c-Src kinase signaling has also been shown to play a pivotal role in regulating cortactin-cytoskeleton function and HA-mediated tumor cell migration during ovarian cancer progression (63). Moreover, another study showed that treatment with CD44 antibody did not inhibit ovarian cancer cell invasion, but inhibited motility (193). Moreover, it has been shown that CD44 splicing isoform switches from variant isoforms (CD44v) to the standard isoform (CD44s) when breast cancer cells undergo EMT (194). Importantly, though, are the most recently

published findings in ovarian cancer that CD44s was upregulated upon TGFβ1-induced EMT, and overexpression of this isoform in ovarian cancer cells induced EMT and invasion (195). Therefore, enhanced expression of CD44s appears to have the potential to confer both stemness and intractable properties upon cancer cells. Hence, the following experiments explored the impact of CD44s expression in ES-2 cells on migration, invasion, and EMT gene expression.

6.2 Material & Methods

6.2.1 Wound Healing Assay.

The spreading and migration abilities of ES-2 parental and ES-2 CD44$^{-/-}$ cells were assessed using the scratch wound healing assay. Cells were seeded into six well tissue culture plates and grown to 100% confluency. Prior to scratching with a P100 pipette tip, cells were incubated overnight with serum free media. After wounding, cellular debris was removed by washing with PBS, and then incubated in 2.5% fetal bovine serum. Wound closure was monitored at 12, 24, and 55 hours and calculated using AxioVision software on the Zeiss AxioObserverD.1 inverted microscope. The wound closure area that was used for measurements was carefully marked, so as to be identifiable at every time point. The difference between the total area of the scratch at any given time period was determined using TScratch analysis software (196) downloaded here: http://www.cse-lab.ethz.ch/software/, and then divided by the original area multiplied by 100 to represent the percent of wound closure. The experiments were repeated three times with three fields of measurements per well.

6.2.2 Transwell Cell Migration. Corning 24-well plate inserts with an 8 micron diameter pore size were bottom surface-coated with Matrigel by adding 500µL of a 1:100 Matrigel (BD Biosciences) solution in PBS to 24 well tissue culture plates followed by addition of inserts to the well. The inserts were incubated for 6 hours at 37°C, washed twice with PBS, and placed at 4°C for storage overnight. To each well, 500µL of serum free media was added and then the modified insert returned to the well. 10,000 ES-2 cells in serum free media were dispensed into the inner chamber of the transwell insert (in triplicate). The plates were incubated for 5 hours in 5% CO_2 at 37°C. The insert was then removed and any non-migrated cells collected by gently swabbing the inner chamber with a Q-tip and rinsing twice with PBS. Inserts were then submerged in 0.2% crystal violet for 15 mins, washed 3 times with deionized water to remove any residual stain, and allowed to air dry. Cells with migratory abilities able to navigate into the matrigel underlayer were counted under a light microscope. The membranes were carefully divided into a numbered grid to aid in manually counting. The experiment was performed twice and analyzed using GraphPad Prism 7.0.

6.2.3 Transwell Cell Invasion. Corning 24-well plate inserts with an 8 micron diameter pore size were bottom surface-coated with matrigel as described above. 40 µL of matrigel was then dispensed into the inner chamber of the insert and incubated at 37°C for 1 hour to solidify. To each well, 500µL of serum free media was added and then the modified insert returned to the well. 100,000 ES-2 cells in serum free media were gently dispensed into the inner chamber of the transwell insert (in triplicate) so as not to

disrupt the matrigel layer. The plates were incubated for 36 hours in 5% CO_2 at 37°C. The insert was then removed and any non-migrated cells collected by aspiration and gently swabbing the inner chamber with a Q-tip and rinsing twice with PBS. Inserts were then submerged in 0.2% crystal violet for 15 mins, washed 3 times with deionized water to remove any residual stain, and allowed to air dry. Cells with invasive abilities able to navigate through the dense matrigel upperlayer were counted under a light microscope. The membranes were carefully divided into a numbered grid to aid in manual counting. The experiment was performed twice and analyzed using GraphPad Prism 7.0.

6.2.4 Quantitative Real-Time PCR.

qRT-PCR was performed by isolating total RNA and generating cDNA as described previously. PCR was conducted by initial denaturation for 10 min at 95°C followed by 40 cycles of 95°C for 15 sec and 60°C for 1 min using the Fast SYBR® Green (Thermo) with primers designed using IDT PrimerQuest Tool (https://www.idtdna.com/primerquest) for Fibronectin 1 Fwd: 5' – CTGGCCAGTCCTACAACCAG – 3', Fibronectin 1 Rev: 5' – CGGGAATCTTCTCTGTCAGCC – 3', β6-Integrin Fwd: 5' – CAGCGTTGGTCTTGTAACGC – 3', β6-Integrin Rev: 5' – AGTTCTTGCTGTGCAGACCG – 3', ETS-1 Fwd: 5' – TGAGGTGCTGAGAGCAGAATG – 3', ETS-1 Rev: 5' – TAGGTCCTTGCCTCACCACT – 3', Vimentin Fwd: 5' – GTCCGCACATTCGAGCAAAG – 3', Vimentin Rev: 5' – CGCTGCTAGTTCTCAGTGCT – 3', ZEB2 Fwd: 5' – AACACCCCTGGCACAACAAC – 3', and ZEB2 Rev: 5' – AATTGCGGTCTGGATCGTGG – 3' on a ViiA7 (Applied Biosystems, Inc.). To

determine the specificity of the PCR primers, the melting curves were collected by denaturing the products at 95°C, then cooling to 65°C, and then slowly melting at 0.5°/sec up to 95°C.

6.2.5 Western Blot. Cells were collected and lysed in RIPA lysis buffer as described previously. Cell lysates (20 μg) were electrophoresed on 10% SDS-polyacrylamide gels under reducing conditions (167), electroblotted to a polyvinylidene difluoride membrane (168), and blocked with 5% bovine serum albumin (BSA) in Tris buffered saline with 0.1% tween (TBST) for 1 h at room temperature (25°C). Membranes were incubated overnight at 4 °C with 1:1000 anti-human FN1 rabbit polyclonal antibody, anti-human ETS-1 rabbit polyclonal antibody, or anti-human ZEB2 rabbit polyclonal antibody from NeoBioLab (Cambridge, MA) in 5% BSA in TBST. 3% BSA block was used for 1:500 anti-human Vimentin mouse monoclonal antibody from SCBT (Dallas, TX). Secondary antibody was goat anti-rabbit horseradish peroxidase (SCBT) at 1:2000 dilution. Proteins were visualized using Amersham ECL Prime Detection Reagent (GE Healthcare) on a Bio-Rad gel documentation system. Blots were performed in triplicate and densitometry analyses were determined using Quantity One software (Bio-Rad) according to the manufacturer's instructions.

6.3 Cell Migration

Since others have reported CD44 regulating motility in ovarian cancer cells (63, 193), we performed scratch wound healing assays as well as modified Boyden chamber assays to assess migration. The bottoms of the transwell inserts were coated with Matrigel to trap

migrating cells as described in the methods section. The principle behind this assay is that more motile cells will be able to migrate through the filter pores into the Matrigel layer. Thus, based upon previous literature that reduced cell migration was associated with induction of epithelial variant CD44 isoform (197), we expected to see an observable decrease in the number of migratory cells with CD44s silencing. However, we did not observe any significant difference in the migratory ability of ES-2 cells with or without CD44 expression either in wound healing (Figure 32) or transwell (Figure 33) assays. Therefore, we concluded that CD44s does not play a role in the migration of EOC cells in the ES-2 cell culture model.

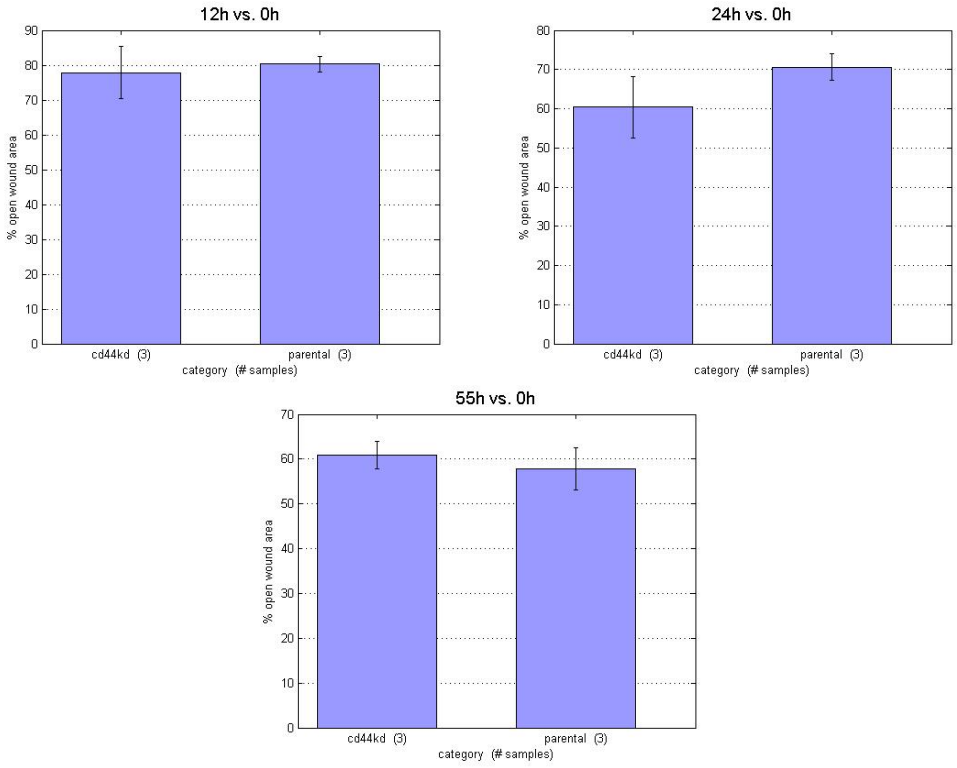

Figure 32. CD44s does not regulate migration in ES-2 cells in wound healing assay. ES-2 cells were plated and grown to confluency, serum starved overnight, and then scratched with a p1000 pipette tip. % of open wound area was measured at 12, 24, and 55 hours. N=3, *p*=n.s. student's t-test, CD44kd=CD44$^{-/-}$ clone 7.

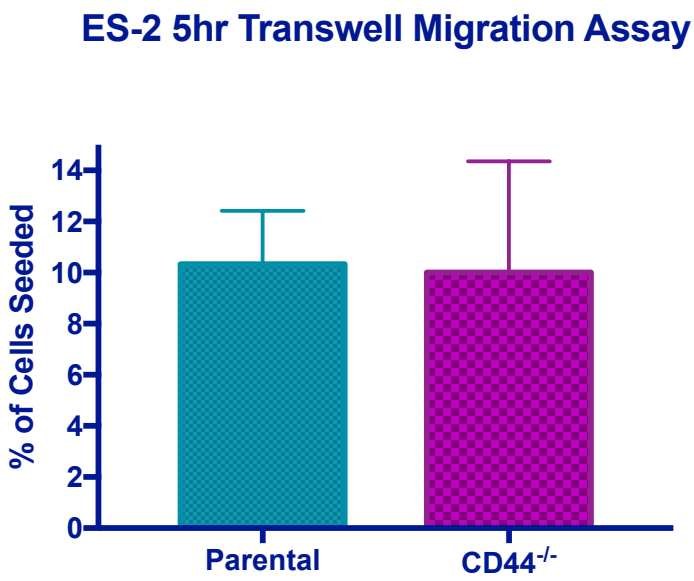

Figure 33. CD44s does not regulate migration in ES-2 cells in transwell migration assay. ES-2 cells were seeded in a modified Boyden chamber and allowed to migrate for 5 hours. % of seeded cells that had migrated through the permeable membrane were stained and counted. N=3, *p*=n.s. student's t-test.

6.4 Cell Invasion

As mentioned already, decades of research have shown that CD44 participates in major oncogenic signaling networks and complexes with oncogenes that promote and regulate every aspect of tumor progression including critical aspects of metastatic disease. However, it is emerging that CD44 may function differently at different stages of cancer progression and may regulate migration and invasion independently. Invasive disease requires epithelial cell penetration of the basement membrane followed by movement through the interstitial ECM. Thus, we sought to do an *in vitro* invasion assay that could simulate cellular movement through such layers. We developed a three-dimensional invasion assay based on a modified Boyden chamber assay. Briefly, a thin layer of undiluted Matrigel was cast over

an 8-µm pore transwell filter. The chamber above the filter was then seeded with ES-2 cells suspended in serum-free medium. In this system, cells must both invade through the gel matrix and migrate through the filter pores as well, a process similar to invasive disease. After 36 hours, the filters were removed and cells that had invaded into the matrix were quantified. However, ES-2 CD44$^{-/-}$ cells displayed similar invasive capacity as parental control cells (Figure 34). Therefore, using ES-2 as a model for epithelial ovarian cancer did not identify a role for CD44s in invasion of EOC cells.

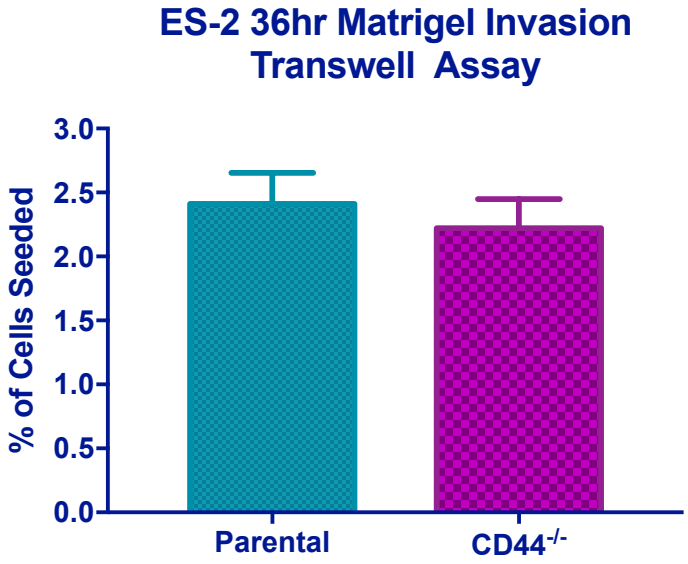

Figure 34. CD44s does not regulate invasion in Matrigel transwell assay. ES-2 cells were seeded in a modified Boyden chamber with a thin layer of Matrigel on top of the permeable membrane. Cells were allowed to invade through the Matrigel for 36 hours. % of seeded cells that had migrated through the permeable membrane were stained and counted. N=3, *p*=n.s., student's t-test.

6.5 EMT

EMT is involved in the acquisition of stemness of epithelial tumor cells, which confers cells with aggressive traits and an invasive phenotype that may result in tumor recurrence and

metastasis. Since CD44 has been shown to promote EMT in many cancer types including ovarian cancer (197), and high CD44s expression in hepatocellular carcinoma was significantly associated with an EMT expression profile (198), we questioned whether CD44s expression might regulate known proteins associated with EMT. We first compared CD44 expression to protein expression of an extensive list of EMT-associate proteins using the TCGA dataset. A subset of 5 proteins exhibiting the highest Pearson and Spearman correlation scores for CD44 co-expression (Table 1) were selected for assessment in ES-2 and SKOV-3 cells. No difference in ETS1 mRNA or protein expression was observed in either ES-2 or SKOV-3 models when CD44 was silenced (Figures 35 and 36). Interestingly, fibronectin, Vimentin, and ZEB2 mRNA levels appear significantly reduced in ES-2 $CD44^{-/-}$ cells (Figure 35, left panel). On the hand, fibronectin and ZEB2 mRNA levels appear significantly increased in SKOV-3 $CD44^{-/-}$ (Figure 25, right panel). However, these apparent changes at the transcriptional level of Vimentin and ZEB2 do not appear to translate into differences in protein amounts of these genes (Figure 36, lower panels). Moreover, the increase in fibronectin mRNA in SKOV-3 did not correspond with an increase in fibronectin protein, and, in fact, SKOV-3 $CD44^{-/-}$ cells exhibited decreased fibronectin protein similar to ES-2 $CD44^{-/-}$ cells (Figure 36, upper left panel). Thus, due to a lack of inconsistency between mRNA and protein changes amongst the two models when CD44 was silenced, it made interpretation of a role for CD44s expression in EMT unmanageable and requiring a more detailed investigation.

Gene	Pearson Score	Spearman Score	*P*-value
Fibronectin 1	0.33	0.36	0.0001
Integrin-β6	0.37	0.35	0.001
ETS1	0.4	0.39	0.057
Vimentin	0.24	0.26	0.053
ZEB2	0.46	0.48	0.661

Table 1. CD44 co-expression correlation scores for top-scoring known EMT genes In TCGA patient samples.

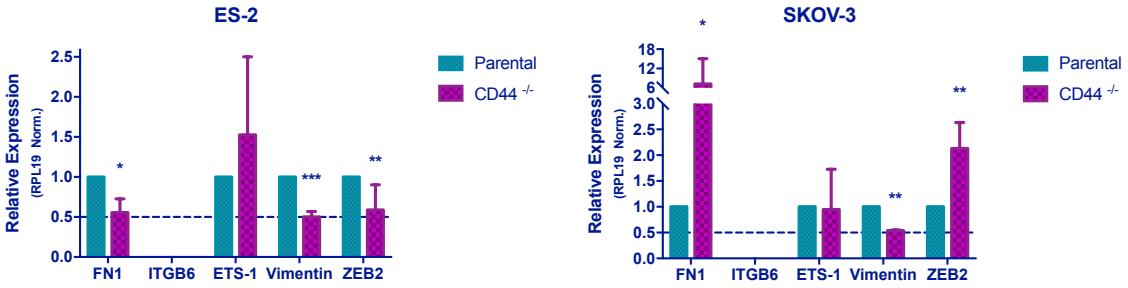

Figure 35. qPCR Analysis for top-scoring EMT proteins co-expressed with CD44. mRNA expression quantified using qRT-PCR for 6 EMT genes in ES-2 (left panel) and SKOV-3 (right panel) cell lines identified as highly co-expressed with CD44 in TCGA patients samples as listed in Table 1. Left panel *p<0.0001, **p=0.0012, ***p=0.0002; Right panel *p=0.0310, **p<0.0001, student's t-test, N=3.

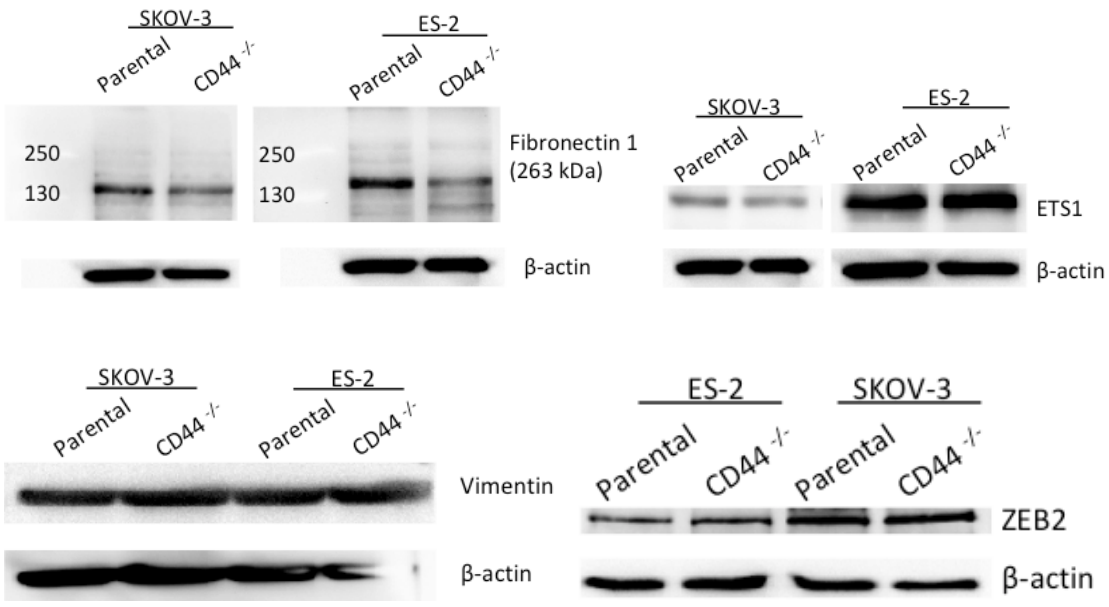

Figure 36. Reduction in fibronectin protein expression in ES-2 CD44$^{-/-}$ EOC cells. Fibronectin 1 (upper left), ETS1 (upper right), vimentin (lower left), and ZEB2 (lower right) protein expression in ES-2 and SKOV-3 cell lines and their CD44$^{-/-}$ clones were determined by western blot analysis. β-actin was used as a loading control for protein. Figure representative of 3 individual replicates.

CHAPTER 7: CD44S IN METASTASIS FORMATION

7.1 Introduction

The previous studies described above provided evidence that silencing CD44s expression decreases proliferation, inhibits spheroid formation, and reduces spheroid adhesion to mesothelial cells *in vitro*. Since these characteristics are associated with tumor formation and metastasis, we questioned whether these effects could impair the ability of cells to develop tumors *in vivo*. Moreover, CD44s-mediated promotion of tumor growth was reported in a melanoma xenograft using an Infusion of soluble recombinant CD44 to compete with endogenous CD44 blocking tumor development (199). Interestingly, siRNA downregulation of CD44 expression suppressed tumor growth and peritoneal dissemination of a human ovarian cancer xenograft in nude mice (200), whereas mice treated with anti-CD44 antibody showed a decrease in the number of total peritoneal ovarian cancer metastases (70). Therefore, because out previous experiments showed that CD44s is required for spheroid formation in ES-2 and cell adhesion to mesothelial cells *in vitro*, we hypothesized that CD44s expression plays a role in the formation of metastases *in vivo*, as well.

The ES-2 line chosen for the present study is derived from a reported clear cell ovarian carcinoma (201), however, has recently been identified to have a genetic profile more closely related to high grade serous carcinoma (HGSOC) (202, 203), the majority of ovarian cancer cases. The reason for using this cell line was that it lends itself easier to transfection

and isogenic clone selection than other ovarian cancer cell lines we have assessed *in vitro* and rapidly forms tumors *in vivo*. Moreover, ES-2 cells generate multifocal peritoneal disease in the same manner HGSOC does thereby justifying its use as a model for carcinoma–mesothelium interactions and disease progression in this disease. We set up a nude mouse xenograft with 4 groups containing 6 mice each injected i.p. with either single cells or spheroids of parental ES-2 and single cells or MCAs of CD44-silenced ES-2. We set up the experiment this way to pursue several goals and answer a few different questions—what is the metastatic potential of single cells versus spheroids of ES-2, and what is the role of CD44s in metastatic formation for both single cells and spheroids by measuring for overall survival and tumor burden.

7.2 Materials & Methods

7.2.1 Animal Study Design.

Athymic nude FOXN1/NU mice were obtained from Harlan Laboratories (Madison, WI). All experimental procedures were performed according to the Institutional Animal Care and Use Committee protocol (#15-252) approved by the Animal Care Committee of UIC. Animals were fed ad libitum and maintained in Association for Assessment and Accreditation of Laboratory Animal Care International approved facilities on a 12 h light 12 h dark cycle. For generation of intraperitoneal tumors, 1×10^6 cells/mouse of parental ES-2 and ES-2 CRISPR-generated CD44 knockout clone were used to generate spheroids or multicellular aggregates (MCA), respectively. Spheroids/MCA were injected intraperitoneally (i.p.) into athymic nude mice (n = 6) and

animals were monitored three times weekly for tumor formation, ascites development, and survival up to 27 days. To generate intraperitoneal tumors from individual cells, 1×10^6 ES-2/mouse were i.p. injected into athymic nude mice (n = 6) and animals were monitored three times weekly for tumor formation, ascites development, and survival up to 24 days. When animals reached humane endpoints, they were sacrificed, dissected, ascites aspirated, and the abdominal region examined for tumors. Tumors were excised, weighed, fixed in paraformaldehyde, and paraffin-preserved as described previously (171) for examination by immunohistochemistry.

7.2.2 Hematoxylin and Eosin Staining. Slides containing paraffin-preserved human tissue sections were rehydrated by incubation in xylenes and graded ethanol solutions followed by incubation in Gill 2 hematoxylin (Thermo Fisher) for 2 mins. Slides were washed in deionized water and then placed in eosin (Sigma-Aldrich) for 30 seconds followed by dehydration in graded ethanols, cleared with xylenes, and mounted with Permount. Stained tissues were evaluated for percent of tumor versus normal tissue and averaged from 3 different 10X fields of view by Andre Kajdacsy-Balla, Osama Elfituri and Hao-Liang Xu (UIC Pathologists), who were blinded to the experimental outcomes of the study.

7.2.3 Western Blot. Cells were collected and lysed in RIPA lysis buffer as described previously. Cell lysates (20 μg) were electrophoresed on 10% SDS-polyacrylamide gels

under reducing conditions (167), electroblotted to a polyvinylidene difluoride membrane (168), and blocked with 10% goat serum in Tris buffered saline with 0.1% tween (TBST) for 1 h at room temperature (25°C). Membranes were incubated overnight at 4 °C with 1:500 anti-human RARRES3 rabbit polyclonal antibody or anti-human RhoGDI2 rabbit polyclonal antibody from Aviva Systems Biology (San Diego, CA) or anti-human CD95 mouse monoclonal antibody from SCBT (Dallas, TX) in 10% goat serum in TBST. Secondary antibody was goat anti-rabbit or anti-mouse horseradish peroxidase (SCBT) at 1:1000 dilution. Proteins were visualized using Amersham ECL Prime Detection Reagent (GE Healthcare) on a Bio-Rad gel documentation system. Blots were performed in triplicate and densitometry analyses were determined using Quantity One software (Bio-Rad) according to the manufacturer's instructions.

7.2.4 Immunohistochemistry. Slides containing paraffin-preserved human tissue sections were rehydrated by incubation in xylenes and graded ethanol solutions followed by blocking of peroxidase activity with 3% H_2O_2 for 10 min. Antigen retrieval was achieved through incubation at 95°C for 15-min in sodium citrate buffer, pH 6.0. After cooling to room temperature, sections were blocked with 10% goat serum in PBS. Primary rabbit anti-human RhoGDI2 antibody and rabbit anti-human-RARRES3 antibody from Aviva Systems Biology (San Diego, CA) was used at 10 µg/ml overnight at 4°C. Primary mouse anti-human CD95 antibody (clone B-10) from Santa Cruz Biotechnology (Dallas, TX) was used at 1:50 dilution overnight at 4°C. Biotin-conjugated goat anti-rabbit or goat anti-mouse secondary antibody was used at a dilution of 1:200 for 20 min at

room temperature. Vectashield avidin-biotin complex and 3,3'-diaminobenzidine reagents were prepared and used as suggested by the manufacturer. Slides were counterstained with hematoxylin, dehydrated and mounted with Permount

7.3 Animal Survival and Tumor Burden

Athymic nude mice were injected intraperitoneally with single cells, spheroids, or multicellular aggregates of ES-2 CD44$^{-/-}$ or parental cells (Figure 37) and monitored for indications of tumor formation and/or ascites production.

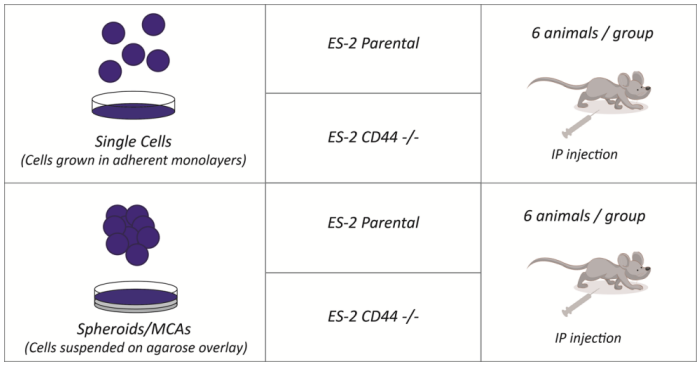

Figure 37. Schematic representation of FOXN1/nu mouse xenograft study design.

There was no difference in overall survival between single cell or spheroid ES-2 parental animals (Figure 38, top left panel) neither was there a difference in survival between CD44 silenced single cells and multi cell aggregate animals either (Figure 38, top right panel), indicating that single cells and spheroids are equally as aggressive in leading to morbidity in these animals. But, when CD44 was silenced, overall survival significantly increased compared to parental regardless of whether they were single cells or spheroid animals

(Figure 38 lower panels). The median survival differences are displayed in Table 2. Since no statistical difference in survival exists between the 2 parental groups nor between the 2 CD44-silenced groups, the single cell and spheroid/MCA groups were combined for further analyses between parental and knockout cells.

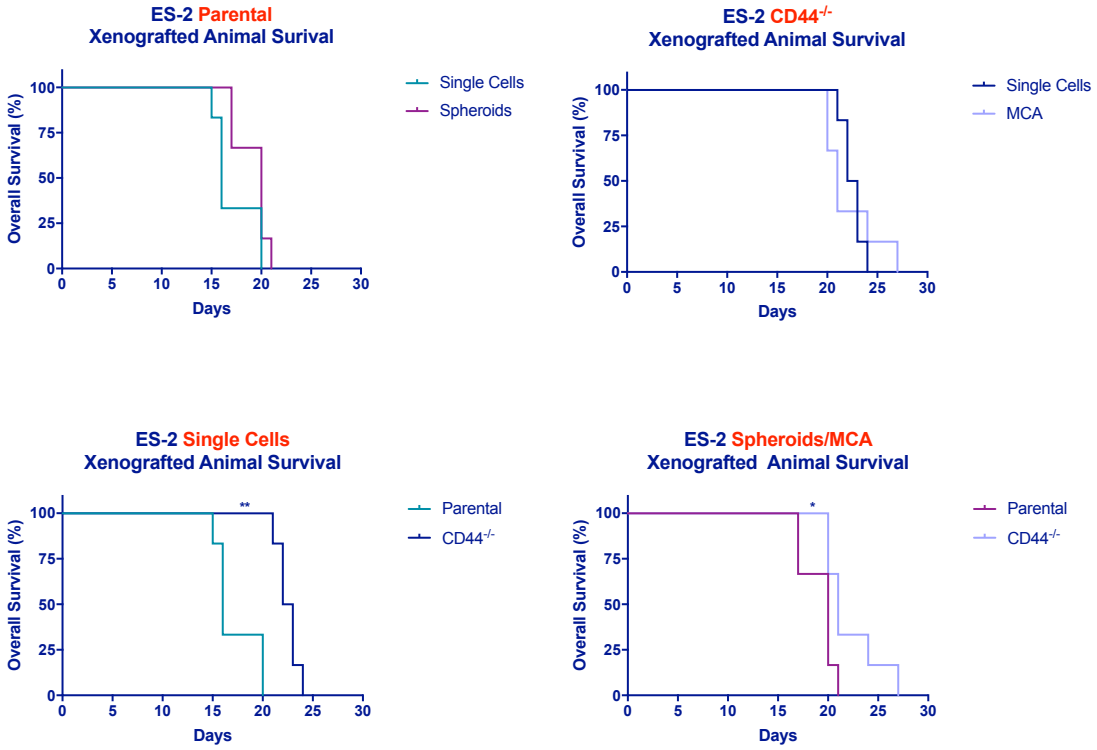

Figure 38. Loss of CD44 increases overall survival *in vivo*. Kaplan-Meier survival curves for ES-2 xenografted mice. Top: Animals with single cells compared to spheroids/MCA in parental or CD44$^{-/-}$; Bottom: CD44$^{-/-}$ compared to parental in single cells or spheroids/MCA. **p<0.001, *p<0.05; log-rank (Mantel Cox) test.

	Median Survival (days)
Parental SC	16
Parental Sph	20
CD44$^{-/-}$ SC	22.5
CD44$^{-/-}$ MCA	21

Table 2. Median overall survival of each animal group.

Next, it was important to try and determine what the underlying factors are which CD44s seems to be playing a role in, in the increased survival of these animals. ES-2 tumor growth and ascites development were observed rapidly, and animals were sacrificed when they appeared clearly morbid. Interestingly, though, we saw that loss of CD44 reduced the amount of ascites produced in these mice (Figure 39, top row, center panel). So although the $CD44^{-/-}$ animals lived 25% longer than parental animals, they exhibited a much lower average volume of ascites production and may, in part, be one of the reasons these animals survived longer as severe abdominal distension in these animals due to ascites build up was a primary reason for euthanasia. However, bowel obstruction by metastatic tumors is the predominant cause of ovarian cancer-related mortality, and tumor burden is often predictive of survival. Nevertheless, no significant difference between total tumor burden was observed between CD44-silenced and parental (Figure 39, top row, left panel).

During metastatic progression, once tumor cells adhere, they need to invade and expand in number in order to establish secondary tumors at metastatic sites. When cancer cells find themselves in the microenvironment of host cell tissues, different tissue types affect them differently so we would expect that growth of secondary lesions that form in each tissue to be different. Since previous findings using a CD44s-expressing cell line showed that in the presence of neutralizing CD44 antibody, implantation of ovarian cancer cells was differentially reduced between the diaphragm and other peritoneal surfaces (70), we hypothesized that CD44s plays a role in metastasis to different secondary sites. We

assessed organ specific tumor burden and observed a significant reduction in mesentery tumor burden with silenced CD44 expression (Figure 39, row 1, right panel). Moreover, although only a subset of animals in each group developed peritoneal wall tumors, the weight of those tumors, which formed, were dramatically reduced with CD44 silencing though not quite reaching statistical significance due to the reduced sample size (Figure 39, row 2, left panel). Interestingly, tumor mass was significantly larger in a number of abdominal organs including the omentum, stomach, and liver (Figure 39). This suggests a growth repressive function for CD44 at these organ sites. No difference was observed in tumor mass in the diaphragm, pancreas, and inguinal lymph nodes (Figure 39). This leads to the conclusion that CD44 expression enhances metastatic tumor growth in the parietal peritoneum (mesentery and peritoneal wall), while suppressing metastatic tumor growth at visceral peritoneum-lined organs (omentum, stomach, and liver). Retroperitoneal metastases (pancreas, kidney, and retroperitoneal fat) appear to be uninfluenced by CD44 expression (Figure 39). Although average kidney tumor weight without CD44 expression was significantly different, standard deviation was relatively high and may not reflect a true significant difference. Finally, extraperitoneal abdominal metastases (diaphragm and inguinal lymph nodes) were also unchanged with CD44 silencing implicating CD44 expression as a key regulator of intraperitoneal metastases—enhancing some and repressing others.

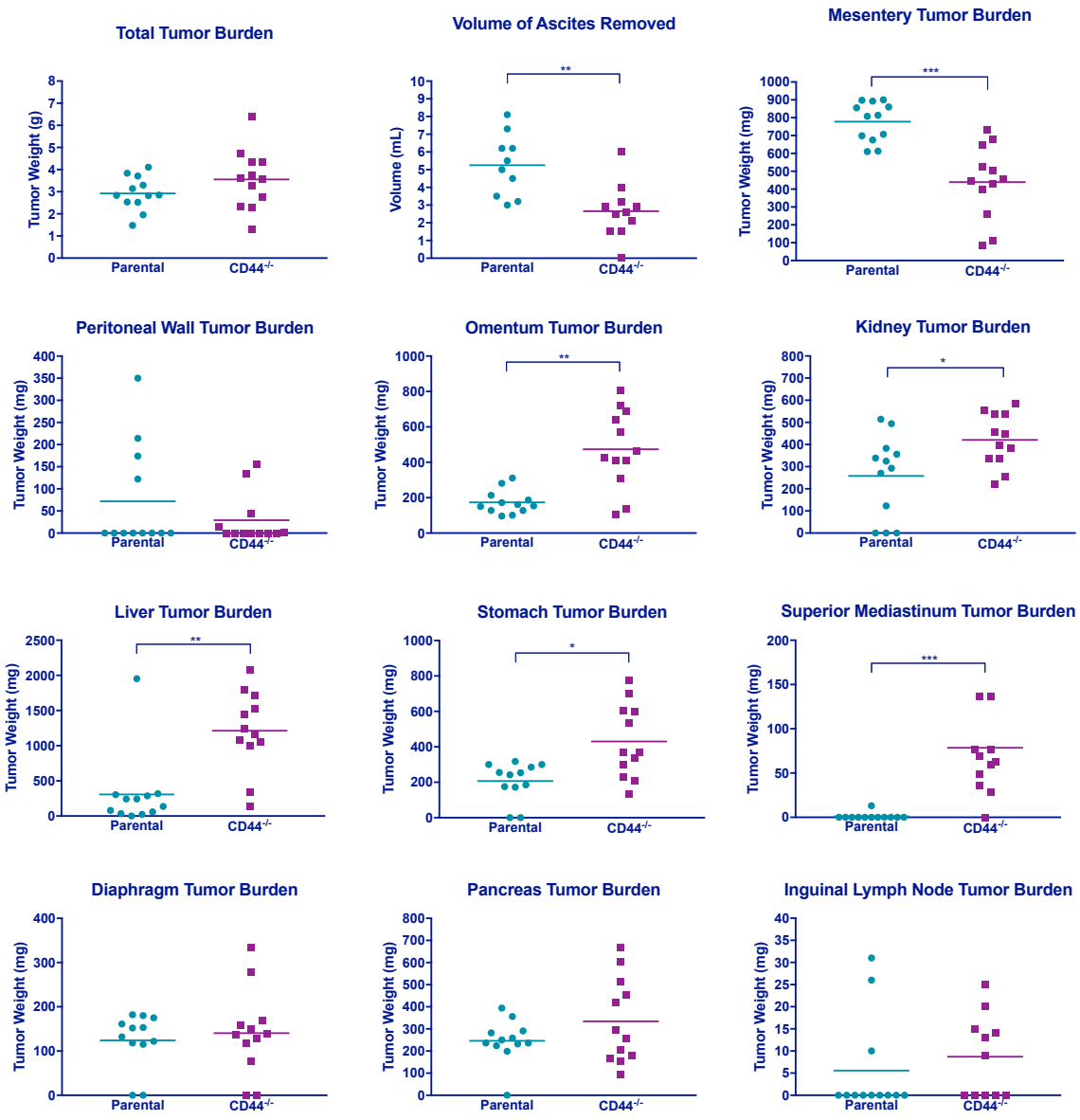

Figure 39. CD44 expression differentially regulates metastasis to peritoneal and thoracic cavity organs. Total tumor burden, volume of ascites removed, and tumor burden at individual sites. N=12; *p<0.05, **p<0.001, ***p<0.0001; Mann-Whitney U.

When we took a closer look at the locations of metastases, we noticed that all, but one animal, with CD44 knockout xenografts, whether single cell or multicellular aggregates, had large tumors growing in the central compartment of the thoracic cavity behind the sternum.

Pathologist Dr. Andre Kajdacsy-Balla, identified them to be tumors of the superior mediastinum (Figure 39, row 3, right panel). Therefore, although parental ES-2 cells seem to be confined to the peritoneal cavity at humane endpoints, these cells appear to now be able to infiltrate the thoracic cavity when expression of CD44 is silenced. What's more is that suppression of CD44s significantly increased the presence of lung metastases as well, both as single cells, but also, and to a greater extent, as multi-cell aggregates (Figure 40). Clinically, HGSOC tumors grow quickly and disseminate widely within the mesothelial cell-covered peritoneal cavity, but also disseminate as an effusion in the mesothelial cell covered pleural space, as well. Thus, CD44s expression acts a suppressor of lung metastases in this model. Therefore, although suppression of CD44s in spheroids reduces peritoneal metastases to a large extent, silencing CD44s enhances metastasis to the lung thereby playing a dual role in metastatic regulation.

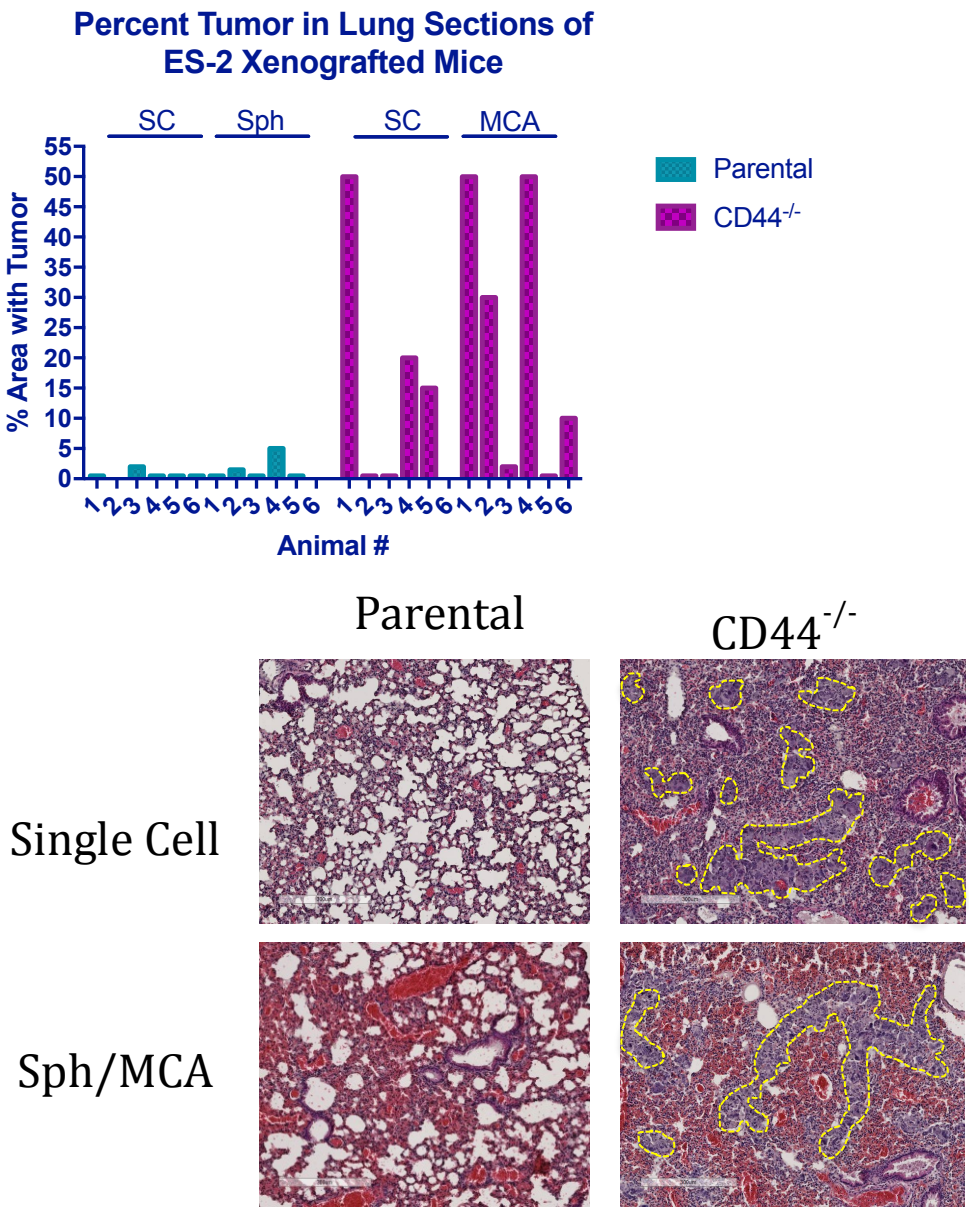

Figure 40. Loss of CD44 increases metastasis to the lungs. Percent area of lung tissue sections displaced by tumor cells (upper panel). H&E staining of mouse lungs representative of each animal group (lower panel). Dotted line indicates tumor areas.

7.4 Putative Lung Metastasis Mechanism

In an effort to understand more mechanistically how CD44s may regulate lung metastasis in EOC, a literature search was completed and a list of 12 reported lung metastases suppressors in cancer was compiled. These proteins were queried for co-expression

correlation in the same TCGA data set described previously. 2 were identified as highly co-expressed with CD44—RhoGDI2 and RARRES3 (Figure 41). The correlation scores and *p*-values are listed in Table 3. Previous studies found that truncated Rho GDP-dissociation inhibitor 2 (RhoGDI2), a cytoplasmic cell signaling regulator, induced pulmonary metastasis, whereas full-length protein did not (204). When RhoGDI2 was transferred back into cells with metastatic ability that lacked its expression, it suppressed experimental lung metastasis (205). Moreover, macrophage-secreted glycoprotein osteopontin in the tumor microenvironment binds to CD44s on bladder cancer cells promoting invasion and clonal growth through CD44s cytoplasmic tail-binding to TIAM1, a Rac guanine nucleotide exchange factor (206). Interestingly, osteopontin, TIAM1, and RhoGDI2 have all been reported to be upregulated in ovarian carcinoma compared to benign tumors (207-209). Thus, this made RhoGDI2 a lead candidate in the signaling of CD44s-regulated lung metastasis in ES-2 mouse xenograft. However, western blot for RhoGDI2 was unchanged in ES-2 $CD44^{-/-}$ cells compared to parental control (Figure 42). Likewise, immunohistochemistry of omental tumors revealed similar intensity of RhoGDI2 protein expression in $CD44^{-/-}$ as parental (Figure 43).

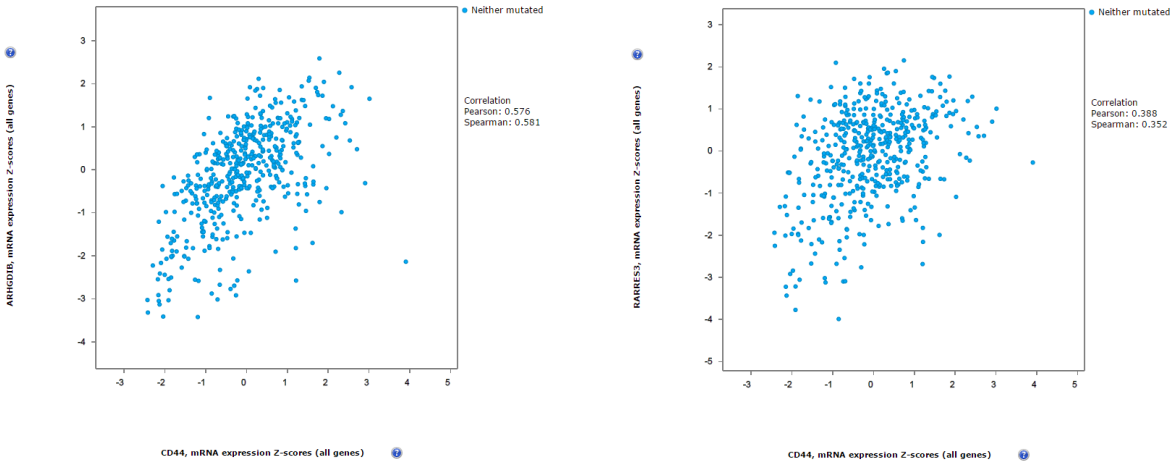

Figure 41. CD44 co-expression correlation plots for top-scoring lung metastasis-related genes. Correlation between expression of CD44 mRNA and Rho Dissociation Inhibitor 2 (RhoGDI2, *ARHGDIB*) mRNA (left panel) and retinoic acid receptor responder 3 (RARRES3) (right panel) in specimens of serous ovarian adenocarcinoma analyzed using cBioportal database and TCGA, Nature 2011, dataset (n=557).

Gene	Pearson Score	Spearman Score	*P*-value
RhoGDI2	0.576	0.581	<0.001
RARRES3	0.388	0.352	0.018

Table 3. CD44 co-expression correlation scores for top-scoring lung metastasis-related genes.

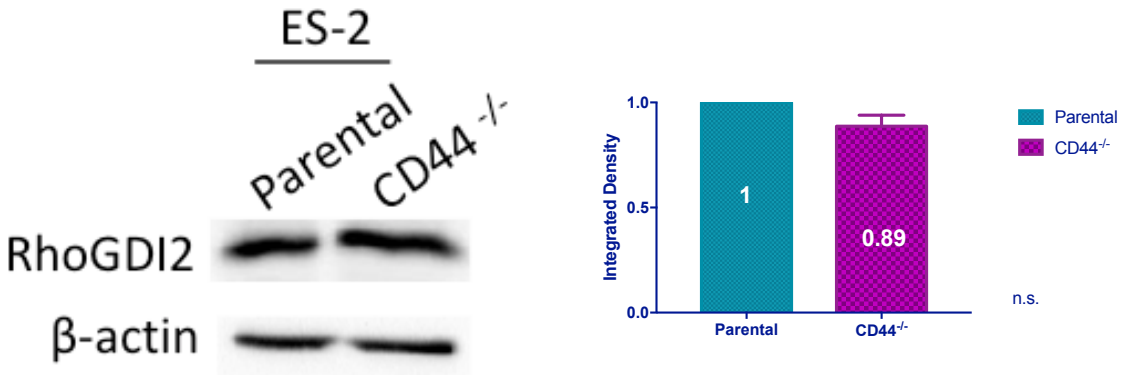

Figure 42. RhoGDI2 protein in ES-2 cells. Expression of RhoGDI2 in ES-2 cells. ACTB was used as a loading control. Images were quantified with digital densitometry using BIO-RAD Chemidoc software. The results of three independent experiments were averaged and plotted.

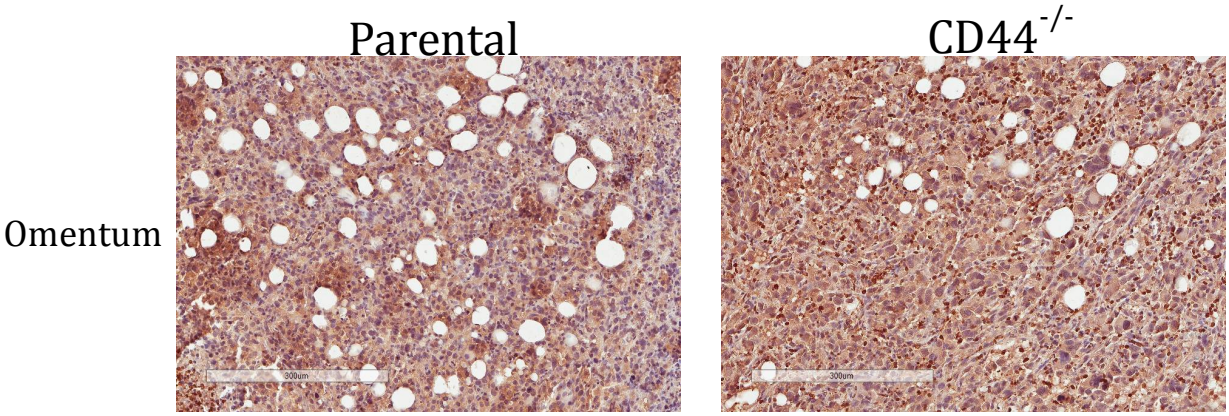

Figure 43. RhoGDI2 protein in omental tumors from ES-2 xenograft. Immunohistochemical staining for RhoGDI2 in omental tumors of $CD44^{-/-}$ compared to parental.

Retinoic Acid Receptor Responder 3 (RARRES3), a small protein responsible for producing signaling lipid secondary messengers (210), but whose function is still widely unknown. It has, however, also been implicated in the regulation of lung metastasis in cancer. RARRES3 downregulation in breast cancer cells facilitated adhesion of tumor cells to the lung parenchyma and formation of lung metastasis (211). Interestingly, western blot for RARRES3 in ES-2 $CD44^{-/-}$ revealed a 36% reduction in expression compared to parental

control (Figure 44). Furthermore, immunohistochemistry in omental tumors similarly displayed reduction in RARRES3 expression (Figure 45, top panels). Importantly, though, the small area of lung tumor we were able to find from ES-2 parental animals exhibited high RARRES3 expression, while CD44$^{-/-}$ tumors in the lung displayed reduced expression of RARRES3 (Figure 45, bottom panels). Thus, CD44s may regulate metastases to the lung in a RARRES3-dependent manner. Though, further studies are needed to better understand a CD44s-RARRES3 signaling axis in EOC.

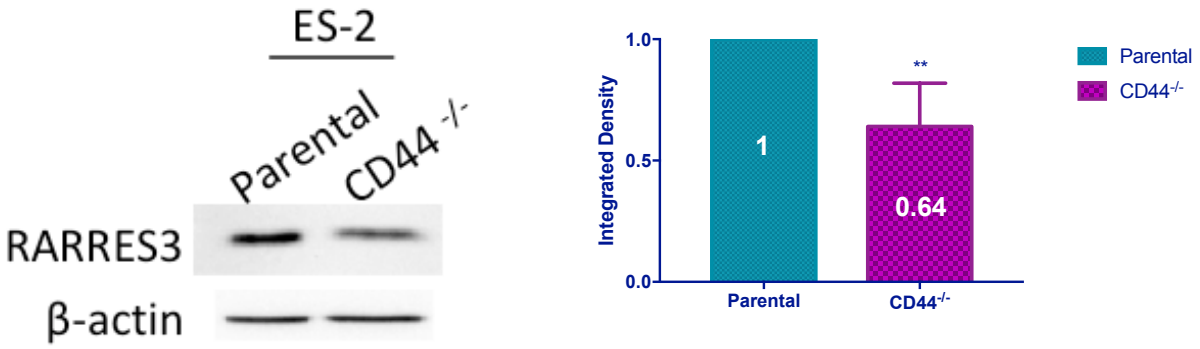

Figure 44. RARRES3 protein in ES-2 cells. Expression of RARRES3 in ES-2 cells. ACTB was used as a loading control. Images were quantified with digital densitometry using BIO-RAD Chemidoc software. The results of six independent experiments were averaged and plotted; ***p*=0.0006, student's t-test.

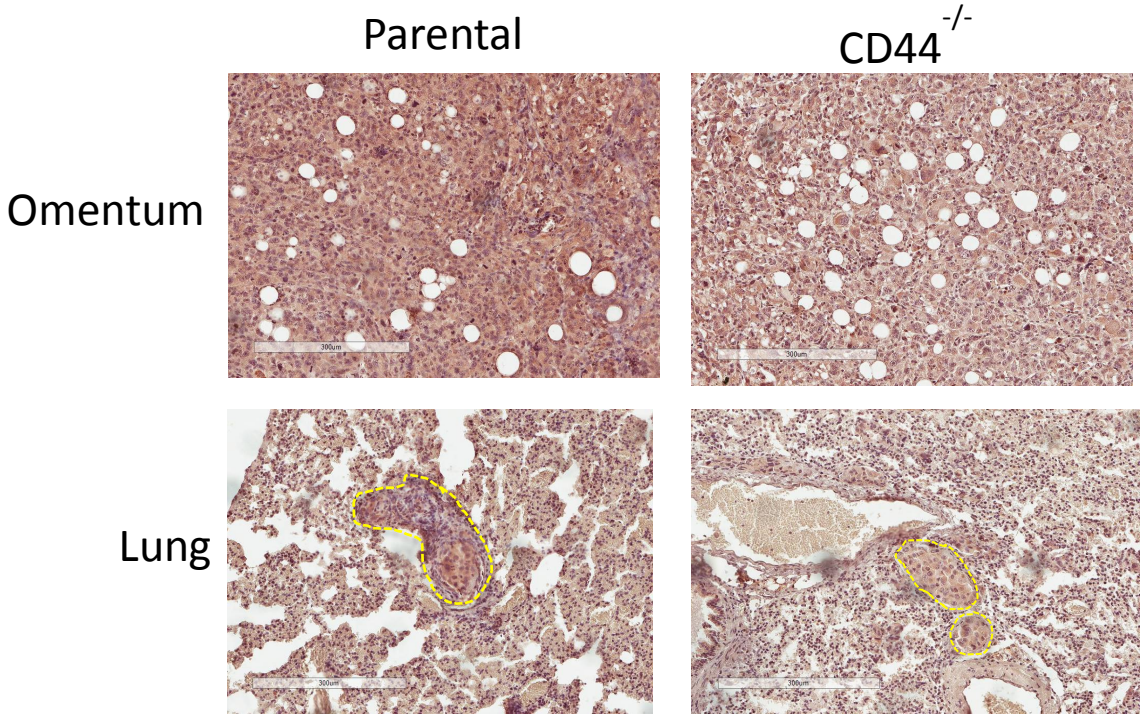

Figure 45. RARRES3 protein in omental and lung tumors from ES-2 xenograft. Immunohistochemical staining for RARRES3 in omental (top) and lung (bottom) tumors of $CD44^{-/-}$ compared to parental.

7.5 Putative Liver Metastasis Mechanism

In an effort to understand more mechanistically how CD44s may regulate liver metastasis in EOC, a literature search was completed and a list of 9 reported liver metastases regulators in cancer was compiled. These proteins were queried for co-expression correlation in the same TCGA data set described previously. One was identified as highly co-expressed with CD44—CD95 (Figure 46). The correlation scores and *p*-value are listed in adjoining table.

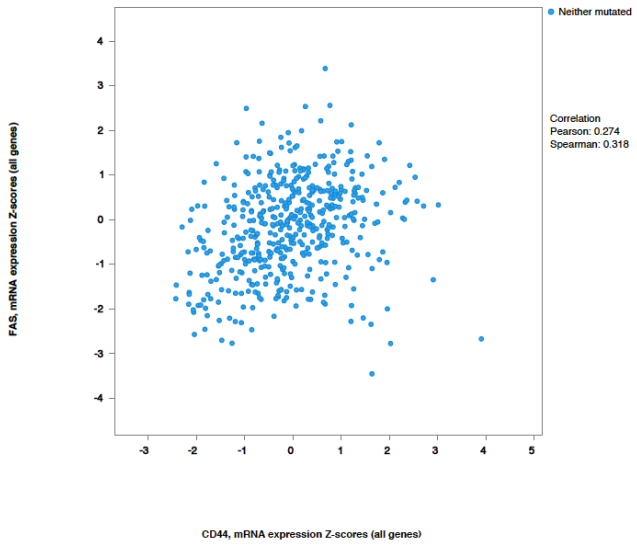

Gene	Pearson Score	Spearman Score	*P*-value
CD95	0.274	0.318	*0.008

Figure 46. CD44 co-expression correlation plot for top-scoring liver metastasis-related gene—CD95. Correlation between expression of CD44 mRNA and CD95 (Fas, APO-1) mRNA in specimens of serous ovarian adenocarcinoma analyzed using cBioportal database and TCGA, Nature 2011, dataset (n=557).

Cluster of Differentiation CD95 (CD95/Apo-1/Fas) receptor-ligand system is one of the key regulators of apoptosis (212) and has also been implicated in the regulation of liver metastasis in cancer (213). Interestingly, western blot for CD95 in ES-2 $CD44^{-/-}$ revealed a 41% reduction in expression compared to parental control (Figure 47). Furthermore, immunohistochemistry in omental tumors similarly displayed reduction in CD95 expression (Figure 48, top panels). Importantly, though, liver metastases present in ES-2 parental animals exhibited high CD95 expression, while $CD44^{-/-}$ tumors in the liver displayed reduced expression of CD95 (Figure 48, bottom panels). Thus, CD44s may regulate metastases to the liver in a CD95-dependent manner. Though, further studies are needed to better understand a CD44s-CD95 signaling axis in EOC.

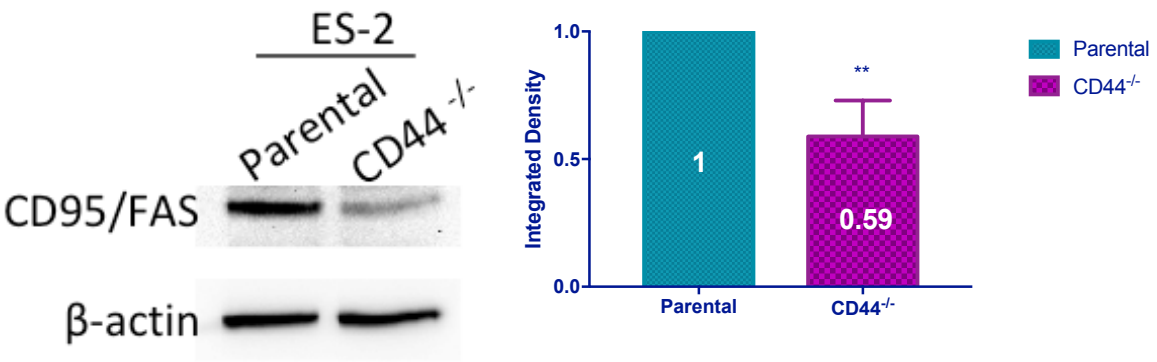

Figure 47. CD95 protein in ES-2 cells. Expression of CD95 in ES-2 cells. ACTB was used as a loading control. Images were quantified with digital densitometry using BIO-RAD Chemidoc software. The results of three independent experiments were averaged and plotted. ***p*=0.0072, student's t-test

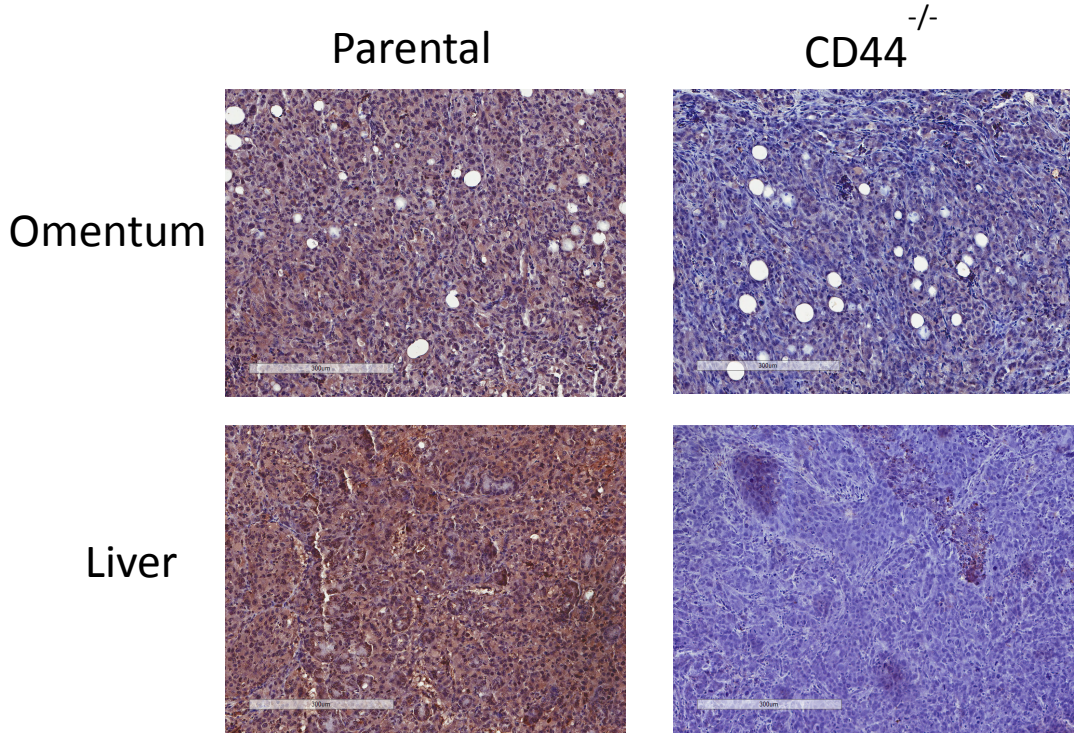

Figure 48. CD95 protein in omental and liver tumors from ES-2 xenograft. Immunohistochemical staining for CD95 in omental (top) and liver (bottom) tumors of $CD44^{-/-}$ compared to parental.

CHAPTER 8: CONCLUSIONS & DISCUSSION

8.1 Summary of results

Multicellular tumor spheroids are excellent *in vitro* models of avascular tumors for understanding cancer biology and metastatic progression. As more evidence continues to implicate CD44s in EOC progression, this work aimed at further characterizing the functional role of CD44s in EOC spheroids and metastatic potential. The concept of CD44 as a cell surface marker for cells with stem-like qualities is largely driven by its association with growth-regulating and metastatic-promoting proteins. The experimental design of this study sought to utilize multiple assays for assessing the role of CD44 in the metastatic cascade. Moreover, use of isoform specific primers provided further evidence for the specific isoform responsible for the observed phenotype in this model of EOC.

Data presented in chapter 3 assessed spheroid formation capacity in cell lines with varying expression of CD44s and variant isoforms, which suggested a potential correlation between CD44s expression with larger spheroids and a higher number of cells forming spheroids. Silencing CD44 expression using CRISPR/CAS9 reduced spheroid formation in SKOV-3 cells and entirely eliminated spheroid formation in ES-2 cells—both primarily CD44s-expressing cell lines. Moreover, although expression of CD44 seemed to promote formation of a pericellular sheath in SEM images of ES-2 parental spheroids, this was unable to be confirmed using available technology or with a 2D culture assay. Nonetheless, whether through a decrease in cell-cell adhesions, loss of pericellular sheath formation, or both, silencing CD44 in ES-2 cells prohibited them from forming the compact multicellular

spheroid structure. This lack in ability to form spheroids was hypothesized, then, to alter either EOC cancer cell survival or metastatic regulation *in vivo*.

While adhesion of cancer cells to each other is certainly important for formation of the spheroid and, ultimately, cell survival, CD44 can also function as an adhesion molecule for cancer cells to other cells types encountered at different steps of the metastatic cascade. The experimental set up in chapter 4 aimed at evaluating the affect on adhesion of CD44s in ES-2 cells to a monolayer of primary mesothelial cells of the peritoneum. These studies in ES-2 cells and spheroids revealed significant reductions in adhesion to LP-3 mesothelial monolayers when CD44 was either function-neutralized with an antibody or silenced in $CD44^{-/-}$ cells. Further clonogenic and proliferation studies described in chapter 5 also revealed a substantial reduction in cell proliferation when expression of CD44 was silenced.

Other known functions of CD44 were examined to comprehensively assess the function of CD44s in EOC cells. As a transmembrane protein recognized for relaying extracellular signals to intracellular signal transducers directing cytoskeletal changes for motility and invasion, it was crucial to characterize the role of CD44s in migration, invasion, and EMT, as well. Chapter 6 experimental design sought to evaluate CD44s in migrating and invading ES-2 cells, while also evaluating expression changes in EMT proteins upon CD44 knockout. However, no significant differences were observed in migration or invasion through Matrigel of ES-2 cells with or without CD44 expression. Moreover, the only EMT-associated protein altered with knockout of CD44s expression was fibronectin (FN). A reduction in

fibronectin with silencing of CD44 may suggest a less mesenchymal phenotype in ES-2 cells lacking CD44s expression, but it is inconclusive on its own without other apparent mesenchymal protein alterations. It's been shown in several cell types that fibronectin interaction with β1-integrin is required for spheroid formation (170, 214). Studies in ovarian cancer have suggested that reduced expression of β1-integrin co-receptors contributes to decreased capacity for spheroid formation by influencing FN matrix assembly and contractile capacity (215). Thus, CD44s-regulated fibronectin expression may have an important role in spheroid formation in conjunction with CD44. It is known, also, that loss of cell surface FN is correlated with the acquisition of metastatic potentials (216). Interestingly, a breast cancer model highly metastatic to the lung showed little FN expression (217) in the tumor ECM compared to the less metastatic variant from which it was derived (218, 219). Therefore, CD44s-downregulation of fibronectin expression may also play a role in enhancing the observed metastasis to the lungs.

Characterization of CD44s function *in vitro* led to the understanding that it predominately functions in enhancing growth and proliferation and in the adhesion of cancer cells to one another in three-dimensional spheroids. Yet, its affect on the formation of metastases and overall survival *in vivo* was critical for fully elucidating the functional role of CD44s in the metastatic potential of EOC cells. Chapter 7 evaluated CD44s expression in a mouse xenograft of EOC, where cells and spheroids expressing CD44s and with CD44s silenced were injected intraperitoneally and animals monitored for tumor development and ascites formation along with overall survival. It was evident that CD44s enhanced metastases to

certain peritoneal sites including the mesentery, while suppressing metastases to other peritoneal sites including the omentum and liver. This may be due to different extracellular matrix compositions, including amount and size of hyaluronan, at each tissue site where CD44 my promote tumor cell adhesion and growth at some sites while preventing it at other sites. The reduction in metastasis to the mesentery with CD44 knockout observed *in vivo* correlates with the reduction in adhesion to LP-3 monolayer observed *in vitro* as this organ is a continuation of the visceral and parietal peritoneum in the abdominal cavity consisting only of a double layer of mesothelium. The omentum, on the other hand, is a much more complex organ composed of two mesothelial sheets enclosing predominantly adipocytes as well as a variety of different immune cells embedded in a loose connective tissue (220). Therefore, the omentum may provide a better tissue microenvironment for metastatic ovarian cancer cells lacking CD44s expression to proliferate and grow once initially adhered to the mesothelium.

Furthermore, our *in vivo* data showed an increase in metastasis to the liver, as well, with CD44 knockout. Additional experiments suggested a CD44-dependent role for CD95/Fas expression in the regulation of liver metastases in this model where silencing CD44s consequently reduced CD95 expression, a pathway with a known role in suppression of metastasis to the liver in other cancer types, as well (213). The CD95 (Apo-1/Fas) receptor-ligand system is one of the key regulators of apoptosis (212). During cancer progression CD95 is frequently downregulated or cells are rendered apoptosis resistant (221, 222) raising the possibility that loss of CD95 is part of a mechanism for tumor evasion (223).

Moreover, it has been reported that loss of CD95 and gain of CD95L expression vary as a function of the degree of dedifferentiation in malignant cells (224), and loss of CD95 expression during dedifferentiation resulted in loss of sensitivity to apoptosis in dedifferentiated breast cancer cells (225). It was reported in a mouse model of melanoma that loss of Fas function was both necessary and sufficient for metastatic development (226), while CD95 ligand (CD95L/FASL) expression at the margin of colorectal liver metastases induces apoptosis in surrounding $CD95^+$ hepatocytes, facilitating the invasion of the tumor into the surrounding liver parenchyma (213). Based on these reports and our data presented here, one mechanism by which ovarian cancer cells may metastasize to the liver involves CD44-dependent downregulation of CD95 so as to reduce sensitivity to FASL and apoptosis during invasion of the tumor into liver parenchyma.

Additionally, loss of CD44s expression had a profound impact on the formation of distant metastases to the lungs and superior mediastinum, while reducing ascites production. Increased metastasis to the superior mediastinum could be due to the enhanced binding of tumor cells lacking CD44 expression with the visceral pleural mesothelium lining the lung (227). Additional experiments suggested a CD44-dependent role for RARRES3 in the regulation of lung metastases in this model where silencing CD44s consequently reduced RARRES3 expression, whose expression is known to suppress pulmonary metastases in other cancer types (228, 229). RARRES3 is a small protein with phospholipase $A_{1/2}$ ($PLA_{1/2}$) activity, responsible for producing signaling lipid secondary messengers in the form of arachidonic and eicosanoid derivatives (210). Interestingly, RARRES3 has also been

identified as a retinoic acid responder gene, and its expression was proposed to cause G_0 growth arrest in breast cancer cells (230). However, it has also been shown that RARRES3 protein inhibits breast cancer metastasis to the lung by blocking adhesion to the lung parenchyma and by stimulating differentiation attributes through its phospholipase activity, thereby blunting metastasis-initiating functions at the lung required to establish a lesion (211). Other studies in breast cancer have provided evidence that RARRES3 targets and modulates acylation of Wnt proteins resulting in suppression of EMT and cancer stem cell properties (231). Studies in colorectal cancer (CRC) revealed an interaction between RARRES3 and metadherin (MTDH) in an opposite way so as to convert CRC cells from a mesenchymal to an epithelial state for suppressing metastasis to the lung (229). Moreover, RARRES3 (alternatively known as RIG1 or TIG3) was demonstrated to downregulate p185 and its downstream PI3K/Akt/mTOR/ VEGF-signaling pathway in ovarian cancer (232). Thus, one could speculate from these reports that reduced RARRES3 expression in this model of ovarian cancer may drive a less differentiated or more mesenchymal phenotype through either regulation of Wnt signaling, metadherin, or mTOR pathways thereby modulating the ability of metastatic tumor cells to specifically attach to the lung parenchyma, which may explain the specific differences observed in lung extravasation capacity. Reduction of RARRES3 expression favored the adhesion of $CD44^{-/-}$ EOC cells to extracellular matrix proteins of the lung. The dense vascular surface area of the lung makes it a particularly attractive microenvironment for supporting the outgrowth of metastases. While the lung parenchyma is composed mainly of Types I and III collagen, elastin, fibronectin, proteoglycans, and glycosaminoglycans (233, 234), the brain extracellular matrix, for

example, has a unique composition, and matrix proteins common in other tissues are virtually absent in the brain (235). In addition to extravasation and homing through an endothelial cellular layer and to a specific matrix, the blood–brain barrier (BBB) may be a limiting step for cell colonization of the brain (236). Thus, CD44-dependent RARRES3 expression may preclude metastasis to the lung in EOC by sustaining some level of differentiation and lack of lung extravasation capacity.

Based on this information, one could conclude that the CD44s isoform functions distinctly from variant isoforms in ovarian cancer metastasis by not only regulating growth and proliferation of EOC cells, but also formation of tumor cell spheroids. As cell growth and anchorage-independent survival are prerequisites for successful formation of distant metastases, this implies an important role for CD44s in disease progression. Loss of CD44s may contribute to reduced cell-cell adhesion as well as adhesion of cell to basement membrane, facilitating detachment of tumor cells from primary sites and penetration into lymph–vascular spaces (237). Moreover, CD44s-regulation of fibronectin, RARRES3, and CD95 expression uncovers suggestive mechanisms for promoting metastasis to distinct sites including the lung and liver.

In conclusion, this dissertation is an account of the novel mechanism for CD44s in epithelial ovarian cancer spheroids highlighting specific functions in spheroid formation, cell proliferation, and suppression of lung and liver metastasis.

8.2 Significance of findings

Disruption of key initial steps of EOC dissemination in the peritoneum, such as peritoneal adhesion, is required to prevent metastatic spread and recolonization. The acquired data, however, shows that CD44s has an important, yet dual, function in promoting metastasis to certain peritoneal organs while suppressing metastasis to others, including distant thoracic sites. Compared with other gynecologic malignancies, the rate of thoracic metastases in ovarian cancer is high and the reported rates of pulmonary metastases in ovarian cancer vary from 1% to 34% (238). Most patients having pulmonary metastases initially present with advanced stage disease. Since nearly all patients also have intra-abdominal disease, the presence of pulmonary metastases indicates that the spread of ovarian cancer into the systemic circulation most likely occurs after intra-abdominal disease has been established (238). Therefore, if CD44s is used as a target for therapeutic management of peritoneal disease in EOC, the findings presented here suggest inevitable development of lung metastases and disease progression. This study supplements the evidence that reduced CD44 expression facilitates formation of pulmonary metastases previously shown in an osteosarcoma xenograft (239) and a transgenic mouse model of breast cancer (240), but now in the EOC xenograft study reported here. Moreover, data presented here also provides evidence that reduced CD44s expression facilitates formation of liver metastases in EOC previously reported, also, in colorectal (241, 242) and breast cancer (243). Thus, therapeutically targeting CD44s would appear to be a promising target for managing ovarian cancer abdominal metastasis, but a poor target for inhibiting distant lung metastases. This raises further questions regarding the underlying mechanisms and the

relevance of CD44 as a therapeutic target in EOC, as well as the likelihood of controlling clinically relevant phenomena of metastasis and resistance to treatment. Better understanding of the signaling pathways involved in CD44s regulation of peritoneal and lung metastases in EOC may lead to development of more rational treatment approaches.

8.3 Recommendations for future work

Having identified a significant role for CD44s in EOC cells and spheroids by regulating spheroid formation, proliferation, mesothelial adhesion, and formation of lung metastases, this work could serve as a starting point for several follow-up studies.

- ESRP1 Overexpression: mRNA splicing factor ESRP1 is known to directly regulate expression of CD44 splice variants, favoring the expression of the epithelial isoforms along with the downregulation of CD44s isoform during lung metastasis in breast cancer (244). Whether isoform switching from CD44s to CD44v via ESRP1 protein overexpression would also reduce spheroid formation and enhance lung metastasis of CD44s-high expressing cell lines would be worth exploring.

- Chemosensitivity Characterization: Cells in spheroids are known for having increased chemoresistance and others have showed CD44s-overexpressing cells to upregulate efflux transporters (195). It would be interesting to assess any role of CD44s in chemosensitivity of EOC cells and whether changes in CD44s isoform expression might affect drug toxicity.

- Other Significant Expression Changes: It is quite likely that there are more proteins with altered expression from CD44 silencing similar to RARRES3. A broad profiling analysis of altered gene expression in $CD44^{-/-}$ cells may provide additional understanding on phenotypic changes when CD44s expression is silenced besides those explored in this study.

CITED LITERATURE

1. Siegel RL, Miller KD, Jemal A. Cancer Statistics, 2017. CA Cancer J Clin. 2017;67(1):7-30.
2. Howlader N NA, Krapcho M, Miller D, Bishop K, Kosary CL, Yu M, Ruhl J, Tatalovich Z, Mariotto A, Lewis DR, Chen HS, Feuer EJ, Cronin KA (eds). . SEER Cancer Statistics Review, 1975-2014 Bethesda, MD: National Cancer Institute; 2017 [Available from: https://seer.cancer.gov/csr/1975_2014/.
3. Yeung TL, Leung CS, Yip KP, Au Yeung CL, Wong ST, Mok SC. Cellular and molecular processes in ovarian cancer metastasis. A Review in the Theme: Cell and Molecular Processes in Cancer Metastasis. American journal of physiology Cell physiology. 2015;309(7):C444-56.
4. Roett MA, Evans P. Ovarian cancer: an overview. American family physician. 2009;80(6):609-16.
5. Marchetti C, Pisano C, Facchini G, Bruni GS, Magazzino FP, Losito S, et al. First-line treatment of advanced ovarian cancer: current research and perspectives. Expert Rev Anticancer Ther. 2010;10(1):47-60.
6. Berek JS, Crum C, Friedlander M. Cancer of the ovary, fallopian tube, and peritoneum. International journal of gynaecology and obstetrics: the official organ of the International Federation of Gynaecology and Obstetrics. 2015;131 Suppl 2:S111-22.
7. Franceschi S, Parazzini F, Negri E, Booth M, La Vecchia C, Beral V, et al. Pooled analysis of 3 European case-control studies of epithelial ovarian cancer: III. Oral contraceptive use. Int J Cancer. 1991;49(1):61-5.
8. Negri E, Franceschi S, Tzonou A, Booth M, La Vecchia C, Parazzini F, et al. Pooled analysis of 3 European case-control studies: I. Reproductive factors and risk of epithelial ovarian cancer. Int J Cancer. 1991;49(1):50-6.
9. Struewing JP, Hartge P, Wacholder S, Baker SM, Berlin M, McAdams M, et al. The risk of cancer associated with specific mutations of BRCA1 and BRCA2 among Ashkenazi Jews. N Engl J Med. 1997;336(20):1401-8.
10. Risch HA, McLaughlin JR, Cole DE, Rosen B, Bradley L, Fan I, et al. Population BRCA1 and BRCA2 mutation frequencies and cancer penetrances: a kin-cohort study in Ontario, Canada. J Natl Cancer Inst. 2006;98(23):1694-706.
11. Chetrit A, Hirsh-Yechezkel G, Ben-David Y, Lubin F, Friedman E, Sadetzki S. Effect of BRCA1/2 mutations on long-term survival of patients with invasive ovarian cancer: the national Israeli study of ovarian cancer. J Clin Oncol. 2008;26(1):20-5.
12. Medeiros F, Muto MG, Lee Y, Elvin JA, Callahan MJ, Feltmate C, et al. The tubal fimbria is a preferred site for early adenocarcinoma in women with familial ovarian cancer syndrome. The American journal of surgical pathology. 2006;30(2):230-6.
13. Buys SS, Partridge E, Black A, Johnson CC, Lamerato L, Isaacs C, et al. Effect of screening on ovarian cancer mortality: the Prostate, Lung, Colorectal and Ovarian (PLCO) Cancer Screening Randomized Controlled Trial. Jama. 2011;305(22):2295-303.
14. Bankhead CR, Kehoe ST, Austoker J. Symptoms associated with diagnosis of ovarian cancer: a systematic review. BJOG : an international journal of obstetrics and gynaecology. 2005;112(7):857-65.
15. Lataifeh I, Marsden DE, Robertson G, Gebski V, Hacker NF. Presenting symptoms of epithelial ovarian cancer. The Australian & New Zealand journal of obstetrics & gynaecology. 2005;45(3):211-4.
16. Eastman A. The formation, isolation and characterization of DNA adducts produced by anticancer platinum complexes. Pharmacology & therapeutics. 1987;34(2):155-66.
17. Pinto AL, Lippard SJ. Binding of the antitumor drug cis-diamminedichloroplatinum(II) (cisplatin) to DNA. Biochimica et biophysica acta. 1985;780(3):167-80.

18. Siddik ZH. Cisplatin: mode of cytotoxic action and molecular basis of resistance. Oncogene. 2003;22(47):7265-79.
19. Lokich J, Anderson N. Carboplatin versus cisplatin in solid tumors: an analysis of the literature. Annals of oncology : official journal of the European Society for Medical Oncology. 1998;9(1):13-21.
20. Jordan MA, Wilson L. Microtubules as a target for anticancer drugs. Nat Rev Cancer. 2004;4(4):253-65.
21. Fuchs DA, Johnson RK. Cytologic evidence that taxol, an antineoplastic agent from Taxus brevifolia, acts as a mitotic spindle poison. Cancer treatment reports. 1978;62(8):1219-22.
22. Schiff PB, Horwitz SB. Taxol stabilizes microtubules in mouse fibroblast cells. Proc Natl Acad Sci U S A. 1980;77(3):1561-5.
23. Lengyel E. Ovarian Cancer Development and Metastasis. The American journal of pathology. 2010;177(3):1053-64.
24. Rossi L, Verrico M, Zaccarelli E, Papa A, Colonna M, Strudel M, et al. Bevacizumab in ovarian cancer: A critical review of phase III studies. Oncotarget. 2017;8(7):12389-405.
25. Pujade-Lauraine E, Ledermann JA, Selle F, Gebski V, Penson RT, Oza AM, et al. Olaparib tablets as maintenance therapy in patients with platinum-sensitive, relapsed ovarian cancer and a BRCA1/2 mutation (SOLO2/ENGOT-Ov21): a double-blind, randomised, placebo-controlled, phase 3 trial. The Lancet Oncology. 2017;18(9):1274-84.
26. Luvero D, Milani A, Ledermann JA. Treatment options in recurrent ovarian cancer: latest evidence and clinical potential. Therapeutic advances in medical oncology. 2014;6(5):229-39.
27. Ushijima K. Treatment for recurrent ovarian cancer-at first relapse. J Oncol. 2010;2010:497429.
28. Kurman RJ, Shih Ie M. The Dualistic Model of Ovarian Carcinogenesis: Revisited, Revised, and Expanded. The American journal of pathology. 2016;186(4):733-47.
29. Labidi-Galy SI, Papp E, Hallberg D, Niknafs N, Adleff V, Noe M, et al. High grade serous ovarian carcinomas originate in the fallopian tube. Nat Commun. 2017;8(1):1093.
30. Cho KR, Shih Ie M. Ovarian cancer. Annual review of pathology. 2009;4:287-313.
31. Silverberg SG. Histopathologic grading of ovarian carcinoma: a review and proposal. International journal of gynecological pathology : official journal of the International Society of Gynecological Pathologists. 2000;19(1):7-15.
32. Marsh DJ, Shah JS, Cole AJ. Histones and their modifications in ovarian cancer - drivers of disease and therapeutic targets. Front Oncol. 2014;4:144.
33. Crum CP, Drapkin R, Miron A, Ince TA, Muto M, Kindelberger DW, et al. The distal fallopian tube: a new model for pelvic serous carcinogenesis. Current opinion in obstetrics & gynecology. 2007;19(1):3-9.
34. Tan DSP, Agarwal R, Kaye SB. Mechanisms of transcoelomic metastasis in ovarian cancer. The Lancet Oncology. 2006;7(11):925-34.
35. Eisenkop SM, Spirtos NM. The clinical significance of occult macroscopically positive retroperitoneal nodes in patients with epithelial ovarian cancer. Gynecol Oncol. 2001;82(1):143-9.
36. Cormio G, Rossi C, Cazzolla A, Resta L, Loverro G, Greco P, et al. Distant metastases in ovarian carcinoma. Int J Gynecol Cancer. 2003;13(2):125-9.
37. Colombo N, Van Gorp T, Parma G, Amant F, Gatta G, Sessa C, et al. Ovarian cancer. Critical reviews in oncology/hematology. 2006;60(2):159-79.
38. Cannistra SA. Cancer of the ovary. N Engl J Med. 2004;351(24):2519-29.
39. Shield K, Ackland ML, Ahmed N, Rice GE. Multicellular spheroids in ovarian cancer metastases: Biology and pathology. Gynecol Oncol. 2009;113(1):143-8.
40. Naora H, Montell DJ. Ovarian cancer metastasis: integrating insights from disparate model organisms. Nat Rev Cancer. 2005;5(5):355-66.

41. Allen HJ, Porter C, Gamarra M, Piver MS, Johnson EA. Isolation and morphologic characterization of human ovarian carcinoma cell clusters present in effusions. Experimental cell biology. 1987;55(4):194-208.
42. Kantak SS, Kramer RH. E-cadherin regulates anchorage-independent growth and survival in oral squamous cell carcinoma cells. The Journal of biological chemistry. 1998;273(27):16953-61.
43. Patel IS, Madan P, Getsios S, Bertrand MA, MacCalman CD. Cadherin switching in ovarian cancer progression. Int J Cancer. 2003;106(2):172-7.
44. Waleh NS, Gallo J, Grant TD, Murphy BJ, Kramer RH, Sutherland RM. Selective down-regulation of integrin receptors in spheroids of squamous cell carcinoma. Cancer research. 1994;54(3):838-43.
45. Islam S, Kim JB, Trendel J, Wheelock MJ, Johnson KR. Vimentin expression in human squamous carcinoma cells: relationship with phenotypic changes and cadherin-based cell adhesion. Journal of cellular biochemistry. 2000;78(1):141-50.
46. Kim YJ, Sauer C, Testa K, Wahl JK, Svoboda RA, Johnson KR, et al. Modulating the strength of cadherin adhesion: evidence for a novel adhesion complex. J Cell Sci. 2005;118(Pt 17):3883-94.
47. Gumbiner BM. Cell adhesion: the molecular basis of tissue architecture and morphogenesis. Cell. 1996;84(3):345-57.
48. Shield K, Riley C, Quinn MA, Rice GE, Ackland ML, Ahmed N. Alpha2beta1 integrin affects metastatic potential of ovarian carcinoma spheroids by supporting disaggregation and proteolysis. J Carcinog. 2007;6:11.
49. Burleson KM, Casey RC, Skubitz KM, Pambuccian SE, Oegema TR, Jr., Skubitz AP. Ovarian carcinoma ascites spheroids adhere to extracellular matrix components and mesothelial cell monolayers. Gynecol Oncol. 2004;93(1):170-81.
50. Hagemann T, Robinson SC, Thompson RG, Charles K, Kulbe H, Balkwill FR. Ovarian cancer cell-derived migration inhibitory factor enhances tumor growth, progression, and angiogenesis. Molecular cancer therapeutics. 2007;6(7):1993-2002.
51. L'Esperance S, Bachvarova M, Tetu B, Mes-Masson AM, Bachvarov D. Global gene expression analysis of early response to chemotherapy treatment in ovarian cancer spheroids. BMC genomics. 2008;9:99.
52. Makhija S, Taylor DD, Gibb RK, Gercel-Taylor C. Taxol-induced bcl-2 phosphorylation in ovarian cancer cell monolayer and spheroids. Int J Oncol. 1999;14(3):515-21.
53. Hamilton CA, Maxwell GL, Chernofsky MR, Bernstein SA, Farley JH, Rose GS. Intraperitoneal bevacizumab for the palliation of malignant ascites in refractory ovarian cancer. Gynecol Oncol. 2008;111(3):530-2.
54. Ween MP, Oehler MK, Ricciardelli C. Role of Versican, Hyaluronan and CD44 in Ovarian Cancer Metastasis. Int J Mol Sci. 2011;12(2):1009-29.
55. Glimelius B, Norling B, Nederman T, Carlsson J. Extracellular matrices in multicellular spheroids of human glioma origin: increased incorporation of proteoglycans and fibronectin as compared to monolayer cultures. APMIS : acta pathologica, microbiologica, et immunologica Scandinavica. 1988;96(5):433-44.
56. Elmasri WM, Casagrande G, Hoskins E, Kimm D, Kohn EC. Cell adhesion in ovarian cancer. Cancer treatment and research. 2009;149:297-318.
57. Ricciardelli C, Rodgers RJ. Extracellular matrix of ovarian tumors. Seminars in reproductive medicine. 2006;24(4):270-82.
58. Sung PL, Jan YH, Lin SC, Huang CC, Lin H, Wen KC, et al. Periostin in tumor microenvironment is associated with poor prognosis and platinum resistance in epithelial ovarian carcinoma. Oncotarget. 2016;7(4):4036-47.
59. Gillan L, Matei D, Fishman DA, Gerbin CS, Karlan BY, Chang DD. Periostin secreted by epithelial ovarian carcinoma is a ligand for alpha(V)beta(3) and alpha(V)beta(5) integrins and promotes cell motility. Cancer research. 2002;62(18):5358-64.

60. Zhu M, Fejzo MS, Anderson L, Dering J, Ginther C, Ramos L, et al. Periostin promotes ovarian cancer angiogenesis and metastasis. Gynecol Oncol. 2010;119(2):337-44.
61. Mitra AK, Sawada K, Tiwari P, Mui K, Gwin K, Lengyel E. Ligand-independent activation of c-Met by fibronectin and alpha(5)beta(1)-integrin regulates ovarian cancer invasion and metastasis. Oncogene. 2011;30(13):1566-76.
62. Desjardins M, Xie J, Gurler H, Muralidhar GG, Sacks JD, Burdette JE, et al. Versican regulates metastasis of epithelial ovarian carcinoma cells and spheroids. J Ovarian Res. 2014;7(1):70.
63. Bourguignon LY, Zhu H, Shao L, Chen YW. CD44 interaction with c-Src kinase promotes cortactin-mediated cytoskeleton function and hyaluronic acid-dependent ovarian tumor cell migration. The Journal of biological chemistry. 2001;276(10):7327-36.
64. Bourguignon LY, Zhu H, Chu A, Iida N, Zhang L, Hung MC. Interaction between the adhesion receptor, CD44, and the oncogene product, p185HER2, promotes human ovarian tumor cell activation. The Journal of biological chemistry. 1997;272(44):27913-8.
65. Bourguignon LY, Zhu H, Zhou B, Diedrich F, Singleton PA, Hung MC. Hyaluronan promotes CD44v3-Vav2 interaction with Grb2-p185(HER2) and induces Rac1 and Ras signaling during ovarian tumor cell migration and growth. The Journal of biological chemistry. 2001;276(52):48679-92.
66. Bourguignon LY, Peyrollier K, Gilad E, Brightman A. Hyaluronan-CD44 interaction with neural Wiskott-Aldrich syndrome protein (N-WASP) promotes actin polymerization and ErbB2 activation leading to beta-catenin nuclear translocation, transcriptional up-regulation, and cell migration in ovarian tumor cells. The Journal of biological chemistry. 2007;282(2):1265-80.
67. Bourguignon LY, Gilad E, Peyrollier K. Heregulin-mediated ErbB2-ERK signaling activates hyaluronan synthases leading to CD44-dependent ovarian tumor cell growth and migration. The Journal of biological chemistry. 2007;282(27):19426-41.
68. Zhu D, Bourguignon LY. Interaction between CD44 and the repeat domain of ankyrin promotes hyaluronic acid-mediated ovarian tumor cell migration. J Cell Physiol. 2000;183(2):182-95.
69. Lessan K, Aguiar DJ, Oegema T, Siebenson L, Skubitz AP. CD44 and beta1 integrin mediate ovarian carcinoma cell adhesion to peritoneal mesothelial cells. The American journal of pathology. 1999;154(5):1525-37.
70. Strobel T, Swanson L, Cannistra SA. In vivo inhibition of CD44 limits intra-abdominal spread of a human ovarian cancer xenograft in nude mice: a novel role for CD44 in the process of peritoneal implantation. Cancer research. 1997;57(7):1228-32.
71. Ponta H, Sherman L, Herrlich PA. CD44: from adhesion molecules to signalling regulators. Nature reviews Molecular cell biology. 2003;4(1):33-45.
72. Naor D, Nedvetzki S, Golan I, Melnik L, Faitelson Y. CD44 in Cancer. Critical reviews in clinical laboratory sciences. 2002;39(6):527-79.
73. Stickeler E, Runnebaum IB, Mobus VJ, Kieback DG, Kreienberg R. Expression of CD44 standard and variant isoforms v5, v6 and v7 in human ovarian cancer cell lines. Anticancer Res. 1997;17(3C):1871-6.
74. Liu D, Sy MS. Phorbol myristate acetate stimulates the dimerization of CD44 involving a cysteine in the transmembrane domain. Journal of immunology (Baltimore, Md : 1950). 1997;159(6):2702-11.
75. Neame SJ, Uff CR, Sheikh H, Wheatley SC, Isacke CM. CD44 exhibits a cell type dependent interaction with triton X-100 insoluble, lipid rich, plasma membrane domains. J Cell Sci. 1995;108 (Pt 9):3127-35.
76. Bretscher A, Edwards K, Fehon RG. ERM proteins and merlin: integrators at the cell cortex. Nature reviews Molecular cell biology. 2002;3(8):586-99.

77. Lokeshwar VB, Bourguignon LY. Post-translational protein modification and expression of ankyrin-binding site(s) in GP85 (Pgp-1/CD44) and its biosynthetic precursors during T-lymphoma membrane biosynthesis. The Journal of biological chemistry. 1991;266(27):17983-9.
78. Tsukita S, Oishi K, Sato N, Sagara J, Kawai A, Tsukita S. ERM family members as molecular linkers between the cell surface glycoprotein CD44 and actin-based cytoskeletons. J Cell Biol. 1994;126(2):391-401.
79. Zhu D, Bourguignon LY. The ankyrin-binding domain of CD44s is involved in regulating hyaluronic acid-mediated functions and prostate tumor cell transformation. Cell motility and the cytoskeleton. 1998;39(3):209-22.
80. Naor D, Sionov RV, Ish-Shalom D. CD44: Structure, Function and Association with the Malignant Process. In: George FVW, George K, editors. Advances in Cancer Research. Volume 71: Academic Press; 1997. p. 241-319.
81. Bennett KL, Modrell B, Greenfield B, Bartolazzi A, Stamenkovic I, Peach R, et al. Regulation of CD44 binding to hyaluronan by glycosylation of variably spliced exons. J Cell Biol. 1995;131(6 Pt 1):1623-33.
82. Di Sante G, Migliara G, Valentini M, Delogu G, Ria F. Regulation of and Regulation by CD44: A Paradigm Complex Regulatory Network. International Trends in Immunity. 2013;1(4):33-42.
83. MISRA S, Markwald RR, Hascall VC, Ghatak S. INTERACTIONS BETWEEN HYALURONAN AND ITS RECEPTORS (CD44, RHAMM) REGULATE THE ACTIVITIES OF INFLAMMATION AND CANCER. Frontiers in Immunology. 2015;6.
84. Jordan AR, Racine RR, Hennig MJP, Lokeshwar VB. The Role of CD44 in Disease Pathophysiology and Targeted Treatment. Frontiers in Immunology. 2015;6(182).
85. Jiang D, Liang J, Noble PW. Hyaluronan as an immune regulator in human diseases. Physiological reviews. 2011;91(1):221-64.
86. Wielenga VJ, Heider KH, Offerhaus GJ, Adolf GR, van den Berg FM, Ponta H, et al. Expression of CD44 variant proteins in human colorectal cancer is related to tumor progression. Cancer research. 1993;53(20):4754-6.
87. Kim H, Yang XL, Rosada C, Hamilton SR, August JT. CD44 expression in colorectal adenomas is an early event occurring prior to K-ras and p53 gene mutation. Archives of biochemistry and biophysics. 1994;310(2):504-7.
88. Wielenga VJ, Smits R, Korinek V, Smit L, Kielman M, Fodde R, et al. Expression of CD44 in Apc and Tcf mutant mice implies regulation by the WNT pathway. The American journal of pathology. 1999;154(2):515-23.
89. Shtivelman E, Bishop JM. Expression of CD44 is repressed in neuroblastoma cells. Mol Cell Biol. 1991;11(11):5446-53.
90. De Marzo AM, Bradshaw C, Sauvageot J, Epstein JI, Miller GJ. CD44 and CD44v6 downregulation in clinical prostatic carcinoma: relation to Gleason grade and cytoarchitecture. Prostate. 1998;34(3):162-8.
91. Gao AC, Lou W, Dong JT, Isaacs JT. CD44 is a metastasis suppressor gene for prostatic cancer located on human chromosome 11p13. Cancer research. 1997;57(5):846-9.
92. Hofmann M, Rudy W, Gunthert U, Zimmer SG, Zawadzki V, Zoller M, et al. A link between ras and metastatic behavior of tumor cells: ras induces CD44 promoter activity and leads to low-level expression of metastasis-specific variants of CD44 in CREF cells. Cancer research. 1993;53(7):1516-21.
93. Weg-Remers S, Ponta H, Herrlich P, Konig H. Regulation of alternative pre-mRNA splicing by the ERK MAP-kinase pathway. Embo j. 2001;20(15):4194-203.
94. Strobeck MW, DeCristofaro MF, Banine F, Weissman BE, Sherman LS, Knudsen ES. The BRG-1 subunit of the SWI/SNF complex regulates CD44 expression. The Journal of biological chemistry. 2001;276(12):9273-8.

95. Reisman DN, Strobeck MW, Betz BL, Sciariotta J, Funkhouser W, Jr., Murchardt C, et al. Concomitant down-regulation of BRM and BRG1 in human tumor cell lines: differential effects on RB-mediated growth arrest vs CD44 expression. Oncogene. 2002;21(8):1196-207.
96. Morrison H, Sherman LS, Legg J, Banine F, Isacke C, Haipek CA, et al. The NF2 tumor suppressor gene product, merlin, mediates contact inhibition of growth through interactions with CD44. Genes Dev. 2001;15(8):968-80.
97. Yu WH, Woessner JF, Jr., McNeish JD, Stamenkovic I. CD44 anchors the assembly of matrilysin/MMP-7 with heparin-binding epidermal growth factor precursor and ErbB4 and regulates female reproductive organ remodeling. Genes Dev. 2002;16(3):307-23.
98. Sherman LS, Rizvi TA, Karyala S, Ratner N. CD44 enhances neuregulin signaling by Schwann cells. J Cell Biol. 2000;150(5):1071-84.
99. Skelton TP ZC, Nocks A, Stamenkovic I. Glycosylation provides both stimulatory and inhibitory effects on cell surface and soluble CD44 binding to hyaluronan. J Cell Biol. 1998;140(2):431-46.
100. Ilangumaran S, Borisch B, Hoessli DC. Signal transduction via CD44: role of plasma membrane microdomains. Leukemia & lymphoma. 1999;35(5-6):455-69.
101. Bao W, Fu HJ, Xie QS, Wang L, Zhang R, Guo ZY, et al. HER2 interacts with CD44 to up-regulate CXCR4 via epigenetic silencing of microRNA-139 in gastric cancer cells. Gastroenterology. 2011;141(6):2076-87 e6.
102. Midgley AC, Rogers M, Hallett MB, Clayton A, Bowen T, Phillips AO, et al. Transforming growth factor-beta1 (TGF-beta1)-stimulated fibroblast to myofibroblast differentiation is mediated by hyaluronan (HA)-facilitated epidermal growth factor receptor (EGFR) and CD44 co-localization in lipid rafts. The Journal of biological chemistry. 2013;288(21):14824-38.
103. Kaya G, Rodriguez I, Jorcano JL, Vassalli P, Stamenkovic I. Selective suppression of CD44 in keratinocytes of mice bearing an antisense CD44 transgene driven by a tissue-specific promoter disrupts hyaluronate metabolism in the skin and impairs keratinocyte proliferation. Genes Dev. 1997;11(8):996-1007.
104. Culty M, Nguyen HA, Underhill CB. The hyaluronan receptor (CD44) participates in the uptake and degradation of hyaluronan. J Cell Biol. 1992;116(4):1055-62.
105. Valent P, Bonnet D, De Maria R, Lapidot T, Copland M, Melo JV, et al. Cancer stem cell definitions and terminology: the devil is in the details. Nat Rev Cancer. 2012;12(11):767-75.
106. Alison MR, Lin WR, Lim SM, Nicholson LJ. Cancer stem cells: in the line of fire. Cancer treatment reviews. 2012;38(6):589-98.
107. Li Y, Laterra J. Cancer stem cells: distinct entities or dynamically regulated phenotypes? Cancer research. 2012;72(3):576-80.
108. Zoller M. CD44: can a cancer-initiating cell profit from an abundantly expressed molecule? Nat Rev Cancer. 2011;11(4):254-67.
109. Dalerba P, Dylla SJ, Park IK, Liu R, Wang X, Cho RW, et al. Phenotypic characterization of human colorectal cancer stem cells. Proc Natl Acad Sci U S A. 2007;104(24):10158-63.
110. Collins AT, Berry PA, Hyde C, Stower MJ, Maitland NJ. Prospective identification of tumorigenic prostate cancer stem cells. Cancer research. 2005;65(23):10946-51.
111. Takaishi S, Okumura T, Tu S, Wang SS, Shibata W, Vigneshwaran R, et al. Identification of gastric cancer stem cells using the cell surface marker CD44. Stem cells (Dayton, Ohio). 2009;27(5):1006-20.
112. Koyama H, Hibi T, Isogai Z, Yoneda M, Fujimori M, Amano J, et al. Hyperproduction of hyaluronan in neu-induced mammary tumor accelerates angiogenesis through stromal cell recruitment: possible involvement of versican/PG-M. The American journal of pathology. 2007;170(3):1086-99.

113. El-Haibi CP, Bell GW, Zhang J, Collmann AY, Wood D, Scherber CM, et al. Critical role for lysyl oxidase in mesenchymal stem cell-driven breast cancer malignancy. Proc Natl Acad Sci U S A. 2012;109(43):17460-5.
114. Krishnamurthy S, Dong Z, Vodopyanov D, Imai A, Helman JI, Prince ME, et al. Endothelial cell-initiated signaling promotes the survival and self-renewal of cancer stem cells. Cancer research. 2010;70(23):9969-78.
115. Khammanivong A, Gopalakrishnan R, Dickerson EB. SMURF1 silencing diminishes a CD44-high cancer stem cell-like population in head and neck squamous cell carcinoma. Molecular cancer. 2014;13:260.
116. Chanmee T, Ontong P, Kimata K, Itano N. Key Roles of Hyaluronan and Its CD44 Receptor in the Stemness and Survival of Cancer Stem Cells. Frontiers in Oncology. 2015;5:180.
117. Bourguignon LY, Peyrollier K, Xia W, Gilad E. Hyaluronan-CD44 interaction activates stem cell marker Nanog, Stat-3-mediated MDR1 gene expression, and ankyrin-regulated multidrug efflux in breast and ovarian tumor cells. The Journal of biological chemistry. 2008;283(25):17635-51.
118. Ohashi R, Takahashi F, Cui R, Yoshioka M, Gu T, Sasaki S, et al. Interaction between CD44 and hyaluronate induces chemoresistance in non-small cell lung cancer cell. Cancer letters. 2007;252(2):225-34.
119. Tamada M, Nagano O, Tateyama S, Ohmura M, Yae T, Ishimoto T, et al. Modulation of glucose metabolism by CD44 contributes to antioxidant status and drug resistance in cancer cells. Cancer research. 2012;72(6):1438-48.
120. Ishimoto T, Nagano O, Yae T, Tamada M, Motohara T, Oshima H, et al. CD44 variant regulates redox status in cancer cells by stabilizing the xCT subunit of system xc(-) and thereby promotes tumor growth. Cancer Cell. 2011;19(3):387-400.
121. Orian-Rousseau V. CD44 Acts as a Signaling Platform Controlling Tumor Progression and Metastasis. Front Immunol. 2015;6:154.
122. Misra S, Heldin P, Hascall VC, Karamanos NK, Skandalis SS, Markwald RR, et al. Hyaluronan-CD44 interactions as potential targets for cancer therapy. FEBS J. 2011;278(9):1429-43.
123. Orian-Rousseau V, Sleeman J. CD44 is a multidomain signaling platform that integrates extracellular matrix cues with growth factor and cytokine signals. Adv Cancer Res. 2014;123:231-54.
124. Yu Q, Toole BP, Stamenkovic I. Induction of apoptosis of metastatic mammary carcinoma cells in vivo by disruption of tumor cell surface CD44 function. J Exp Med. 1997;186(12):1985-96.
125. Ghatak S, Misra S, Toole BP. Hyaluronan oligosaccharides inhibit anchorage-independent growth of tumor cells by suppressing the phosphoinositide 3-kinase/Akt cell survival pathway. The Journal of biological chemistry. 2002;277(41):38013-20.
126. Li L, Hao X, Qin J, Tang W, He F, Smith A, et al. Antibody against CD44s inhibits pancreatic tumor initiation and postradiation recurrence in mice. Gastroenterology. 2014;146(4):1108-18.
127. Jin L, Hope KJ, Zhai Q, Smadja-Joffe F, Dick JE. Targeting of CD44 eradicates human acute myeloid leukemic stem cells. Nat Med. 2006;12(10):1167-74.
128. Heider KH, Sproll M, Susani S, Patzelt E, Beaumier P, Ostermann E, et al. Characterization of a high-affinity monoclonal antibody specific for CD44v6 as candidate for immunotherapy of squamous cell carcinomas. Cancer immunology, immunotherapy : CII. 1996;43(4):245-53.
129. Iida J, Clancy R, Dorchak J, Somiari RI, Somiari S, Cutler ML, et al. DNA aptamers against exon v10 of CD44 inhibit breast cancer cell migration. PLoS One. 2014;9(2):e88712.
130. Tremmel M, Matzke A, Albrecht I, Laib AM, Olaku V, Ballmer-Hofer K, et al. A CD44v6 peptide reveals a role of CD44 in VEGFR-2 signaling and angiogenesis. Blood. 2009;114(25):5236-44.
131. Shah V, Taratula O, Garbuzenko OB, Taratula OR, Rodriguez-Rodriguez L, Minko T. Targeted nanomedicine for suppression of CD44 and simultaneous cell death induction in ovarian cancer: an

optimal delivery of siRNA and anticancer drug. Clinical cancer research : an official journal of the American Association for Cancer Research. 2013;19(22):6193-204.
132. Zou L, Song X, Yi T, Li S, Deng H, Chen X, et al. Administration of PLGA nanoparticles carrying shRNA against focal adhesion kinase and CD44 results in enhanced antitumor effects against ovarian cancer. Cancer gene therapy. 2013;20(4):242-50.
133. Saegusa M, Machida D, Hashimura M, Okayasu I. CD44 expression in benign, premalignant, and malignant ovarian neoplasms: relation to tumour development and progression. J Pathol. 1999;189(3):326-37.
134. Cho EY, Choi Y, Chae SW, Sohn JH, Ahn GH. Immunohistochemical study of the expression of adhesion molecules in ovarian serous neoplasms. Pathology international. 2006;56(2):62-70.
135. Kayastha S, Freedman AN, Piver MS, Mukkamalla J, Romero-Guittierez M, Werness BA. Expression of the hyaluronan receptor, CD44S, in epithelial ovarian cancer is an independent predictor of survival. Clinical cancer research : an official journal of the American Association for Cancer Research. 1999;5(5):1073-6.
136. Uhl-Steidl M, Muller-Holzner E, Zeimet AG, Adolf GR, Daxenbichler G, Marth C, et al. Prognostic value of CD44 splice variant expression in ovarian cancer. Oncology. 1995;52(5):400-6.
137. Afify AM, Ferguson AW, Davila RM, Werness BA. Expression of CD44S and CD44v5 is more common in stage III than in stage I serous ovarian carcinomas. Appl Immunohistochem Mol Morphol. 2001;9(4):309-14.
138. Sillanpaa S, Anttila MA, Voutilainen K, Tammi RH, Tammi MI, Saarikoski SV, et al. CD44 expression indicates favorable prognosis in epithelial ovarian cancer. Clinical cancer research : an official journal of the American Association for Cancer Research. 2003;9(14):5318-24.
139. Ross JS, Sheehan CE, Williams SS, Malfetano JH, Szyfelbein WM, Kallakury BV. Decreased CD44 standard form expression correlates with prognostic variables in ovarian carcinomas. American journal of clinical pathology. 2001;116(1):122-8.
140. Rodriguez-Rodriguez L, Sancho-Torres I, Mesonero C, Gibbon DG, Shih WJ, Zotalis G. The CD44 receptor is a molecular predictor of survival in ovarian cancer. Med Oncol. 2003;20(3):255-63.
141. Cannistra SA, Abu-Jawdeh G, Niloff J, Strobel T, Swanson L, Andersen J, et al. CD44 variant expression is a common feature of epithelial ovarian cancer: lack of association with standard prognostic factors. J Clin Oncol. 1995;13(8):1912-21.
142. Speiser P, Wanner C, Breitenecker G, Kohlberger P, Kainz C. CD-44 is not involved in the metastatic spread of ovarian cancer in vivo. Anticancer Res. 1995;15(6b):2767-9.
143. Sanchez Lockhart M, Hajos SE, Basilio FM, Mongini C, Alvarez E. Splice variant expression of CD44 in patients with breast and ovarian cancer. Oncol Rep. 2001;8(1):145-51.
144. Ryabtseva OD, Lukianova NY, Shmurakov YA, Polishchuk LZ, Antipova SV. Significance of adhesion molecules expression for estimation of serous ovarian cancer prognosis. Experimental oncology. 2013;35(3):211-8.
145. Chen H, Hao J, Wang L, Li Y. Coexpression of invasive markers (uPA, CD44) and multiple drug-resistance proteins (MDR1, MRP2) is correlated with epithelial ovarian cancer progression. British journal of cancer. 2009;101(3):432-40.
146. Gao Y, Foster R, Yang X, Feng Y, Shen JK, Mankin HJ, et al. Up-regulation of CD44 in the development of metastasis, recurrence and drug resistance of ovarian cancer. Oncotarget. 2015;6(11):9313-26.
147. Zhang J, Chang B, Liu J. CD44 standard form expression is correlated with high-grade and advanced-stage ovarian carcinoma but not prognosis. Hum Pathol. 2013;44(9):1882-9.
148. Paik DY, Janzen DM, Schafenacker AM, Velasco VS, Shung MS, Cheng D, et al. Stem-like epithelial cells are concentrated in the distal end of the fallopian tube: a site for injury and serous cancer initiation. Stem cells (Dayton, Ohio). 2012;30(11):2487-97.

149. Wang YC, Yo YT, Lee HY, Liao YP, Chao TK, Su PH, et al. ALDH1-bright epithelial ovarian cancer cells are associated with CD44 expression, drug resistance, and poor clinical outcome. The American journal of pathology. 2012;180(3):1159-69.
150. Zhang S, Balch C, Chan MW, Lai HC, Matei D, Schilder JM, et al. Identification and characterization of ovarian cancer-initiating cells from primary human tumors. Cancer research. 2008;68(11):4311-20.
151. Chen J, Wang J, Chen D, Yang J, Yang C, Zhang Y, et al. Evaluation of characteristics of CD44+CD117+ ovarian cancer stem cells in three dimensional basement membrane extract scaffold versus two dimensional monocultures. BMC cell biology. 2013;14:7.
152. Chen J, Wang J, Zhang Y, Chen D, Yang C, Kai C, et al. Observation of ovarian cancer stem cell behavior and investigation of potential mechanisms of drug resistance in three-dimensional cell culture. Journal of bioscience and bioengineering. 2014.
153. He QZ, Luo XZ, Wang K, Zhou Q, Ao H, Yang Y, et al. Isolation and characterization of cancer stem cells from high-grade serous ovarian carcinomas. Cellular physiology and biochemistry : international journal of experimental cellular physiology, biochemistry, and pharmacology. 2014;33(1):173-84.
154. Liao J, Qian F, Tchabo N, Mhawech-Fauceglia P, Beck A, Qian Z, et al. Ovarian cancer spheroid cells with stem cell-like properties contribute to tumor generation, metastasis and chemotherapy resistance through hypoxia-resistant metabolism. PLoS One. 2014;9(1):e84941.
155. Du YR, Chen Y, Gao Y, Niu XL, Li YJ, Deng WM. Effects and mechanisms of anti-CD44 monoclonal antibody A3D8 on proliferation and apoptosis of sphere-forming cells with stemness from human ovarian cancer. Int J Gynecol Cancer. 2013;23(8):1367-75.
156. Cannistra SA, Kansas GS, Niloff J, DeFranzo B, Kim Y, Ottensmeier C. Binding of ovarian cancer cells to peritoneal mesothelium in vitro is partly mediated by CD44H. Cancer research. 1993;53(16):3830-8.
157. Preca BT, Bajdak K, Mock K, Sundararajan V, Pfannstiel J, Maurer J, et al. A self-enforcing CD44s/ZEB1 feedback loop maintains EMT and stemness properties in cancer cells. Int J Cancer. 2015.
158. Gardner MJ, Catterall JB, Jones LM, Turner GA. Human ovarian tumour cells can bind hyaluronic acid via membrane CD44: a possible step in peritoneal metastasis. Clinical & experimental metastasis. 1996;14(4):325-34.
159. Gao L, Yan L, Lin B, Gao J, Liang X, Wang Y, et al. Enhancive effects of Lewis y antigen on CD44-mediated adhesion and spreading of human ovarian cancer cell line RMG-I. Journal of experimental & clinical cancer research : CR. 2011;30:15.
160. Ween MP, Hummitzsch K, Rodgers RJ, Oehler MK, Ricciardelli C. Versican induces a pro-metastatic ovarian cancer cell behavior which can be inhibited by small hyaluronan oligosaccharides. Clinical & experimental metastasis. 2011;28(2):113-25.
161. Haria D, Trinh BQ, Ko SY, Barengo N, Liu J, Naora H. The homeoprotein DLX4 stimulates NF-kappaB activation and CD44-mediated tumor-mesothelial cell interactions in ovarian cancer. The American journal of pathology. 2015;185(8):2298-308.
162. Henry JC, Park JK, Jiang J, Kim JH, Nagorney DM, Roberts LR, et al. miR-199a-3p targets CD44 and reduces proliferation of CD44 positive hepatocellular carcinoma cell lines. Biochem Biophys Res Commun. 2010;403(1):120-5.
163. Gao Y, Feng Y, Shen JK, Lin M, Choy E, Cote GM, et al. CD44 is a direct target of miR-199a-3p and contributes to aggressive progression in osteosarcoma. Sci Rep. 2015;5:11365.
164. Hu Y, Wang J, Qian J, Kong X, Tang J, Wang Y, et al. Long noncoding RNA GAPLINC regulates CD44-dependent cell invasiveness and associates with poor prognosis of gastric cancer. Cancer research. 2014;74(23):6890-902.

165. Cheng W, Liu T, Wan X, Gao Y, Wang H. MicroRNA-199a targets CD44 to suppress the tumorigenicity and multidrug resistance of ovarian cancer-initiating cells. Febs j. 2012;279(11):2047-59.
166. Nakshatri H, Srour EF, Badve S. Breast cancer stem cells and intrinsic subtypes: controversies rage on. Current stem cell research & therapy. 2009;4(1):50-60.
167. Laemmli UK. Cleavage of structural proteins during the assembly of the head of bacteriophage T4. Nature. 1970;227(5259):680-5.
168. Matsudaira P. Sequence from picomole quantities of proteins electroblotted onto polyvinylidene difluoride membranes. The Journal of biological chemistry. 1987;262(21):10035-8.
169. Liu J, Ma L, Xu J, Liu C, Zhang J, Liu J, et al. Co-expression of CD44 and ABCG2 in spheroid body-forming cells of gastric cancer cell line MKN45. Hepatogastroenterology. 2013;60(125):975-80.
170. Casey RC, Burleson KM, Skubitz KM, Pambuccian SE, Oegema TR, Jr., Ruff LE, et al. Beta 1-integrins regulate the formation and adhesion of ovarian carcinoma multicellular spheroids. The American journal of pathology. 2001;159(6):2071-80.
171. Kim M, Rooper L, Xie J, Rayahin J, Burdette JE, Kajdacsy-Balla AA, et al. The lymphotactin receptor is expressed in epithelial ovarian carcinoma and contributes to cell migration and proliferation. Molecular cancer research : MCR. 2012;10(11):1419-29.
172. Clarris BJ, Fraser JR. On the pericellular zone of some mammalian cells in vitro. Experimental cell research. 1968;49(1):181-93.
173. McBride WH, Bard JB. Hyaluronidase-sensitive halos around adherent cells. Their role in blocking lymphocyte-mediated cytolysis. J Exp Med. 1979;149(2):507-15.
174. Underhill CB, Toole BP. Transformation-dependent loss of the hyaluronate-containing coats of cultured cells. J Cell Physiol. 1982;110(2):123-8.
175. Knudson CB, Toole BP. Changes in the pericellular matrix during differentiation of limb bud mesoderm. Developmental biology. 1985;112(2):308-18.
176. Evanko SP, Tammi MI, Tammi RH, Wight TN. Hyaluronan-Dependent Pericellular Matrix. Advanced drug delivery reviews. 2007;59(13):1351-65.
177. Thiberge S, Nechushtan A, Sprinzak D, Gileadi O, Behar V, Zik O, et al. Scanning electron microscopy of cells and tissues under fully hydrated conditions. Proc Natl Acad Sci U S A. 2004;101(10):3346-51.
178. Uroukov IS, Patton D. Optimizing environmental scanning electron microscopy of spheroidal reaggregated neuronal cultures. Microscopy research and technique. 2008;71(11):792-801.
179. Davidowitz RA, Selfors LM, Iwanicki MP, Elias KM, Karst A, Piao H, et al. Mesenchymal gene program-expressing ovarian cancer spheroids exhibit enhanced mesothelial clearance. The Journal of clinical investigation. 2014;124(6):2611-25.
180. Iwanicki MD, RA; Ng, MR; Besser, A; Muranen, T; Merritt, M; Danuser, G; Ince, TA; Brugge, JS. Ovarian cancer spheroids use myosin-generated force to clear the mesothelium. Cancer Discovery. 2011;1(2):144-57.
181. Casey RC, Skubitz AP. CD44 and beta1 integrins mediate ovarian carcinoma cell migration toward extracellular matrix proteins. Clinical & experimental metastasis. 2000;18(1):67-75.
182. Pamir MN, Black PM, Fahlbusch R. Meningiomas: a comprehensive text. 1 ed. Philadelphia, Pa: Saunders/Elsevier; 2010.
183. Park YS, Huh JW, Lee JH, Kim HR. shRNA against CD44 inhibits cell proliferation, invasion and migration, and promotes apoptosis of colon carcinoma cells. Oncol Rep. 2012;27(2):339-46.
184. Nam K, Oh S, Lee KM, Yoo SA, Shin I. CD44 regulates cell proliferation, migration, and invasion via modulation of c-Src transcription in human breast cancer cells. Cellular signalling. 2015;27(9):1882-94.

185. Gadhoum Z, Leibovitch MP, Qi J, Dumenil D, Durand L, Leibovitch S, et al. CD44: a new means to inhibit acute myeloid leukemia cell proliferation via p27Kip1. Blood. 2004;103(3):1059-68.
186. Gadhoum Z, Delaunay J, Maquarre E, Durand L, Lancereaux V, Qi J, et al. The effect of anti-CD44 monoclonal antibodies on differentiation and proliferation of human acute myeloid leukemia cells. Leukemia & lymphoma. 2004;45(8):1501-10.
187. Mosmann T. Rapid colorimetric assay for cellular growth and survival: application to proliferation and cytotoxicity assays. Journal of immunological methods. 1983;65(1-2):55-63.
188. Franken NA, Rodermond HM, Stap J, Haveman J, van Bree C. Clonogenic assay of cells in vitro. Nat Protoc. 2006;1(5):2315-9.
189. Gu C, Du Y, Gao Y, Yao Z, Gu X, Zhang Q, et al. Anti-CD44 mAb remodels biological behaviors of spheroid cells with stemness from human ovarian cancer cell line SKOV-3. Chinese Science Bulletin. 2012;57(11):1288-97.
190. Bravo-Cordero JJ, Hodgson L, Condeelis J. Directed Cell Invasion and Migration During Metastasis. Curr Opin Cell Biol. 2012;24(2):277-83.
191. Schaeffer D, Somarelli JA, Hanna G, Palmer GM, Garcia-Blanco MA. Cellular migration and invasion uncoupled: increased migration is not an inexorable consequence of epithelial-to-mesenchymal transition. Mol Cell Biol. 2014;34(18):3486-99.
192. Zhao P, Xu Y, Wei Y, Qiu Q, Chew TL, Kang Y, et al. The CD44s splice isoform is a central mediator for invadopodia activity. J Cell Sci. 2016;129(7):1355-65.
193. Casey RC, Koch KA, Oegema TR, Jr., Skubitz KM, Pambuccian SE, Grindle SM, et al. Establishment of an in vitro assay to measure the invasion of ovarian carcinoma cells through mesothelial cell monolayers. Clinical & experimental metastasis. 2003;20(4):343-56.
194. Brown RL, Reinke LM, Damerow MS, Perez D, Chodosh LA, Yang J, et al. CD44 splice isoform switching in human and mouse epithelium is essential for epithelial-mesenchymal transition and breast cancer progression. The Journal of clinical investigation. 2011;121(3):1064-74.
195. Bhattacharya R, Mitra T, Chaudhuri SR, Roy SS. Mesenchymal splice isoform of CD44 (CD44s) promotes EMT/invasion and imparts stem-like properties to ovarian cancer cells. Journal of cellular biochemistry. 2017.
196. Geback T, Schulz MM, Koumoutsakos P, Detmar M. TScratch: a novel and simple software tool for automated analysis of monolayer wound healing assays. BioTechniques. 2009;46(4):265-74.
197. Jeong HM, Han J, Lee SH, Park HJ, Lee HJ, Choi JS, et al. ESRP1 is overexpressed in ovarian cancer and promotes switching from mesenchymal to epithelial phenotype in ovarian cancer cells. Oncogenesis. 2017;6(11):e391.
198. Mima K, Hayashi H, Imai K, Kuroki H, Nakagawa S, Okabe H, et al. High CD44s expression is associated with the EMT expression profile and intrahepatic dissemination of hepatocellular carcinoma after local ablation therapy. Journal of hepato-biliary-pancreatic sciences. 2013;20(4):429-34.
199. Bartolazzi A, Peach R, Aruffo A, Stamenkovic I. Interaction between CD44 and hyaluronate is directly implicated in the regulation of tumor development. J Exp Med. 1994;180(1):53-66.
200. Li CZ, Liu B, Wen ZQ, Li HY. Inhibition of CD44 expression by small interfering RNA to suppress the growth and metastasis of ovarian cancer cells in vitro and in vivo. Folia biologica. 2008;54(6):180-6.
201. Lau DH, Lewis AD, Ehsan MN, Sikic BI. Multifactorial mechanisms associated with broad cross-resistance of ovarian carcinoma cells selected by cyanomorpholino doxorubicin. Cancer research. 1991;51(19):5181-7.
202. Kwok AL, Wong OG, Wong ES, Tsun OK, Chan KK, Cheung AN. Caution over use of ES2 as a model of ovarian clear cell carcinoma. Journal of clinical pathology. 2014;67(10):921-2.

203. Domcke S, Sinha R, Levine DA, Sander C, Schultz N. Evaluating cell lines as tumour models by comparison of genomic profiles. Nat Commun. 2013;4:2126.
204. Ota T, Maeda M, Suto S, Tatsuka M. LyGDI functions in cancer metastasis by anchoring Rho proteins to the cell membrane. Molecular carcinogenesis. 2004;39(4):206-20.
205. Gildea JJ, Seraj MJ, Oxford G, Harding MA, Hampton GM, Moskaluk CA, et al. RhoGDI2 is an invasion and metastasis suppressor gene in human cancer. Cancer research. 2002;62(22):6418-23.
206. Ahmed M, Sottnik JL, Dancik GM, Sahu D, Hansel DE, Theodorescu D, et al. An Osteopontin/CD44 Axis in RhoGDI2-Mediated Metastasis Suppression. Cancer Cell. 2016;30(3):432-43.
207. Tapper J, Kettunen E, El-Rifai W, Seppala M, Andersson LC, Knuutila S. Changes in gene expression during progression of ovarian carcinoma. Cancer Genet Cytogenet. 2001;128(1):1-6.
208. Li H, Cui X, Chen D, Yang Y, Piao J, Lin Z, et al. Clinical implication of Tiam1 overexpression in the prognosis of patients with serous ovarian carcinoma. Oncology letters. 2016;12(5):3492-8.
209. Weber GF, Lett GS, Haubein NC. Osteopontin is a marker for cancer aggressiveness and patient survival. British journal of cancer. 2010;103(6):861-9.
210. Han BG, Cho JW, Cho YD, Kim SY, Yoon HJ, Song HK, et al. Expression, purification and biochemical characterization of the N-terminal regions of human TIG3 and HRASLS3 proteins. Protein expression and purification. 2010;71(1):103-7.
211. Morales M, Arenas EJ, Urosevic J, Guiu M, Fernandez E, Planet E, et al. RARRES3 suppresses breast cancer lung metastasis by regulating adhesion and differentiation. EMBO molecular medicine. 2014;6(7):865-81.
212. Muschen M, Warskulat U, Beckmann MW. Defining CD95 as a tumor suppressor gene. Journal of molecular medicine (Berlin, Germany). 2000;78(6):312-25.
213. Yoong KF, Afford SC, Randhawa S, Hubscher SG, Adams DH. Fas/Fas ligand interaction in human colorectal hepatic metastases: A mechanism of hepatocyte destruction to facilitate local tumor invasion. The American journal of pathology. 1999;154(3):693-703.
214. Robinson EE, Foty RA, Corbett SA. Fibronectin matrix assembly regulates alpha5beta1-mediated cell cohesion. Mol Biol Cell. 2004;15(3):973-81.
215. Sodek KL, Ringuette MJ, Brown TJ. Compact spheroid formation by ovarian cancer cells is associated with contractile behavior and an invasive phenotype. Int J Cancer. 2009;124(9):2060-70.
216. Hynes RO. Fibronectins. New York: Springer-Verlag; 1990.
217. Werbajh SE, Urtreger AJ, Puricelli LI, de Lustig ES, Bal de Kier Joffé E, Kornblihtt AR. Downregulation of fibronectin transcription in highly metastatic adenocarcinoma cells. FEBS Letters. 1998;440(3):277-81.
218. Colombo LLB, Y.P.; Klein, S.; Stillitane-D'Elia, I. Selección in vivo de una línea tumoral con alta incidencia de metástasis pulmonares. Medicina (Buenos Aires). 1980;40(6/2):827-8.
219. Bal de Kier Joffe E, Puricelli L, de Lustig ES. Modified adhesion behavior after in vitro passage of two related murine mammary adenocarcinomas with different metastasizing ability. Invasion & metastasis. 1986;6(5):302-12.
220. Bianchini F, Kaaks R, Vainio H. Overweight, obesity, and cancer risk. Lancet Oncology. 2002;3(9):565-74.
221. Peter ME, Legembre P, Barnhart BC. Does CD95 have tumor promoting activities? Biochimica et biophysica acta. 2005;1755(1):25-36.
222. Debatin KM, Krammer PH. Death receptors in chemotherapy and cancer. Oncogene. 2004;23(16):2950-66.
223. Chen L, Park SM, Tumanov AV, Hau A, Sawada K, Feig C, et al. CD95 promotes tumour growth. Nature. 2010;465(7297):492-6.
224. Muschen M, Warskulat U, Schmidt B, Schulz WA, Haussinger D. Regulation of CD95 (Apo-1/Fas) ligand and receptor expression in human embryonal carcinoma cells by interferon gamma and all-trans retinoic acid. Biological chemistry. 1998;379(8-9):1083-91.

225. Muschen M, Moers C, Warskulat U, Niederacher D, Betz B, Even J, et al. CD95 ligand expression in dedifferentiated breast cancer. J Pathol. 1999;189(3):378-86.
226. Owen-Schaub LB, van Golen KL, Hill LL, Price JE. Fas and Fas Ligand Interactions Suppress Melanoma Lung Metastasis. The Journal of Experimental Medicine. 1998;188(9):1717-23.
227. Drake RL, Vogl W, Mitchell AWM. Gray's anatomy for students. Third;3rd; ed. Philadelphia, PA: Churchill Livingstone/Elsevier; 2015.
228. Minn AJ, Gupta GP, Siegel PM, Bos PD, Shu W, Giri DD, et al. Genes that mediate breast cancer metastasis to lung. Nature. 2005;436(7050):518-24.
229. Wang Z, Wang L, Hu J, Fan R, Zhou J, Wang L, et al. RARRES3 suppressed metastasis through suppression of MTDH to regulate epithelial-mesenchymal transition in colorectal cancer. Am J Cancer Res. 2015;5(6):1988-99.
230. DiSepio D, Ghosn C, Eckert RL, Deucher A, Robinson N, Duvic M, et al. Identification and characterization of a retinoid-induced class II tumor suppressor/growth regulatory gene. Proc Natl Acad Sci U S A. 1998;95(25):14811-5.
231. Hsu T, Jiang S, Chan W, Eckert RL, Scharadin TM, Chang T. Involvement of RARRES3 in the regulation of Wnt proteins acylation and signaling activities in human breast cancer cells. Cell Death Differ. 2015;22(5):801-14.
232. Ou C-C, Hsu S-C, Hsieh Y-H, Tsou W-L, Chuang T-C, Liu J-Y, et al. Downregulation of HER2 by RIG1 involves the PI3K/Akt pathway in ovarian cancer cells. Carcinogenesis. 2008;29(2):299-306.
233. Suki B, Ito S, Stamenovic D, Lutchen KR, Ingenito EP. Biomechanics of the lung parenchyma: critical roles of collagen and mechanical forces. Journal of applied physiology (Bethesda, Md : 1985). 2005;98(5):1892-9.
234. Pelosi P, Rocco PR. Effects of mechanical ventilation on the extracellular matrix. Intensive care medicine. 2008;34(4):631-9.
235. Dityatev A, Seidenbecher CI, Schachner M. Compartmentalization from the outside: the extracellular matrix and functional microdomains in the brain. Trends in neurosciences. 2010;33(11):503-12.
236. Cardoso FL, Brites D, Brito MA. Looking at the blood-brain barrier: molecular anatomy and possible investigation approaches. Brain research reviews. 2010;64(2):328-63.
237. Gong Y, Sun X, Huo L, Wiley EL, Rao MS. Expression of cell adhesion molecules, CD44s and E-cadherin, and microvessel density in invasive micropapillary carcinoma of the breast. Histopathology. 2005;46(1):24-30.
238. Kerr VE, Cadman E. Pulmonary metastases in ovarian cancer. Analysis of 357 patients. Cancer. 1985;56(5):1209-13.
239. Gvozdenovic A, Arlt MJ, Campanile C, Brennecke P, Husmann K, Born W, et al. Silencing of CD44 gene expression in human 143-B osteosarcoma cells promotes metastasis of intratibial tumors in SCID mice. PLoS One. 2013;8(4):e60329.
240. Lopez JI, Camenisch TD, Stevens MV, Sands BJ, McDonald J, Schroeder JA. CD44 attenuates metastatic invasion during breast cancer progression. Cancer research. 2005;65(15):6755-63.
241. Kunimura T, Yoshida T, Sugiyama T, Morohoshi T. The Relationships Between Loss of Standard CD44 Expression and Lymph Node, Liver Metastasis in T3 Colorectal Carcinoma. Journal of gastrointestinal cancer. 2009;40(3-4):115-8.
242. Choi SH, Takahashi K, Eto H, Yoon SS, Tanabe KK. CD44s expression in human colon carcinomas influences growth of liver metastases. International Journal of Cancer. 2000;85(4):523-6.
243. Allison KH, Fligner CL, Tony Parks W. Radiographically Occult, Diffuse Intrasinusoidal Hepatic Metastases From Primary Breast Carcinomas: A Clinicopathologic Study of 3 Autopsy Cases. Archives of Pathology & Laboratory Medicine. 2004;128(12):1418-23.

244. Yae T, Tsuchihashi K, Ishimoto T, Motohara T, Yoshikawa M, Yoshida GJ, et al. Alternative splicing of CD44 mRNA by ESRP1 enhances lung colonization of metastatic cancer cell. Nat Commun. 2012;3:883.

APPENDIX I

Cell line Authentication

Cell Line Authentication (STR)

Name: Hilal Gurler
Request number: 13439
Date initiated: 06/08/2016
Date finalized: 06/08/2016

Quality Controls

QC Qubit

Sample Name	Cell Line	Concentration (ng/ul)
1	SKOV-3	111
2	OVCAR-4	312
3	CAOV-3	208
4	ES-2	214
5	OAW-28	540
6	Kuramochi	51.4
7	Ovsaho	768

STR Results

Sample	1.SKOV-3																
Marker	TH01	TH01	D21S11	D21S11	D21S11	D5S818	D13S317	D13S317	D7S820	D7S820	D16S539	CSF1PO	AMEL	vWA	vWA	TPOX	TPOX
Allele	9	9.3	30	31	31.2	11	8	11	13	14	12	11	X	17	18	8	11

Sample	2.OVCAR-4												
Marker	TH01	D21S11	D21S11	D5S818	D13S317	D7S820	D7S820	D16S539	CSF1PO	AMEL	vWA	vWA	TPOX
Allele	9	28	31	13	9	10	11	11	10	X	14	18	8

Page 1 of 2

Sample	3.CAOV-3												
Marker	TH01	D21S11	D5S818	D13S317	D7S820	D16S539	CSF1PO	CSF1PO	AMEL	vWA	vWA	TPOX	TPOX
Allele	7	30	12	12	10	9	10	13	X	16	18	8	10

Sample	4.ES-2															
Marker	TH01	D21S11	D21S11	D5S818	D5S818	D13S317	D7S820	D16S539	D16S539	CSF1PO	CSF1PO	AMEL	vWA	vWA	TPOX	TPOX
Allele	9.3	32.2	33.2	11	13	11	11	11	13	10	15	X	16	17	8	12

Sample	5.OAW-28										
Marker	TH01	D21S11	D5S818	D13S317	D7S820	D16S539	CSF1PO	AMEL	vWA	vWA	TPOX
Allele	9	29	12	11	11	13	11	X	17	19	8

Sample	6.Kuramochi															
Marker	TH01	D21S11	D21S11	D5S818	D13S317	D13S317	D7S820	D7S820	D16S539	CSF1PO	CSF1PO	AMEL	vWA	vWA	TPOX	TPOX
Allele	9	30	32.2	12	9	12	10	11	10	11	12	X	16	19	8	12

Sample	7.Ovsaho													
Marker	TH01	D21S11	D5S818	D5S818	D13S317	D7S820	D7S820	D16S539	CSF1PO	CSF1PO	AMEL	vWA	TPOX	TPOX
Allele	6	31	12	13	8	8	10	9	10	12	X	14	8	11

Sample	PTC																
Marker	TH01	TH01	D21S11	D21S11	D5S818	D13S317	D13S317	D7S820	D7S820	D16S539	D16S539	CSF1PO	AMEL	AMEL	vWA	vWA	TPOX
Allele	6	9.3	29	31.2	12	9	11	8	11	9	13	12	X	Y	16	19	11

Cell Line Authentication (STR)

Name: Joelle Sacks
Request number: 14712
Date initiated: 9/6/2016
Date finalized: 9/12/2016

Quality Controls

QC Qubit

Sample	Concentration [ng/ul]
1. Skov3-C2	16.2
2. Skov3-C6	5.84

STR Results

Sample	1.SKOV3-C2												
Marker	TH01	TH01	D21S11	D21S11	D5S818	D13S317	D13S317	D7S820	D16S539	CSF1PO	AMEL	vWA	TPOX
Allele	9	9.3	30	31.2	11	8	11	14	12	11	X	18	11

Sample	2.SKOV3-C6																		
Marker	TH01	TH01	D21S11	D21S11	D21S11	D5S818	D13S317	D13S317	D7S820	D7S820	D7S820	D16S539	CSF1PO	CSF1PO	AMEL	vWA	vWA	TPOX	TPOX
Allele	9	9.3	30	31	31.2	11	8	10	12	13	14	12	11	12	X	17	18	8	11

Sample	PTC																
Marker	TH01	TH01	D21S11	D21S11	D5S818	D13S317	D13S317	D7S820	D7S820	D16S539	D16S539	CSF1PO	AMEL	AMEL	vWA	vWA	TPOX
Allele	6	9.3	29	31.2	12	9	11	8	11	9	13	12	X	Y	16	19	11

Sample Comparison

Table 3A: STR Profile Results

	Test Sample	***Reference Sample***
Cell line designation e.g. name and catalog number	ES-2	ES-2
Date sample collected (if known)	6/8/2016	NCBI data
Passage or Population Doubling (if known)		
STR Profile Result (enter name of kit if used)	UIC RRC	
D5S818	11,13	11,13
D13S317	11	11
D7S820	11	11
D16S539	11,13	11,13
vWA	16,17	16,17
TH01	9.3	9.3
Amelogenin	X	X
TPOX	8,12	8,12
CSF1PO	10,15	10,15

Table 3B: Percent Match Calculations

TOTAL ALLELES in the Test Sample	14
TOTAL ALLELES in the Reference Sample	14
SHARED ALLELES, Test and Reference Samples	14
Percent Match for Test and Reference Samples	**100%**

Percent Match can be calculated using an appropriate Match Algorithm (2,3). For this Worksheet:

$$\text{Match Algorithm} = \frac{\text{SHARED ALLELES} \times 2}{\text{TOTAL ALLELES in the Test Sample} + \text{TOTAL ALLELES in the Reference Sample}}$$

Percent Match = Match Algorithm result x 100

Table 3C: Interpretation of Results

Are there multiple peaks that would be consistent with a mixture?	YES/**NO**
Is the percent match result in the range 0-55 %? This result is consistent with the two samples being unrelated (different donors)	YES/**NO**
Is the percent match result in the range 56-79 %? This result is indeterminant and may need further testing	YES/**NO**
Is the percent match result in the range 80-100 %? This result is consistent with the two samples being related (same donor)	**YES**/NO

Sample Comparison

Table 3A: STR Profile Results

	Test Sample	***Reference Sample***
Cell line designation e.g. name and catalog number	SKOV-3	SKOV-3
Date sample collected (if known)	6/8/2016	ATCC Data
Passage or Population Doubling (if known)		
STR Profile Result (enter name of kit if used)	UIC RRC	
D5S818	11	11
D13S317	8,11	8,11
D7S820	13,14	13,14
D16S539	12	12
vWA	17,18	17,18
TH01	9,9.3	9,9.3
Amelogenin	X	X
TPOX	8,11	8,11
CSF1PO	11	11

Table 3B: Percent Match Calculations

TOTAL ALLELES in the Test Sample	14
TOTAL ALLELES in the Reference Sample	14
SHARED ALLELES, Test and Reference Samples	14
Percent Match for Test and Reference Samples	**100%**

Percent Match can be calculated using an appropriate Match Algorithm (2,3). For this Worksheet:

$$\text{Match Algorithm} = \frac{\text{SHARED ALLELES} \times 2}{\text{TOTAL ALLELES in the Test Sample + TOTAL ALLELES in the Reference Sample}}$$

Percent Match = Match Algorithm result x 100

Table 3C: Interpretation of Results

Are there multiple peaks that would be consistent with a mixture?	YES/**NO**
Is the percent match result in the range 0-55 %? This result is consistent with the two samples being unrelated (different donors)	YES/**NO**
Is the percent match result in the range 56-79 %? This result is indeterminant and may need further testing	YES/**NO**
Is the percent match result in the range 80-100 %? This result is consistent with the two samples being related (same donor)	**YES**/NO

Sample Comparison

Table 3A: STR Profile Results

	Test Sample	***Reference Sample***
Cell line designation e.g. name and catalog number	OVCAR-4	OVCAR-4
Date sample collected (if known)	6/8/2016	NIH/NCI
Passage or Population Doubling (if known)		
STR Profile Result (enter name of kit if used)	UIC RRC	
D5S818	13	13
D13S317	9	9
D7S820	10,11	10,11
D16S539	11	11
vWA	14,18	14,18
TH01	9	9
Amelogenin	X	X
TPOX	8	8
CSF1PO	10	10

Table 3B: Percent Match Calculations

TOTAL ALLELES in the Test Sample	11
TOTAL ALLELES in the Reference Sample	11
SHARED ALLELES, Test and Reference Samples	11
Percent Match for Test and Reference Samples	**100%**

Percent Match can be calculated using an appropriate Match Algorithm (2,3). For this Worksheet:

$$\text{Match Algorithm} = \frac{\text{SHARED ALLELES} \times 2}{\text{TOTAL ALLELES in the Test Sample} + \text{TOTAL ALLELES in the Reference Sample}}$$

Percent Match = Match Algorithm result x 100

Table 3C: Interpretation of Results

Are there multiple peaks that would be consistent with a mixture?	YES/**NO**
Is the percent match result in the range 0-55 %? This result is consistent with the two samples being unrelated (different donors)	YES/**NO**
Is the percent match result in the range 56-79 %? This result is indeterminant and may need further testing	YES/**NO**
Is the percent match result in the range 80-100 %? This result is consistent with the two samples being related (same donor)	**YES**/NO

Sample Comparison

Table 3A: STR Profile Results

	Test Sample	***Reference Sample***
Cell line designation e.g. name and catalog number	OVSAHO	OVSAHO
Date sample collected (if known)	6/8/2016	NCBI
Passage or Population Doubling (if known)		
STR Profile Result (enter name of kit if used)	UIC RRC	
D5S818	12,13	12,13
D13S317	8	8
D7S820	8,10	8,10
D16S539	9	9
vWA	14	14
TH01	6	6
Amelogenin	X	X
TPOX	8,11	8,11
CSF1PO	10,12	10,12

Table 3B: Percent Match Calculations

TOTAL ALLELES in the Test Sample	13
TOTAL ALLELES in the Reference Sample	13
SHARED ALLELES, Test and Reference Samples	13
Percent Match for Test and Reference Samples	**100%**

Percent Match can be calculated using an appropriate Match Algorithm (2,3). For this Worksheet:

$$\text{Match Algorithm} = \frac{\text{SHARED ALLELES} \times 2}{\text{TOTAL ALLELES in the Test Sample} + \text{TOTAL ALLELES in the Reference Sample}}$$

Percent Match = Match Algorithm result x 100

Table 3C: Interpretation of Results

Are there multiple peaks that would be consistent with a mixture?	YES/**NO**
Is the percent match result in the range 0-55 %? This result is consistent with the two samples being unrelated (different donors)	YES/**NO**
Is the percent match result in the range 56-79 %? This result is indeterminant and may need further testing	YES/**NO**
Is the percent match result in the range 80-100 %? This result is consistent with the two samples being related (same donor)	**YES**/NO

Sample Comparison

Table 3A: STR Profile Results

	Test Sample	***Reference Sample***
Cell line designation e.g. name and catalog number	ES-2 CD44$^{-/-}$ G1+2 Clone 7	ES-2
Date sample collected (if known)	6/8/2016	NCBI
Passage or Population Doubling (if known)		
STR Profile Result (enter name of kit if used)	UIC RRC	
D5S818	11,13	11,13
D13S317	11	11
D7S820	11	11
D16S539	11,13	11,13
vWA	16,17	16,17
TH01	9.3	9.3
Amelogenin	X	X
TPOX	8,12	8,12
CSF1PO	10,15	10,15

Table 3B: Percent Match Calculations

TOTAL ALLELES in the Test Sample	14
TOTAL ALLELES in the Reference Sample	14
SHARED ALLELES, Test and Reference Samples	14
Percent Match for Test and Reference Samples	**100%**

Percent Match can be calculated using an appropriate Match Algorithm (2,3). For this Worksheet:

$$\text{Match Algorithm} = \frac{\text{SHARED ALLELES} \times 2}{\text{TOTAL ALLELES in the Test Sample} + \text{TOTAL ALLELES in the Reference Sample}}$$

Percent Match = Match Algorithm result x 100

Table 3C: Interpretation of Results

Are there multiple peaks that would be consistent with a mixture?	YES/**NO**
Is the percent match result in the range 0-55 %? This result is consistent with the two samples being unrelated (different donors)	YES/**NO**
Is the percent match result in the range 56-79 %? This result is indeterminant and may need further testing	YES/**NO**
Is the percent match result in the range 80-100 %? This result is consistent with the two samples being related (same donor)	**YES**/NO

Sample Comparison

Table 3A: STR Profile Results

	Test Sample	***Reference Sample***
Cell line designation e.g. name and catalog number	SKOV-3 CD44$^{-/-}$ G1+2 Clone 2	SKOV-3
Date sample collected (if known)	6/8/2016	ATCC
Passage or Population Doubling (if known)		
STR Profile Result (enter name of kit if used)	UIC RRC	
D5S818	11	11
D13S317	8,11	8,11
D7S820	14	13,14
D16S539	12	12
vWA	18	17,18
TH01	9,9.3	9,9.3
Amelogenin	X	X
TPOX	11	8,11
CSF1PO	11	11

Table 3B: Percent Match Calculations

TOTAL ALLELES in the Test Sample	11
TOTAL ALLELES in the Reference Sample	14
SHARED ALLELES, Test and Reference Samples	11
Percent Match for Test and Reference Samples	**88%**

Percent Match can be calculated using an appropriate Match Algorithm (2,3). For this Worksheet:

$$\text{Match Algorithm} = \frac{\text{SHARED ALLELES} \times 2}{\text{TOTAL ALLELES in the Test Sample} + \text{TOTAL ALLELES in the Reference Sample}}$$

Percent Match = Match Algorithm result x 100

Table 3C: Interpretation of Results

Are there multiple peaks that would be consistent with a mixture?	YES/**NO**
Is the percent match result in the range 0-55 %? This result is consistent with the two samples being unrelated (different donors)	YES/**NO**
Is the percent match result in the range 56-79 %? This result is indeterminant and may need further testing	YES/**NO**
Is the percent match result in the range 80-100 %? This result is consistent with the two samples being related (same donor)	**YES**/NO

Sample Comparison

Table 3A: STR Profile Results

	Test Sample	***Reference Sample***
Cell line designation e.g. name and catalog number	SKOV-3 CD44$^{-/-}$ G1+2 Clone 6	SKOV-3
Date sample collected (if known)	6/8/2016	ATCC
Passage or Population Doubling (if known)		
STR Profile Result (enter name of kit if used)	UIC RRC	
D5S818	11	11
D13S317	8,10	8,11
D7S820	12,13,14	13,14
D16S539	12	12
vWA	17,18	17,18
TH01	9,9.3	9,9.3
Amelogenin	X	X
TPOX	8,11	8,11
CSF1PO	11,12	11

Table 3B: Percent Match Calculations

TOTAL ALLELES in the Test Sample	16
TOTAL ALLELES in the Reference Sample	14
SHARED ALLELES, Test and Reference Samples	13
Percent Match for Test and Reference Samples	**87%**

Percent Match can be calculated using an appropriate Match Algorithm (2,3). For this Worksheet:

$$\text{Match Algorithm} = \frac{\text{SHARED ALLELES} \times 2}{\text{TOTAL ALLELES in the Test Sample + TOTAL ALLELES in the Reference Sample}}$$

Percent Match = Match Algorithm result x 100

Table 3C: Interpretation of Results

Are there multiple peaks that would be consistent with a mixture?	YES/**NO**
Is the percent match result in the range 0-55 %? This result is consistent with the two samples being unrelated (different donors)	YES/**NO**
Is the percent match result in the range 56-79 %? This result is indeterminant and may need further testing	YES/**NO**
Is the percent match result in the range 80-100 %? This result is consistent with the two samples being related (same donor)	**YES**/NO

Approved animal use protocol

UIC UNIVERSITY OF ILLINOIS AT CHICAGO

Office of Animal Care and
Institutional Biosafety Committees (MC 672)
Office of the Vice Chancellor for Research
206 Administrative Office Building
1737 West Polk Street
Chicago, Illinois 60612-7227

February 10, 2016

Maria Barbolina
Biopharmaceutical Sciences
M/C 865

Dear Dr. Barbolina:

The protocol indicated below was reviewed at a convened ACC meeting in accordance with the Animal Care Policies of the University of Illinois at Chicago on **1/19/2016**. *The protocol was not initiated until final clarifications were reviewed and approved on* **2/9/2016**. *The protocol is approved for a period of* ***3*** years with annual continuation.

Title of Application: Molecular Mechanisms of Metastasis Formation and Survival in Ovarian Carcinoma

ACC Number: 15-252

Initial Approval Period: 2/9/2016 to 1/19/2017

Current Funding: ***Currently protocol NOT matched to specific funding source. Modification will need to be submitted prior to Just in time or acceptance of award to match protocol to external funding source. All animal work proposed in the funding application must be covered by an approved protocol. UIC is the only performance site currently approved for this protocol.***

This institution has Animal Welfare Assurance Number A3460.01 on file with the Office of Laboratory Animal Welfare (OLAW), NIH. **This letter may only be provided as proof of IACUC approval for those specific funding sources listed above in which all portions of the funding proposal are matched to this ACC protocol.**

In addition, all investigators are responsible for ensuring compliance with all federal and institutional policies and regulations related to use of animals under this protocol and the funding sources listed on this protocol. Please use OLAW's "*What Investigators Need to Know about the Use of Animals*" (http://grants.nih.gov/grants/olaw/InvestigatorsNeed2Know.pdf) as a reference guide. Thank you for complying with the Animal Care Policies and Procedures of UIC.

Sincerely yours,

John P. O'Bryan, PhD
Chair, Animal Care Committee
JPO /*mbb*
cc: BRL, ACC File

Phone (312) 996-1972 • Fax (312) 996-9088 • www.research.uic.edu

APPENDIX II

Permissions to Reprint/Reproduce

ELSEVIER LICENSE
TERMS AND CONDITIONS

Nov 29, 2017

This Agreement between Mrs. Joelle Sacks ("You") and Elsevier ("Elsevier") consists of your license details and the terms and conditions provided by Elsevier and Copyright Clearance Center.

License Number	4238380076977
License date	Nov 29, 2017
Licensed Content Publisher	Elsevier
Licensed Content Publication	The American Journal of Pathology
Licensed Content Title	The Dualistic Model of Ovarian Carcinogenesis Revisited, Revised, and Expanded
Licensed Content Author	Robert J. Kurman,Ie-Ming Shih
Licensed Content Date	Apr 1, 2016
Licensed Content Volume	186
Licensed Content Issue	4
Licensed Content Pages	15
Start Page	733
End Page	747
Type of Use	reuse in a thesis/dissertation
Portion	figures/tables/illustrations
Number of figures/tables/illustrations	2
Format	both print and electronic
Are you the author of this Elsevier article?	No
Will you be translating?	No
Original figure numbers	Figures 1 and 2
Title of your thesis/dissertation	Adhesion and Beyond: CD44 in Ovarian Cancer Spheroids
Expected completion date	Jan 2018
Estimated size (number of pages)	100
Requestor Location	Mrs. Joelle Sacks 950 W Cullerton St Unit G CHICAGO, IL 60608 United States Attn: Mrs. Joelle Sacks
Publisher Tax ID	98-0397604

Permissions to Reprint/Reproduce (continued)

Rockefeller University Press LICENSE TERMS AND CONDITIONS

Dec 18, 2017

This is a License Agreement between Mrs. Joelle Sacks ("You") and Rockefeller University Press ("Rockefeller University Press") provided by Copyright Clearance Center ("CCC"). The license consists of your order details, the terms and conditions provided by Rockefeller University Press, and the payment terms and conditions.

All payments must be made in full to CCC. For payment instructions, please see information listed at the bottom of this form.

License Number	4251960340461
License date	Dec 17, 2017
Licensed content publisher	Rockefeller University Press
Licensed content title	The journal of cell biology
Licensed content date	Dec 31, 1969
Type of Use	Thesis/Dissertation
Requestor type	Academic institution
Format	Print, Electronic
Portion	chart/graph/table/figure
Number of charts/graphs/tables/figures	1
The requesting person/organization is:	Joelle Sacks/University of Illinois at Chicago
Title or numeric reference of the portion(s)	Figure 1
Title of the article or chapter the portion is from	The extracellular matrix: A dynamic niche in cancer progression
Editor of portion(s)	N/A
Author of portion(s)	Pengfei Lu, Valerie M. Weaver, Zena Werb
Volume of serial or monograph.	196
Issue, if republishing an article from a serial	4
Page range of the portion	396
Publication date of portion	February 20, 2012
Rights for	Main product
Duration of use	Life of current and all future editions
Creation of copies for the disabled	no
With minor editing privileges	no
For distribution to	Worldwide
In the following language(s)	Original language of publication
With incidental promotional use	no
The lifetime unit quantity of new product	Up to 499
Title	Adhesion and Beyond: CD44 in Ovarian Cancer Spheroids
Instructor name	n/a
Institution name	n/a
Expected presentation date	Jan 2018
Billing Type	Invoice
Billing Address	Mrs. Joelle Sacks 950 W Cullerton St Unit G CHICAGO, IL 60608 United States Attn: Mrs. Joelle Sacks
Total (may include CCC user fee)	0.00 USD

Permissions to Reprint/Reproduce (continued)

Keywords: hyaluronan, CD44, RHAMM, inflammation, cancer

Citation: Misra S, Hascall VC, Markwald RR and Ghatak S (2015) Interactions between hyaluronan and its receptors (CD44, RHAMM) regulate the activities of inflammation and cancer. *Front. Immunol.* 6:201. doi: 10.3389/fimmu.2015.00201

Received: 07 February 2015; **Accepted:** 13 April 2015;
Published: 06 May 2015

Edited by:
David Naor, Hebrew University of Jerusalem, Israel

Reviewed by:
Toru Hiraga, Matsumoto Dental University, Japan
Carmela Ricciardelli, University of Adelaide, Australia

***Correspondence:** Suniti Misra and Shibnath Ghatak, Department of Regenerative Medicine and Cell Biology, Medical University of South Carolina, 173 Ashley Avenue, Charleston, SC 29425, USA, misra@musc.edu; ghatak@musc.edu

TABLE OF CONTENTS

Write a comment...

Add

Permissions to Reprint/Reproduce (continued)

Title: Multicellular spheroids in ovarian cancer metastases: Biology and pathology

Author: Kristy Shield,M. Leigh Ackland,Nuzhat Ahmed,Gregory E. Rice

Publication: Gynecologic Oncology

Publisher: Elsevier

Date: April 2009

Logged in as:
Joelle Sacks
Account #:
3001223570

LOGOUT

Order Completed

Thank you for your order.

This Agreement between Mrs. Joelle Sacks ("You") and Elsevier ("Elsevier") consists of your license details and the terms and conditions provided by Elsevier and Copyright Clearance Center.

Your confirmation email will contain your order number for future reference.

printable details

License Number	4242850189372
License date	Dec 05, 2017
Licensed Content Publisher	Elsevier
Licensed Content Publication	Gynecologic Oncology
Licensed Content Title	Multicellular spheroids in ovarian cancer metastases: Biology and pathology
Licensed Content Author	Kristy Shield,M. Leigh Ackland,Nuzhat Ahmed,Gregory E. Rice
Licensed Content Date	Apr 1, 2009
Licensed Content Volume	113
Licensed Content Issue	1
Licensed Content Pages	6
Type of Use	reuse in a thesis/dissertation
Portion	figures/tables/illustrations
Number of figures/tables/illustrations	1
Format	both print and electronic
Are you the author of this Elsevier article?	No
Will you be translating?	No
Original figure numbers	Figure 1
Title of your thesis/dissertation	Adhesion and Beyond: CD44 in Ovarian Cancer Spheroids
Expected completion date	Jan 2018
Estimated size (number of pages)	100

Requestor Location	Mrs. Joelle Sacks 950 W Cullerton St Unit G CHICAGO, IL 60608 United States

VITA

NAME:	Joelle Devon Sacks
EDUCATION:	B.A., Chemistry, Boston University, Boston, Massachusetts, 2009
	M.S., Biomedical Sciences, Northeastern University, Boston, Massachusetts, 2012
	Ph.D., Biopharmaceutical Sciences, University of Illinois at Chicago, Chicago, Illinois, 2018
PROFESSIONAL EXPERIENCE:	Research Intern, Epizyme, Inc., Cambridge, Massachusetts, 2011-2012
	Laboratory Technician, Siemens Healthcare Diagnostics, East Walpole, Massachusetts, 2009-2010
	Summer Research Intern, Phylonix Pharmaceuticals, Cambridge, Massachusetts, 2009
	Summer Intern, Douglass Hanly Moir Pathology, Sydney, Australia, 2008
PROFESSIONAL MEMBERSHIP:	American Association for Cancer Research American Association of Pharmaceutical Scientists American Association for the Advancement of Science American Society for Biochemistry and Molecular Biology
PUBLICATIONS:	**Sacks, JD** and Barbolina, MV. Expression and Function of CD44 in Epithelial Ovarian Carcinoma. *Biomolecules*, 2015. 5(4): p. 3051-3066.
	Desjardins M, Xie J, Gurler H, Muralidhar GG, **Sacks JD**, Burdette JE, et al. Versican regulates metastasis of epithelial ovarian carcinoma cells and spheroids. *J Ovarian Res*. 2014;7(1):70.
	Knutson SK, Wigle TJ, Warholic NM, Sneeringer CJ, Allain CJ, Klaus CR, **Sacks JD**, Raimondi A, Majer CR, Song J, Scott MP, Jin L, Smith JJ, Olhava EJ, Chesworth R, Moyer MP, Richon VM, Copeland RA, Keilhack H, Pollock RM, Kuntz KW. A selective inhibitor of EZH2 blocks H3K27 methylation and kills mutant lymphoma cells. *Nat Chem Biol*. 2012;8(11):890-6
AWARDS:	AAPS Annual Meeting Biotech Section Travelship Award, 2016 Boston University Funded Research Opportunities Grant, 2008-2009